Thermoelectric generation for a self-powered autonomous sensor in satellites

By

J. Machín Llanos

in partial fulfilment of the requirements for the degree of

Master of Science
in Aerospace Engineering

at the Delft University of Technology,
to be defended publicly on Tuesday June 4, 2017 at 10:00 AM.

Student number:	4420438	
Affiliation:	Chair of Space Systems Engineering.	
Course code:	AE5810	
Project duration:	September 1, 2016 – July 4, 2017	
Supervisor:	ir. J. Bouwmeester	
Thesis committee:	Prof. dr. E.K.A. Gill,	TU Delft, Space systems engineering chairholder
	Dr. R. M. Groves	TU Delft, Structural Integrity and Composites
	ir. J. Bouwmeester,	TU Delft, Space systems engineering
	J. Carvajal Godínez,	TU Delft, Space systems engineering

An electronic version of this thesis is available at http://repository.tudelft.nl/.

Abstract

There are several benefits of using autonomous sensors in spacecraft. Avoidance of wired connections reduces cost, mass, and increases the flexibility and reliability of the system. The impact of wire reduction can be significant, especially for small satellites with many sensors, like temperature and sun sensors. Previous research has already focused on wireless intra- spacecraft communications. This research tests the self-powering capabilities of a system based on a COTS thermoelectric generator connected to a Bluetooth Low energy communication system, with a built-in controller and temperature sensor, and a power management interface. The system will be considered as a candidate for an autonomous temperature sensor in a future PocketQube mission of the university.

Controlled temperature differences can be achieved in a test environment, allowing the measurement of the generator power capabilities. It is tested that the system requires, for operation, a minimum temperature difference of 2.31 degrees between the extremes of the thermoelectric generator. It generates a peak power of 234 μW for that difference. In addition, the voltage difference obtained of 35.5 mV exceeds the minimum voltage required by the power management subsystem to be used. The power management sub-system consists of an ultra-low power converter that provides an output voltage of 4.1 V and a measured power efficiency of 32 % Moreover, thanks to the management of the Bluetooth sleeping modes, with the built-in controller and several operational amplifier comparators, an average power consumption of 5 μW is required during operation. The case studied would allow measuring temperature and sending the data over a Bluetooth link to the on-board computer every 16.2 seconds

It is concluded that the technology, based on COTS components, can be implemented and considered as the first step for a fully autonomous sensor with thermoelectric power generation in small satellites. Its implementation may provide substantial advantages for remote or/and locations where wiring is difficult to integrate. The tested performance values provide the foundation to develop the technology further.

The results of this thesis will be presented in the 68th International Astronautical Congress 2017, the 25-29 of September, organised by the International Astronautical Federation (IAF) in Adelaide, Australia. See Appendix O.

Acknowledgements

This MSc thesis would have not been completed without the support of a big amount of people. I would like to start thanking my thesis supervisor, Jasper Bouwmeester. His guidance and contributions for the thesis has been indispensable for my work. I have learnt a lot from his corrections and his way of approaching every single technological premise. I could already see the value and effect of these lessons in the last steps of my thesis. I would also like to thank the members of my committee for taking the time to correct my thesis and for their interest. In addition, I cannot forget Tatiana, Stefano, Johan, Dadui and Marsil for their time and friendly help whenever I had a technical problem.

I would also like to thank all of my friends. It is inevitable to focus on the people that have share my time in Delft but I still have a special place in my heart for all my friends in Madrid. It is also inevitable to see how much easier is to go through academic difficulties when you have a stimulating and enjoyable working environment. Thank you to all my friends that shared my working days in the MSc room of the Space Engineering department.

I would like to thank all the support of my family. Also, I want to thank my second family, the ones that made me feel like home in Delft, thanks Dani, Clara, Vicky, Lu and Nico.

However, my biggest gratitude goes to my parents, my sister, and my girlfriend. Most of the success of this thesis is because of them, who provided me with their unconditional help and love. This project is for them.

Table of Contents

List of Figures

List of Tables

Chapter 1 Introduction

Satellite miniaturization has created a paradigm shift in spacecraft design. Satellite miniaturization emerged mainly because of electronic size reduction and the will of educational institutions, and small and medium enterprises to develop their own-missions. Space missions benefit from the use of smaller, faster-to-develop, and cheaper spacecraft. As a result, new space applications have emerged thanks to the benefits provided (Straub 2012). Satellite miniaturization is also a chance to create new mission concepts, for example distributed network of multiple small satellites can provide a more higher temporal resolution to cover the whole earth (Sandau, Brieß et al. 2010). These concepts arise from the reconsideration of the spacecraft architecture and the adaptation of technologies to the new spacecraft performance requirements. While miniaturization and the use of commercial electronics helps to drive development and cost down per satellite, the complexity of assembly testing and integration is still high compared to commercial assembly lines for mass market productions. Solutions are needed to lower this complexity.

This MSc thesis focuses on the application of self-powering, more specifically thermoelectric harvesting, for autonomous sensors in small satellites to obtain a reduction in system size and an improvement of small satellite integration and development times. An autonomous sensor is a self-working unit; it measures and sends the data to a central computer while powering itself. While harvesting techniques use the physical environmental conditions of the sensor surroundings to provide with the power required for functioning.

1.1 Motivation

Several researchers have already spotted the benefits of using autonomous sensors in spacecrafts. The focus has been on the benefits that the use of a wireless intra-spacecraft communication entails (Amini, Aalbers et al. 2006, Amini, Gill et al. 2007, Zheng and Armstrong 2010). The main benefits, which can also be considered for energy harvesting, can be summarized as:

Mass reduction. The elimination of wirings implies a reduction of mass. Cables and all the interface components encompass 10% of the dry mass of a spacecraft(Amini, Aalbers et al. 2006).

Space reduction. Reducing the wirings implies a reduction of space occupied. In addition it entails better disposition options. Small satellites, due to their size constraints, can benefit from this aspect.

Complexity reduction. There is a reduction in the integration and assembly time. There aren't wires to allocate, support or connect.

Failure isolation. The independence respecting to other subsystems allows the mitigation of combined failures. For example, wiring busses failures can spread to other elements.

Better and new concepts. The utilization of autonomous systems allows placing sensors in complex positions, using them in deployable parts or just enhancing existing concepts. Self-powering technology was used in one of the first sun sensors in a small satellite (De Boom, Leijtens et al. 2004).

Increase flexibility. Allows the introduction of changes in advance stages of the project. And it allows an easier replacement and upgrade of the units, the so-called "plug and play" devices.

To summarise, the avoidance of wired connections can reduce weight, volume, increase flexibility, and increase the reliability of the system; all these benefits can be extrapolated to self-powering. To provide a self-powering capability two methods can be used: batteries or energy harvesting. Using a battery provides a limited time of operation. However, the use of energy harvesting increases the lifespan of the operation. The real final product will be able to provide an assessment of the feasibility of obtaining these benefits. For example, it is expected that all the additional modules needed for an autonomous sensor will create an overall bigger size than a wired sensor for short wiring distances.

1.2 Literature study

Autonomous sensors require three functioning segments: autonomous-powering, wireless communication and data acquisition. Several institutions have already researched wireless communication for a spacecraft. However, energy harvesting and autonomous-powering research is not widespread and has not followed a clear trend. Specific concepts have been investigated but most of the research has a limit scope without proper ending prototypes being built or developed, especially in thermoelectric harvesting and radio frequency harvesting, the main self-powering technologies considered to be researched apart from solar powered applications already developed and tested in detail.

Radio frequency harvesting and thermoelectric harvesting are selected as the best candidates for their implementation in a small satellite. Thermal harvesting, based on the Seebeck effect, obtains energy from the temperature difference between two junctions with different conductor types. Radio frequency (RF) harvesting obtains the energy with an antenna from RF waves. It can be provided by a dedicated RF source or it can be obtained from any environmental RF source. The identified harvesting would focus on a dedicated RF source, a technology that is being developed already in on-ground applications (Visser 2012). The rejection of other energy harvesting techniques has been done in a previous Literature Study, following the requirements presented in Appendix-A.

This section goes through the different contributions on the field of energy harvesting for satellite use, the contribution of this thesis and its objectives, and the contribution that it has for TUDelft's chair of Space Systems Engineering (SSE).

1.2.1 Work in the field

Companies and research institutions have already researched self-powering to make its possible advantages a reality. Research has already been carried out in this area in collaboration between Thales and the University of Toulouse (Takacs, Aubert et al. 2012, Takacs, Aubert et al. 2013, Takacs, Aubert et al. 2014).This research was made with a specific application in mind. It departs with the premise that the environmental conditions, found in the exterior part of a Geostationary Broadcasting Satellite, harvested with radio frequency harvesting and thermoelectric harvesting, could provide power for autonomous health monitoring in the external side. This premise is proven by analysis of the thermoelectric harvesting and testing in lab the RF harvesting energy link.

The simulation of the power obtained with thermoelectric generators was carried with positive results. The simulation takes into account a thermoelectric generator with the hot plate facing the sun and the cold face facing space. This design provides a considerable temperature difference between the plates, providing a considerable power. The simulation gives an average electrical power of 15 mW for a temperature gradient of 30 degrees (Takacs, Aubert et al. 2012). This research does not test these premises.

Moreover, an analysis of radio frequency harvesting for health monitoring is also done. Radio frequency energy is obtained from the minor lobes created by antennas in the satellite. The feasibility results are also positive. To obtain these results they use a self-design rectenna, analysing the worst-case scenario, where the impedance of the rectenna doesn't match with the load impedance, which generates a stronger conclusion of feasibility (Takacs, Aubert et al. 2014).

In the Technische Universitat Dresden research has been done on system studies for the application of thermoelectric harvesting in satellites. They have evaluated the main possible locations of the devices inside conventional satellites, possible applications for TEGs, as powering electrochromatic devices (ECD) that change their optical properties with the application of voltage, , and the possible feasibility of integration into small satellites. The main outcomes of their research is that the low temperature differences expected in small satellites, less than 3.5 degrees, and the low efficiency of these devices do not allow to feed the electrical power into the main power system. It is stated that an autonomous system would be the only current possible application of this technology. Foreseeing this future application, they plan to launch a TEG, in 2017, on a small satellite built by TU Dresden, to characterize its performance with space conditions (von Lukowicz, Abbe et al. 2016).

1.2.2 TUDelft's Chair of Space Systems Engineering contribution

Small satellites interest educational institutions because of its affordability and its project development time scale; students can work in a space project and see results before finishing their educational lifetime. Delft University of Technology´s chair of Space Systems Engineering (SSE) aim is to develop small satellite technology further. For years TUDelft has been developing student small satellites and projects and has developed the state of the art with scientific and space industry agreements, for example within the MISAT grant program (Gill, Monna et al. 2007). Research on the use of autonomous sensors and wireless technology for satellites has already been done at the chair. An autonomous wireless sun sensor was successfully developed by the university and the company TNO (Bouwmeester, Aalbers et al. 2008) and demonstrated on the Delfi-C3 Cubesat launched in 2008. The chair also carried out a PhD on Wireless Communication On-board Satellites (Amini 2016) and an MSc thesis based on a proof of concept BLE (Bluetooth Low Energy) communication in a Cubesat (Schoemaker). A higher-level objective of this research is to continue with this research direction and implement self-powering to wireless sensors in future small satellites launched by the SSE chair.

The chair wants to keep on the lead of small satellite technology. Therefore the attention is now on the development of PocketCubes, and the development of its new satellite, the Delfi-PQ. PocketCubes are composed of building blocks of approximately 5 cm wide. They provide a better value-to-cost for huge networks of satellites. And its much smaller size forces the development of new interesting concepts. Delfi-PQ will also be faster to develop and launch providing advantages for student collaboration and project continuation. All this technology and development knowledge could also be implemented in other satellite concepts, for example, CubeSats.

Fig. 1 Delfi-PQ artist impression

1.3 Conceptual Thesis Design

This section presents the contribution of the thesis to the body of knowledge already presented in the previous section. Furthermore, this section presents the objectives, questions, and methodology stated/agreed to fill this void in knowledge.

1.3.1 MSc thesis contribution

The research above-mentioned, in subsection 1.2.1 from Thales and Toulouse University, departs from the analysis of a GEO satellite. The research considers huge ΔT conditions so it does not analyse the possible limits of the thermoelectric technology. Neither have they tested the expected conditions on a thermoelectric module. These researches analyse the use of TEGs in satellite with positive results but did not obtain an end-to-end system both analysed and tested. In addition, they analyse the system with an expected temperature difference of 30 degrees, a relatively high value, which is not expected to occur frequently at random places in the satellite, nor is it expected to be needed for useful low power applications. Also, their approach for RF harvesting cannot be used for small satellites due to the expected low and uncertain RF ambient conditions. Research of on-ground applications also found similar problems as it is said in (Visser 2012), "The availability... of sufficient power cannot be guaranteed under all circumstances… however powering … by means of radio waves that are emitted by a dedicated source".

The use of dedicated sources could provide the required power without jeopardizing other benefits as the flexibility in the design.

Research by the DLR and Dresden university, focus on the feasibility of using the TEG to add energy into the main power system. The research states that TEGs are promising for implementation of new autonomous systems based on low power demand. These conclusions are all based on a maximum temperature difference, 3.5 degrees, which they identify can be obtained from a CubeSat of the Institute of Aerospace Engineering at TU Dresden. However, they do not state if that is enough for a complete autonomous system nor analyse the possible extra components needed to overcome thermoelectric harvesting flaws, like ultra-low output voltage, to make the system a reality.

There are possible research paths that can be carried in this MSc thesis. This thesis will assess a case study that will develop a real proof of concept and characterize its true performance specification. The proof of concept will be based on thermoelectric harvesting rather than RF harvesting because of time constraints. The result is intended to be the first full system test for a small satellite design. The research will provide the first full prototype addition to the body of knowledge of the use of Thermoelectric harvesting in small satellites. For this purpose thermoelectric harvesting will be used to power a temperature sensor for housekeeping purposes. A temperature sensor is used as it is considered one of the easiest to implement and one of the lowest power consumption sensors. In addition, the research will focus on obtaining the lowest possible environmental requirements for the system. The focus will be taken into obtaining a system that for example could be used in the previous availability of a maximum 3.5 degrees of temperature difference. In addition, a low temperature difference is sought as it will provide the technology limits and so applications with a higher available temperature difference could also be used. This research wants to continue with the wireless technology on-board spacecraft research of the SSE chair focusing on the powering section of the autonomous sensors. It is expected that more work would have to be done in the areas of application study and optimization of design.

1.3.2 Research questions and objective

After the identified possible contribution that can be made, research questions and a research objective are presented to give a clearer path of action. The initial research question states the following:

> "Can thermoelectric harvesting power an autonomous powered sensor in a small satellite?"

It is considered that a sensor is powered when it can gather data, process data, and send data to a main computer. The data received shall provide accurate information of what has been measured. For the proper completion and for guiding the research of the project sub-research questions should be stated:

> "How and under which minimal conditions can thermoelectric harvesting power an autonomous powered sensor?"

> "Are the required conditions, for powering, feasible in a small satellite environment?"

From these research questions, and with the actual body of knowledge conditions, the research objective is:

> "Assess the feasibility of the introduction of self-powering techniques, specifically thermoelectric harvesting, in the use of autonomous sensors in small satellites and provide with recommendations for further actions."

1.3.3 Methodology

The methodology will provide a stance on how to obtain an answer to the research questions. To provide a feasibility study two different approaches have been found, analysis and testing as the research of (Takacs, Aubert et al. 2012).

Breadboard and laboratory testing is selected for this project for practical reasons, as it will provide with hands-on-the-sensor lessons for the SSE chair. In addition, it is considered that it will allow finding unexpected problems that may create a risk on the proof of concept, obtaining a better quality conclusion. However, a theoretical investigation is needed to provide a departure point for testing.

The system is made of several subsystems. Therefore, testing all at once would be a risky process to carry on. That is why this project focuses on modular testing. Every subsystem is characterized independently with a test. Characterization is important as it enhances the final analysis of its integration with the other subsystems (Denker and Muhtaroğlu 2013). The characterization requires the theoretical enumeration of properties and if needed, the test of any of those properties. The values expected to be measured consist of ultra-low electrical values. This means that special attention is given to the uncertainty analysis and to guarantee the correctness of the results.

The final results will have to fulfil a series of requirements to be able to provide a reliable research outcome. Test achievement conditions and requirements will be defined during the first phases of the test. These conditions will be used to provide conclusions and answers to the project.

Confirmation bias and the correct annotation of every testing condition, with an impact on the result, are considered among the most important risks on the methodology. One key issue of this study is that a positive answer is more satisfying, and it can mean trying to change the assumptions or test conditions until a favourable result emerges.

In conclusion, the research objective is achieved by the test of the powering of a low power sensor by thermoelectric harvesting. In addition, a final prototype will be designed and tested. The final prototype will provide the limitations of the design analysed.

1.3.4 Document Structure

The philosophy of end-to-end development that characterizes PocketQube design can be seen through the project. As presented before, The design and test of a full system requires the division into functional units. Therefore, a modular test approach has been used. Each subsystem will be tested individually providing an assessment of their capabilities and a preview on what problems the final design may have. This philosophy can directly be seen with the document structure.

The documents starts, in Chapter 2, presenting the full self-powered autonomous sensor system. The different modules of the system and a brief explanation of the state of the art of each module is presented. Afterwards, the first module is characterized, the Thermoelectric Generator, in Chapter 3. This chapter provides the expected powering characteristics of the load. The next test characterizes the Power conversion module, found in Chapter 4. In addition, the test done to connect the Thermoelectric generator to the Power conversion module is also presented. The Power Management module is tested before the load as the main objective of this thesis is on the powering characteristics of the system and the power converter was identified as a possible critical aspect of the design.

Afterwards, in Chapter 5, the load, comprising the Bluetooth Low Energy module and the temperature sensor, is tested and characterized. Then, the whole system is connected in Chapter 6, also the power control module is tested and characterized. The thesis document ends with Chapter 7 in which the Conclusions and Recommendations are presented with a Discussion on the work done.

Chapter 2 The Self-powered Autonomous Temperature sensor

The previous chapter presented the problem and the way to address it. Providing a solution starts with the proper definition of what is a self-powered autonomous sensor, the definition of its main characteristics and sections, and the theory required to solve the problem. This section provides a general overview of the system. Every single module is presented in detail with the information required to complete the tests and obtain results and conclusions.

2.1 The Self-powered autonomous sensor system

Dissecting the name, self-powered autonomous sensor, presents the main characteristics of the system. Self-powered implies that the system itself has a power generation module and an external system does not power it; it is self-sufficient. Batteries normally power self-powering sensors however the need for a long-term power source leads to energy harvesting. Autonomous implies that the system communicates through wireless communication achieving an independent system when it is also used with self-powering or a battery. Furthermore, the whole system is designed to sense data.

Energy harvesting provides low power density. Therefore, these systems require lowering their power consumption by using low-power components and power managing. Low average power is obtained as autonomous sensors are inactive most of the time, one of its most important characteristics. The relation between the active time and the total period time is defined by the duty cycle, denoted as follows,

$$D = \frac{t_{ON}}{T} = \frac{advertising\ time}{advertising\ time + charging\ time} \quad (1)$$

In which, D is the duty cycle [-], T is the sensing period [seconds], and t_{ON} is the total time that the system is active. The advertising time in the equation represents the wake-up, the sensing and the sending of data. Overall performance characteristics can be defined with the duty cycle as the average power consumed and the maximum attainable duty cycle.

$$\overline{P_c} = (1 - D)P_{sleep} + DP_{active} \quad (2)$$

$$D_{MAX} = \frac{\overline{P_g} - P_{sleep}}{P_{active} - P_{sleep}} \quad (3)$$

In which $\overline{P_c}$ is the average power consumed by the system, $\overline{P_g}$ is the average power generated [W], P_{sleep} is the power consumed by the load while idle [W], P_{active} is the power consumed by the load while active [W], and D_{MAX} is the maximum duty cycle to provide energy for the functioning of the sensor for a certain power generation [-]. For using this concept a storage component is needed to power peaks of sensor activity and charge during sleep mode. Figure 3 shows a simplified graph representing the power profile of an autonomous sensor with a distinction between the power active, or peaks, and the sleep power, considerably lower than the active mode.

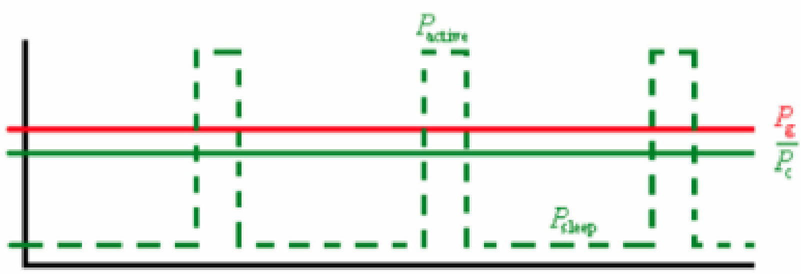

Fig. 2 Duty cycle representation with average power values generated, P_g, and consumed, P_c. (M. T. Penella 2007).

2.1.1 System model

Several modules form an autonomous self-powered sensor system, each with a different functionality. The modules are:

Power source, provides the energy for the system operation. Batteries could be used for this module, but this project focuses on thermoelectric harvesting.

Management electronics, they provide the interface between the electrical characteristics of the power source and the power necessities of the different elements: the controller, transceiver and sensor, to be powered. The storage system is also considered in this module as it also serves as an interface. In addition, these electronics provide the control of the modes of operation of the powered sensor elements.

Micro-controller for control and signal processing of the system. The microcontroller stays in low power state when it doesn't need to carry actions, sleep mode. In this specific case the microcontroller, CC2541 Radio Frequency chip, is inside the COTS BLE module used guaranteeing an easier use and lower power consumption.

Transceiver for data communication. It needs to transmit the data to the OBC (On Board Computer) Low power protocols can be used as BLE and ZigBee. This project uses Bluetooth Low Energy (BLE).

Sensor, the data-acquisition module. It provides with the functional application of the whole system. In this case the embedded temperature sensor of the CC2541 is used.

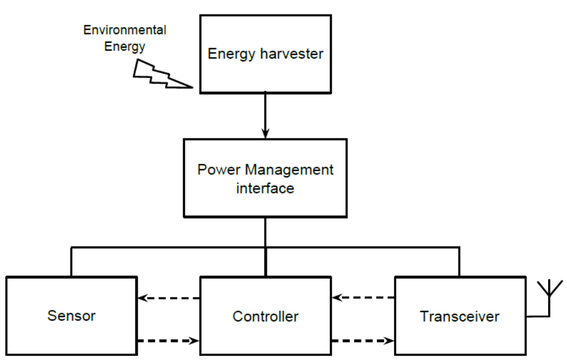

Fig. 3 Block diagram of a self-powering autonomous sensor system. Dashed arrows represent data communication Normal arrows represent power transmission.

2.1.2 System design

The system should follow guidelines determined by the limitations and requirements of the used platform, small satellites, and the step in which the state of the art technology is right now, searching an end-to-end proof of concept. Different design requirements are identified:

Low environmental source conditions. The prototype is designed to be able to operate in the lowest temperature difference achievable. This allows an easy implementation and to foresee the limitations of the technology. It is also considered that the introduction of one of these modules would be difficult for high heat flow paths due to the criticality for the overall performance of the system of these paths and the possible low thermal conduction of the thermoelectric modules (von Lukowicz, Abbe et al. 2016).

Size. One of the main constraints of every technology introduced in a small satellite is size. For this project, the temperature sensor used in Delfi-n3xt is used as a reference. Temperature sensor images are presented in Appendix N.

Complexity. The main aim is to provide a proof of concept of an end-to-end system and powered by thermoelectric harvesting, no specific requirements of application are required. Therefore, the lowest level of complexity is used in each functional area of the design as long as the objectives can be achieved

2.2 The thermoelectric harvester

A thermoelectric harvester is used as power source. Commercial TEGs can be obtained easily, marketed as proper thermoelectric generators or most commonly as Peltier coolers. The following section presents the modelling theory used to estimate the final performance of both the coolers and the generators. In addition, the COTS Thermoelectric modules used in this thesis are presented.

2.2.1 Thermoelectricity theory

Thermoelectricity is the relation that exists between heat and electrical phenomena. Thanks to this phenomena electrical power can be obtained from temperature differences or heat flow can be obtained from electrical power. This subsection presents several concepts of the theory of thermoelectricity.

Seebeck effect

The Seebeck effect is the vital thermoelectric effect for this project. The Seebeck effect generates electrical power when there is a temperature gradient between two dissimilar conductors in contact. The effect can be modelled as follows*:

$$V_{TEG} = \alpha \Delta T \tag{4}$$

In which α is the Seebeck coefficient $[\frac{mV}{K}]$, and ΔT is the temperature gradient between the two extremes of the contact materials $[{}^{\underline{o}}C]$.

Peltier effect

The contrary effect to the Seebeck effect is the Peltier effect. When there is a voltage difference there will always be a heat-flow, and this counter effect needs to be taken into account for any model. The Peltier Effect generates a heat-

* Most of the bibliography related to thermoelectric harvesting uses the equations described in this section for each pair of conductors. In this thesis, the equations are directly used to represent a final thermoelectric COTS module, formed by several pairs connected together.

flow when a voltage difference is applied between the extremes of two different materials. The effect can be modelled as follows:

$$\dot{Q}_P = \pi * I_{TEG} = \alpha \mathrm{T} I_{TEG} \tag{5}$$

In which π_{ab} is the Peltier coefficient $[V]$, $\dot{Q}_P$ corresponds to the heat flow generated by the Peltier effect $[W]$, I as the current $[A]$, and T as the temperature $[K]$. Thermoelectric coolers or heaters are based on this effect. The relation between the Seebeck and Peltier coefficient is obtained from the Kelvin relationship of the thermoelectric effect (Stephen Beeby 2010).

Power generation

The TEG is modelled as a real voltage generator, with its internal resistance. Power is obtained with the voltage obtained by the Seebeck effect, and the current as obtained with Ohm's Law. The output power in the load is equal to,

$$P_{out} = VI = \frac{(\alpha_{ab}\Delta T)^2}{(R_L + R_i)^2} R_L \tag{6}$$

In which R_L is the load resistance $[\Omega]$, and R_i is the internal resistance of the generator $[\Omega]$. The expected values are represented with a linear IV curve and power is maximum when R_L and R_i are equal. The following figure represents the electrical characteristics, output power curve and IV curve, of a standard thermoelectric generator.

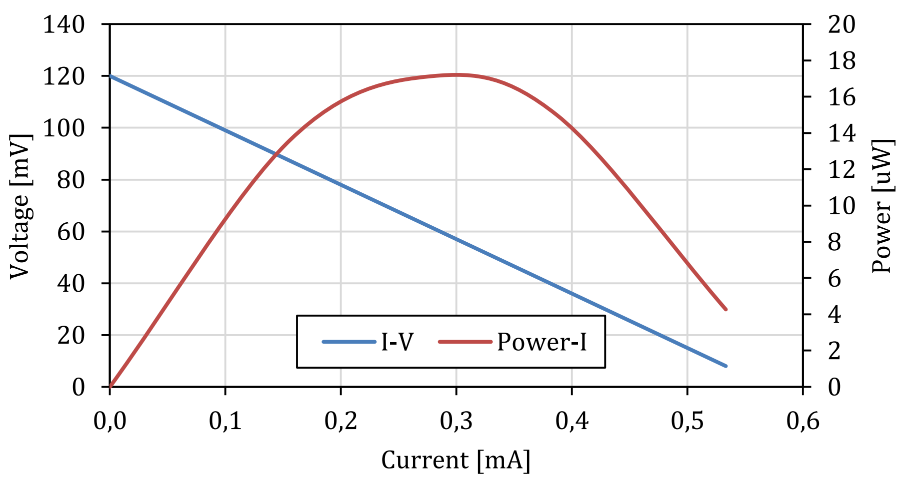

Fig. 4 Graph representing the shape of a IV curve and a Power vs. Current curve for a thermoelectric generator. The values used for this graph are $\alpha = 60\frac{mV}{K}$ and $R_{int} = 210\ \Omega$ for $\Delta T = 2.0\ K$.

Heat balance equation

The heat balance equation of any thermoelectric module is composed of three terms, the Peltier heat, the heat conduction and the Joule heat. The heat balance equation is of importance for final performance characterisation like the efficiency of the module. Depending on the application the heat balance is calculated in different sides of the thermoelectric module. For a thermoelectric generator calculating the heat absorbed is important to know the efficiency of the system. The heat absorbed in the hot side of the module is equal to,

$$\dot{Q}_h = \alpha T_h I + k(T_h - T_c) - \frac{1}{2} I^2 R_i \tag{7}$$

In which $\dot{Q}_h$corresponds to the heat flow absorbed from the hot side [W], and k corresponds to the thermal conductance of the device $[W]$. For a thermoelectric cooler, the heat absorbed at the cold side is important to calculate the efficiency of the system. The heat absorbed at the cold side is equal to,

$$\dot{Q}_c = \alpha T_c I - k(T_h - T_c) - \frac{1}{2} I^2 R_i \tag{8}$$

In which $\dot{Q}_c$corresponds to the heat flow absorbed from the cold side [W].

Maximum performance values

For a thermoelectric cooler there are maximum performance values that can be obtained due to equation (8). The maximum $\dot{Q}_c$ that can be obtained corresponds to $\Delta T = 0.$ The maximum $\dot{Q}_c$ is equal to,

$$\dot{Q}_{c_{max}} = \alpha T_h I_{max} - \frac{1}{2} {I_{max}}^2 R_{int} \tag{9}$$

If the maximum temperature difference is searched, then $\dot{Q}_c$ needs to be equal to zero, and the maximum value of current should be searched. This leads to have the following temperature gradient equation,

$$\Delta T = \frac{\alpha T_c \mathrm{I} - \frac{1}{2} \mathrm{I}^2 R_{int}}{k} \tag{10}$$

The derivation of the previous equation with respect to the current going through the TEG is equal to,

$$\frac{\partial \Delta T}{\partial I} = \alpha T_c - \mathrm{I} R_{int} = 0 \tag{11}$$

Which gives the maximum current that is needed to generate the maximum temperature difference,

$$I_{max} = \frac{\alpha T_c}{R_{int}} \tag{12}$$

And,

$$\Delta T_{max} = \frac{\alpha T_c I_{max} - \frac{1}{2} {I_{max}}^2 R_{int}}{k} \tag{13}$$

2.2.2 The Thermoelectric generator in the system

There are two performance values that need to be reached by the TEG. There is a minimum voltage required for the use of the DC-DC converter in the power management module and enough power should be generated so that after power losses through the power management module there is still enough current for charging the output capacitor. The Seebeck coefficient and the internal resistance of the TEG are the parameters that have a bigger influence on the output power and voltage.

2.2.2.1 Thermoelectric module selection

Two COTS modules are selected as possible candidates for the sensor system. They have been selected after a trade-off seeking high Seebeck coefficient and low internal resistance. A commercialized Peltier cooler and a commercialized thermoelectric generator have been sought. In the end, one of them has better capabilities for voltage provision but will provide with less power while the other one will provide with more voltage but lower voltage output. Both of them are the best ones for both worlds, among the total thermoelectric modules provided by known suppliers.

The first module selected is the TGP-651 from Micropelt Technologies, commercialized as a thermoelectric generator and the other module is the ET20,68,F1A,1313,11 from Laird Technologies, commercialized as a Peltier cooler, called from now on as ET20,68.

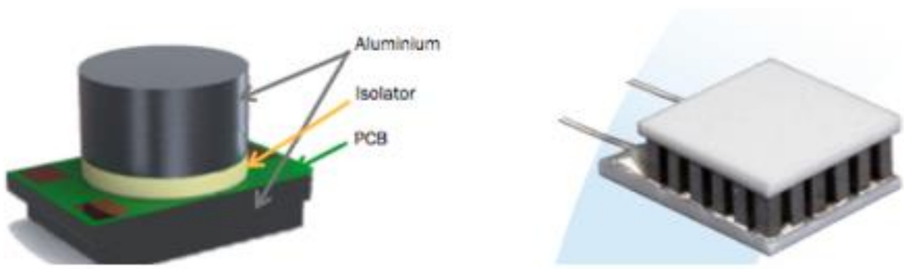

Fig. 5 Thermoelectric modules used for the project. (left) TGP-651. (right) ET20-68.

Both modules are commercialized for different applications. It is expected that the TEG-G would be the best for the application foreseen. However, the definition of power harvester does not encompass all the different application conditions. The different characteristics of both modules are presented in the following tables. Due to the different applications foreseen for them, the manufacturers provide different characteristics.

TGP-651 (TEG-G)	*Values*
Internal Resistance (Typical)	210 Ω
Internal Resistance (Maximum)	242 Ω
Seebeck coefficient	60 mV/K
Dimensions	15 x 10 x 9,5 mm

Table 1 Parameters of the TGP-651 thermoelectric module.

ET20-68 (TEG-C)	*Values*
Internal Resistance	3.55 Ω
Maximum heat generated	9.3 W
Maximum Current	2.0 A
Maximum Temperature gradient	67.0 K
Dimensions	13.2 x 13.2 x 2.2 mm

Table 2 Parameters of the ET20-68 thermoelectric module.

From the data obtained from the datasheet of the ET20-68 and presented in Table 2, the Seebeck coefficient can be obtained. Calculating the coefficient with equations (9) and (13) different values are obtained. To take into account both maximum conditions, equation (12), with $T_c = T_h - \Delta T_{max}$, are used into (9) to obtain the following Seebeck coefficient,

$$\alpha = \frac{2Q_{max}}{I_{max}(T_h - \Delta T_{max})} \tag{14}$$

The final Seebeck coefficient for the module is presented in the following table, Table 3.

ET20-68 (TEG-C)	*Value*
Seebeck coefficient	$25.5\ \mathrm{mV/K}$

Table 3 Seebeck parameter obtained for the commercial Peltier cooler, ET20-68.

The values presented show that the TGP-651 will produce more voltage per temperature difference than the ET20-68. However, the power obtained will be higher from the ET20,68 due to the difference in internal resistance.

2.3 The communications subsystem

Several wireless communication protocols can be used for intra-spacecraft communication. Their most important requirements are low-power consumption and overcoming signal interference problems such as achieving high SNR, and mitigate the harm to other sensitive devices in the satellite. For small satellite applications, ZigBee and Bluetooth meet the requirements while low-energy WiFi could be considered for higher data rate applications (Amini, Gill et al. 2007). Previous analysis in the chair of SSE TUDelft has also determined that BLE has a slightly better power consumed per transmitted bit performance for data bus communication and with acknowledge packets (Schoemaker).

The rest of this subsection will provide the information on the BLE communications protocol needed to understand the rest of the sections of this project that involve Bluetooth LE. The specific component used for communications, the BLE113 from Silicon Labs is also presented.

2.3.1 Bluetooth low energy protocol (BLE)

Bluetooth low energy was made to satisfy new wireless communication requirements, for small devices and with low power requirements, which the already developed Bluetooth protocols could not fulfil. It serves novel concepts that appeared after the electronics miniaturization trend and the emergence of the Internet of things (IoT). It requires an ultra-low average power consumption, suitable for applications running for long times with autonomous power sources. It also has a lower cost, size, and easier personalization compared to previous Bluetooth protocols. Communication is achieved by connections or advertising:

Advertising, also named broadcasting. It communicates by sending data to any scanning receiver.

Connecting, is used for bigger data packets and dual way transmission. It is a private communication with agreed communication periods and more complex communication instructions than advertising.

Both communication methods comply with the rules defined by the Generic Access Profile (GAP) The Generic Access profile provides the communication rules for the systems to interchange data in a standard, universal understood manner. The method used in this project is advertising. Two different roles can the Bluetooth module have for advertising type communication:

Broadcaster, the device sends non-connectable advertising data.

Observer, the device scans for non-connectable data packets sent by advertising.

Both roles are similar in activity profile but one uses the transceiver for transmitting and the other one for receiving. The role that is researched in this project corresponds to the functionalities of a broadcaster. However, it can be considered that the observer will follow a similar shape of power consumption, for example waiting for an activation packet by using an observer role.

2.3.2 Bluetooth Advertising

Advertising is the method used due to the simplification in the communication events power managing. Connecting would require different requests back and forward to guarantee a successful connection. In addition, by using advertising the need to use the transmitter capability is eliminated, reducing power consumption. For more complex systems there may be the need of creating connections to allow more flexibility and fault-tolerance operation. Advertising allows removing BLE capabilities, to obtain lower power consumption for this first proof of concept.

The total advertising data consists of a maximum of 47 bytes. A total of 8 bytes correspond to the Preamble, the Access Address and the CRC. While a packet Payload of (2-39 bytes) corresponds to the main part of the message. Advertising allows wireless transmission of data as long as the data to be transmitted is less than 31 bytes. Advertising can use, together or independently, three frequency channels (37, 38, and 39) and the successful reception of data depends if the scanning and advertising overlap. The total time required for sending an advertising packet in the three channels is around $1\,ms$ (Lindh 2016). However, additional time would be needed for the controller to process the actions and for the sensor to acquire data.

2.3.3 BLE module selection

The BLE device used for this project is the BLE113 developed by Bluegiga Technology from Silicon Labs. This device provides the best achievable power performance from the known available products in the market. In addition, it has been already used in the department for other applications, so it will be easier to use the same device as long as there are not compelling reasons to change it for a specific application. The BLE113 characteristics are presented in the following table.

BLE113	*Values*
Input Voltage	2.0 – 3.6 V
TX current ($0\ dBm$)	20.7 mA
RX current	14.3 mA
Active (No RF activity)	6.7 mA
Sleep Mode 1	270 μA
Sleep Mode 2	1 μA
Sleep Mode 3	0.5 μA
Dimensions	9.15 x 15.75 x 2.1 mm
Dimensions with testing Breakout-Board	28.0 x 51.0 x 3.9 mm
Dimensions of dedicated Breakout-Board	28.0 x 23.0 x 3.9 mm

Table 4 Datasheet values for the BLE module used, the BLE113 device.

The power consumption is reduced to a magnitude of 1000 when kept in sleep mode; this is the key for the application foreseen. The dimensions, an important requirement for the viability of this application, change a lot with the breakout boards used. Two breakout boards have been tested for this project. The comparison between both breakout boards, their flaws and advantages, are presented in Chapter 5, where the BLE113 is tested. The importance of the breakout board design is paramount. A honed breakout board should be designed for this specific application, reducing the current leakage and the dimensions. The projected dimensions of the breakout board used for the specific autonomous sensor application were inferred after comparing both breakout boards and the space availability for pins.

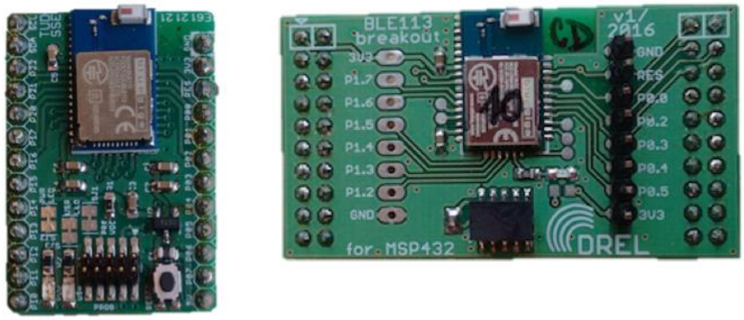

Fig. 6 Breakout boards for the BLE113 developed in the SSE chair. The left one is called from now on BB_LED and the right one as BB_test.

In addition, the BLE113 provides easy design of applications thanks to the internal low power MCU, the TI's CC2541 chip, a temperature sensor embedded in the controller, and a dedicated scripting language called BGScript. The BLE 113 has also several GPIO (General Purpose Input Output) pins that can be used. One of them will be used as a wake-up pin to communicate when to sense and advertise data.

2.4 The power management subsystem

The problem is clear; the electrical values provided by the thermoelectric harvester do not allow powering the communications segment directly. An interface is needed to provide a proper connection and control the advertising events. The power management module encompasses the group of components that serve as the interface between the electrical requirements of the load and the values obtained by the thermoelectric generator. In addition, it provides a logical segment to control the powering, at the right time, of the Bluetooth low energy module.

The power management module is divided into two sections, the voltage conversion, and the control section. Ultra-low start-up and functioning voltage, reduced current leakage, and power conversion efficiency are the main constraints for the interface. The main components of the converter segment is an ultra-low voltage converter based on a SoC, a transformer and a boost oscillator. The power control segment is based on a power switch, and a logic system of comparators.

2.4.1 The voltage converter

The specific requirements for obtaining the lowest possible temperature difference only leaves, to the best of our knowledge, one option for a COTS voltage converter. The voltage converter system uses the LTC3108 chip from Linear Technology. The LTC3108 is an ultra-low voltage converter system-on-chip. In addition to a 1:100 transformer and a charge pump capacitor it can provide a range of selectable outputs around $3\ V$ for inputs starting at $20\ mV$. All the characteristics of the LTC3108 component are presented in Table 5. The datasheet does not provide values for efficiencies using a voltage output different than 4.5 V.

LTC3108	*Values**
Minimum input voltage	20 mV
Output Voltage	2.35 V, 3.3 V, 4.1 V, 5 V
Power efficiency $V_{in} = 50\ mV\ V_{out} = 4.5\ V$	40 %
Power efficiency $V_{in} = 30\ mV\ V_{out} = 4.5\ V$	35 %
Input resistance	$4\ \Omega - 7\ \Omega$

Table 5 LTC3108 datasheet specifications (LinearTechnology).

The TEG is a dual-polarity power source. The current design system is not capable of withstanding this characteristic. This burden has already been considered. However, for the first phase of the testing the focus will be on a single electrical polarity power source. Adding a rectifier circuit will decrease the efficiency of the whole system burdening the first performance assessment. The LTC3109 from Linear Technology provides a dual-polarity power source but requires higher voltage input values, around 30 mV.

Providing a higher voltage reduces the output current. In addition, power is consumed in the process. The efficiency can be considered to be its most important characteristic. It will depend on the internal process of the LTC3108 and in the whole system design, or PCB design. It is critical to obtain more output current than the one required in sleep mode from the load plus losses as quiescent currents from other components. If this condition does not hold, there will not be any charging.

Several extra components, capacitors and a transformer, are recommended for energy harvesting with inputs close to the minimum input voltage. The following figure provides the main scheme of summarised internal capabilities and the external components recommended and needed.

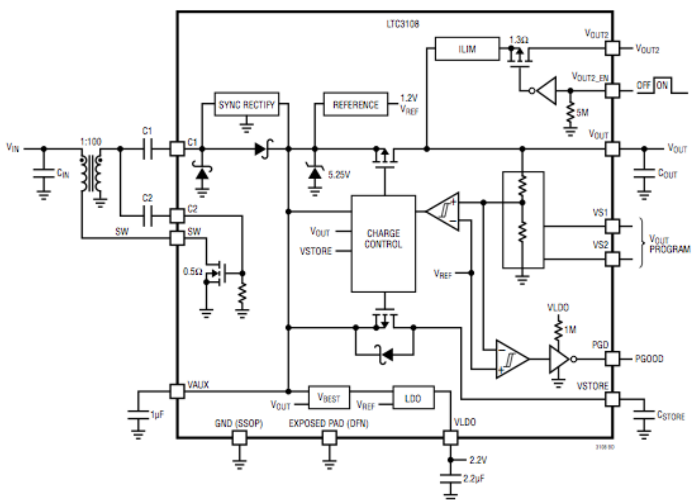

Fig. 7 Sketch with summarized LTC3108 internal functionalities and recommended outside layout for energy harvesting applications (LinearTechnology).

The extra modules presented in the previous figure are the ones required for an ultra-low input voltage, of the order of 20 mV. However, for higher values of input voltage the efficiency of the system decreases and so, different ratios of the transformer should be used.

There are two internal functionalities that can be used for the control system as well. The converter provides a LDO output. This output provides a stable 2.2 V reference that can be used for any reference level required in the control segment comparators. In addition, there is a pin, the PGD, which provides a signal when the output storage component reaches the designated final voltage. The real operation needs to be characterized to establish if it can be used to control the wake up of the Bluetooth module.

2.4.1.1 Storage Capacitors

The output and input capacitor needs to be modelled with the specific application in mind. The rest of the components do not require any extra modelling, as the values from the datasheet are the only ones needed as they depend on the input voltage used, and they are stated in the specific datasheet. Capacitors cover different functionalities for the power management sub-system. The output and input capacitors are used for interfacing with load and power source. For sizing the capacitors, variants of the following equation are used:

$$I(t) = C\frac{dV(t)}{dt} \qquad (15)$$

In which, $I(t)$ is the current through the capacitor $[A]$, C is the capacitance $[F]$, $dV(t)$ is the voltage change in the capacitor $[V]$, and dt is the time differential. Real capacitors have parasitic elements. These parasitic elements are important for low-power use. The parasitic resistance of the capacitor is called ESR (Equivalent Series Resistance). In addition, the dielectric used to separate the two conductive extremes of a capacitor is not a perfect insulator, so current goes through. These features are represented in the next figure.

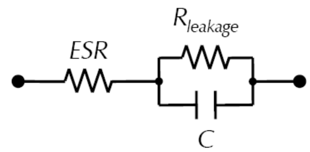

Fig. 8 Non-ideal capacitor model.

The leakage current will have an impact on the output capacitor, as the expected charging currents are in the order of the μA. And the ESR will have an impact on the start-up voltage, as it will reduce the effective voltage obtained from the capacitor. The output capacitor has two different functions, charging from a low current and then discharging a lot of energy in tiny time frames. Peak loads correspond to the "on" moment of the load in the duty cycle. For charging the equation obtained from Equation (15) is,

$$I_{pulse} = C_{out} \frac{V_{out} - V_{load_{min}}}{t_{pulse}} \qquad (16)$$

in which I_{pulse} is the total current consumed by the load, t_{pulse} is the time of the pulsed load, V_{out} is the voltage obtained from the converter, the initial voltage of the capacitor, and $V_{load_{min}}$ is the minimum voltage required by the load.† The previous equation can be rearranged for sizing the capacitor:

$$C_{out} \geq \frac{I_{pulse} t_{pulse}}{V_{out} - V_{min,load}} \qquad (17)$$

The product $C * ESR$ is considered as the time constant. For 5 time constants the charged voltage is equal to the 99,3% of what is provided. Similar equation as Equation (16) can be used for charging instead of discharging,

$$I_{sleep} - I_{out} = C_{out} \frac{V_{min,load} - V_{out}}{t_{charging}} \qquad (18)$$

2.4.1.2 Final voltage converter module:

A Printed Circuit Board (PCB) is designed to incorporate all the components of the module together. For the design process two PCBs were manufactured, with different sizes and level of complexity in the design. The bigger and less complex PCB was produced to reduce the risk of a possible delay due to wrong design of the smaller one. It was expected, that the big PCB is less prone to design failures. Both of the final products can be seen in Figure 9. The design schemes of the Breakout board are presented in Appendix C, including the breakout board disposition scheme. In addition, the first test environment, the protoboard, is also presented, in Appendix J.

† I_{pulse} could be considered as the current required by the load minus the charging current. However the latter is in the order of the μA, being negligible for the operation.

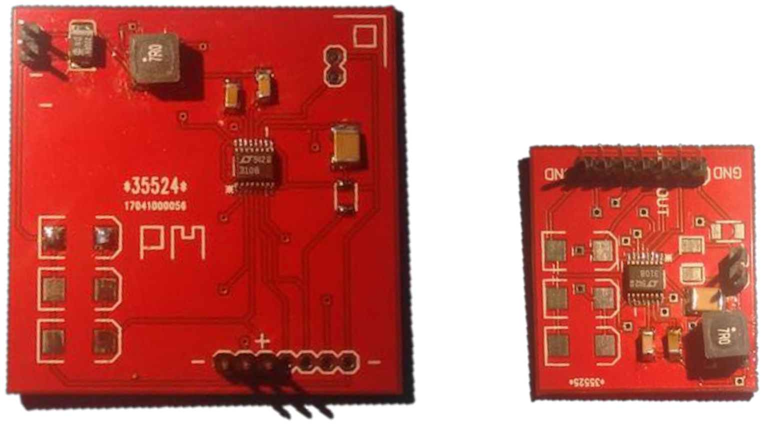

Fig. 9 Two different designs of the PCB prototyping for the Power Management module. Both PCBs are on scale.

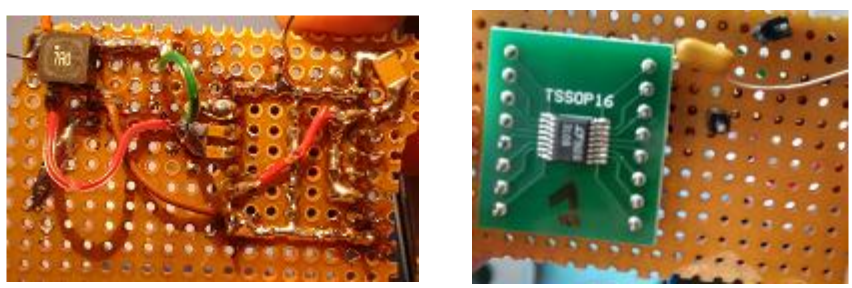

Fig. 10 Upper and bottom side of the protoboard Power converter module.

2.4.2 The control segment

Supplying power from the storage element needs to be controlled to administrate the duty cycle of the system. In addition, it should control when there is enough energy to carry the initialization or start-up, and the sensing events. This is all done by the use of three components, a Low Dropout Linear Regulator (LDO), and two comparators, one transformed into a Schmitt trigger.

2.4.2.1 Activity profile

The storage element starts charging and when it reaches the minimum operating voltage of the BLE113 it would start discharging to start-up the module. However, if not enough energy is present in the capacitor, the BLE module will try to start-up but it will have to stop the process. This process would repeat indefinitely. Therefore a switch needs to be present to close itself when the capacitor has been charged to complete the start-up of the BLE module. In addition, the switch needs to remain closed to be able to keep the system in sleep mode. The right time to close is provided by a Schmitt trigger, built with an operational amplifier comparator. Another signal needs to specify when to start sensing and advertising. This signal is provided by a non-inverter comparator.

In addition, to control when the system needs to act, a stable operation is required to minimize any possible restart of the system. To guarantee a stable operation of the BLE module, a stable input voltage signal should be supplied. This is provided by a linear regulator or a switching regulator.

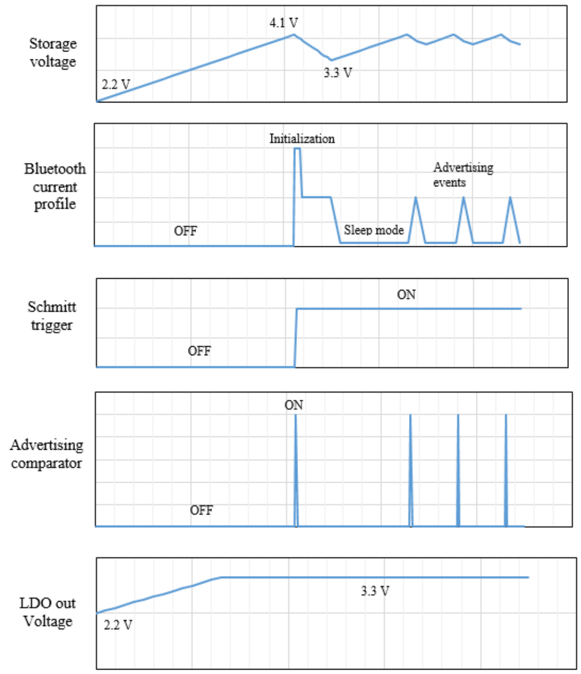

Fig. 11 Qualitative comparison of the signals involved in the Power management control segment .

In Fig.11 the different signals provided by the different elements of the system are represented, the values of the graphs are qualitative, obtained from the profiles of the experiments, to provide with the idea of the control mechanism. The storage voltage starts to charge, in the figure it is only represented from $2.2\ V$, obtaining the same output profile of the LDO. When the storage system reaches above $3.3\ V$ the regulator stabilizes its outcome providing only $2.2\ V$. The power converter provides an output voltage of $4.1\ V$, so the capacitor should be sized to store the initialization energy from this maximum to the limit of the stabilization of the LDO, $3.3\ V$. Therefore, the Schmitt trigger activates at $4.1\ V$, allowing the BLE to initialize, and it remains closed, ON signal, to keep the module in sleep mode. From $3.3\ V$ the capacitor starts charging to reach the maximum again, when the maximum is reached the comparator is activated sending a signal to start the sensing and advertising. It can be seen that the voltage of the storage capacitor decreases less than when initializing, as the energy required for the advertising is less.

2.4.2.2 Switch and input stabilization

A stable input can be provided by a switching regulator or a linear regulator. Each of them has its advantages and disadvantages. The efficiency of a switching regulator is higher than the one obtained from a linear regulator. This is because a linear regulator can only provide a buck converter capability. However, a switching regulator normally requires the inclusion of additional external components to provide with the full functionality. The linear regulator provides its function with minimal adaptation, requiring less complexity of design.

With the aim of reducing the complexity of the system a linear regulator has been selected. The component used is the TPS781, that provides with a constant output voltage of $3.3\ V$. The power dissipation that occurs, required for the storage component, is equal to:

$$P_{diss} = (V_{in} - V_{out})I_{out}$$

In which P_{diss} is the power lost in the linear regulator, V_{in} is the input voltage, V_{out} is the output voltage, in this case $3.3\,V$, and I_{out} is the output current going through the load, regulator and storage component. In addition, the component has a quiescent current of $500\ nA$.

2.4.2.3 Sensing and advertising control

The signal for sensing and advertising is provided by a comparator. A non-inverting comparator so when the storage voltage sought is sensed, the output will be a HIGH state. The internal LDO output of the power converter is used as reference signal and powering signal, as it is stable and always present when the storage voltage is above $2.2V$. The input voltage with the help of a voltage divider would provide with 2.2 V to the comparator when it reaches the specified previously 4.1 V.

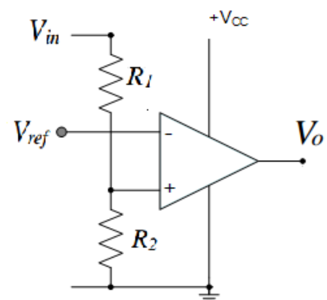

Fig. 12 Non inverting comparator with the use of an operational amplifier for the control of the sensing moments.

The resistances should be of a high value to provide the lowest possible current consumption. And the operational amplifier, comparator, used should require a low quiescent current and supply current consumption. The comparator used is the TLV3691. The output signal changes when the voltage obtained in the positive terminal of the comparator is equal to the reference voltage and it will remain positive as long as the following relation is kept $V_{ref} < V_{+}$.

2.4.2.4 Initialization control

For the initialization a hysteresis process is used. It turns ON and OFF for different input voltage levels, not as the single turning voltage of the last comparator design presented. The design should provide a turning ON signal when reached 4.1 V and a turned off when reached 3.3 V. The hysteresis process is represented in Figure 13 (right). This functionality is provide by the so-called Schmitt trigger, represented in Figure 13 (left).

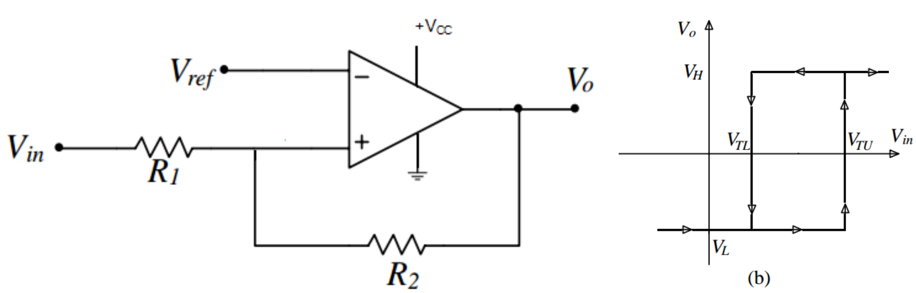

Fig. 13 Non inverting Schmitt trigger. (left) circuit, (right) hysteresis cycle.

The equations that determine the performance of the Schmitt trigger are the following,

$$V_{TU} = \frac{V_{REF}(R_2 + R_1)}{(R_2)} \tag{19}$$

$$V_{TL} = \frac{V_{REF}(R_2 + R_1) - V_{cc}R_1}{(R_2)} \tag{20}$$

In which V_{cc} corresponds to the supply voltage to the comparator, V_{REF} is the voltage used as a reference, V_{TL} is the lower turning point, and V_{TU} is the high turning point.

2.4.2.1 Final power control circuit

All the components presented in this section should be connected together to create the circuit required to control the operation of the Bluetooth module. The final circuit used is presented in the following figure:

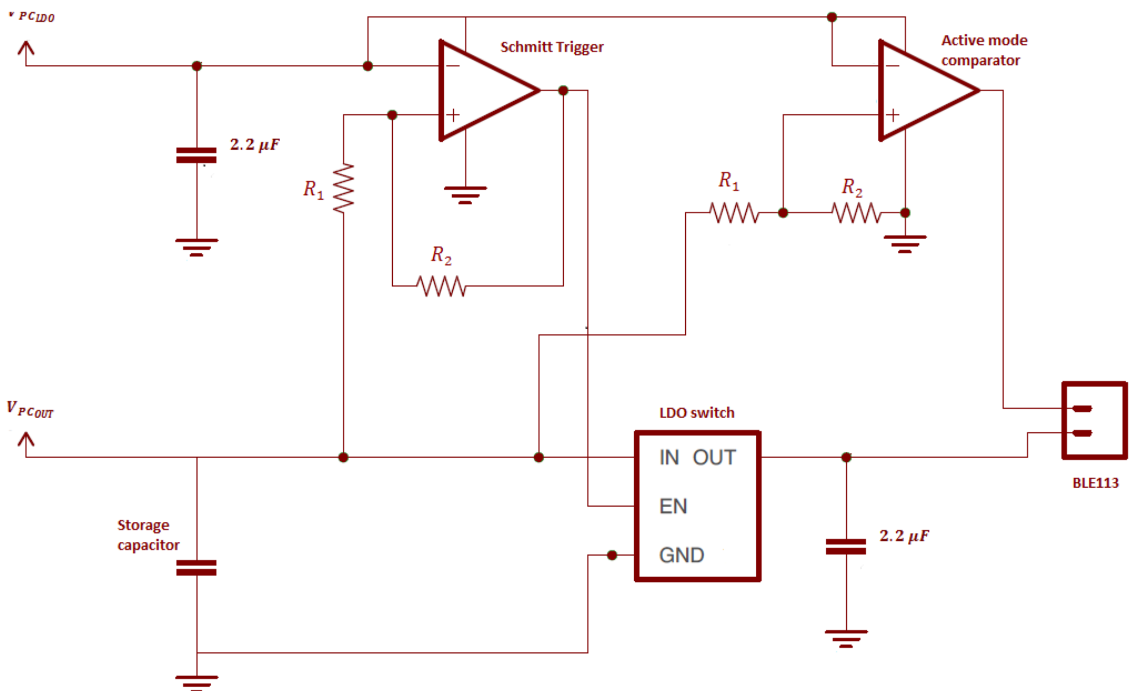

Fig. 14 Circuit for the Power management control segment.

The capacitors used in the circuit are for obtaining a stable operation of the LDO outputs. The values represented in the circuit for the resistances need to be of high value to drain the smallest amount of current, to reduce current leakages, and be able to provide enough current through for the operation of the comparator.

Chapter 3 Thermoelectric Characterization Test

3.1 Introduction

This chapter starts presenting the objectives and the test set-up for the thermoelectric characterization test. Then, to assess if the test set-up can answer the main questions satisfactorily section 3.2 presents the systematic uncertainty analysis. After that, in Section 3.3, the obtained results and the uncertainty for each value are presented. The end of the chapter, Section 3.4, gives the final conclusions on the results and on the test design and procedure.

3.1.1 Test objectives

The test expects to clarify the thermoelectric modules performance, present qualitative data for future designs, and provide the working conditions for the present thesis project. The objectives that have been identified are the following:

T-O-1: Validate the Seebeck coefficient values given in the thermoelectric modules datasheets.
T-O-2: Provide power generation information, including current and voltage values for a temperature difference of $2ºC$.[‡]
T-O-3: Determine the I-V curve of the thermoelectric modules.
T-O-4: Determine the power curves of the modules with respect to the load.

3.1.2 Test Set-up

The test consists of two aluminium plates constraining, in contact with thermal paste, the tested thermoelectric module. The bottom part of the system stays in contact with an electric heater to produce a temperature difference in the extremes of the thermoelectric generator, which will be measured by thermocouples into drilled holes in the aluminium plates, with thermal paste inside. Thermal insulation is used around to decrease the temperature non-uniformity of the TEG. Figure 15 presents a sketch of the described test set-up while images of the real test layout can be found in Appendix E.

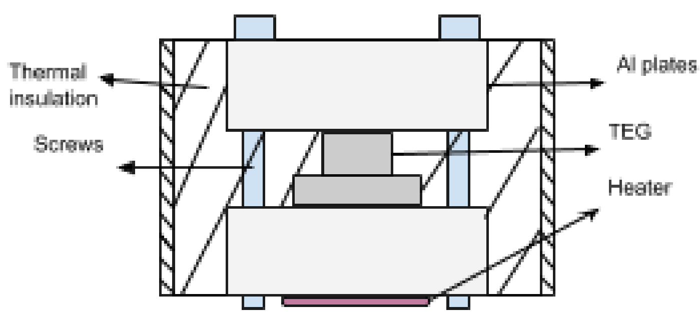

Fig. 15 Test set-up sketch for the thermoelectric generator characterization test.

The output voltage from the TEG is measured while measuring the temperature difference provided by the thermocouples. In addition, the output wires are connected to different loads to obtain the voltage and current through the different loads and hence, calculate the power provided. The specifications of the test instruments can be found in Appendix F.

[‡] A previous analysis has identified that a temperature difference of two degrees is the minimum required for the operation of the load.

3.2 Uncertainty analysis

The uncertainty analysis is conducted to give veracity to the test results. The analysis measures quantitatively the range in which the result is guaranteed within a certain level of confidence. It is an important input for test design, as it determines the design with the lowest possible uncertainty. The following chapter is based on the theory developed in Appendix D..

3.2.1 Qualitative uncertainty analysis

Two parameters have to be obtained through measured values, the Seebeck coefficient and the power obtained in the load. The Seebeck coefficient is obtained with the following equation,

$$\alpha = \frac{V_{oc}}{\Delta T} \tag{21}$$

In which, α is the Seebeck coefficient of the TEG module, V_{oc} is the open circuit voltage of the module, and ΔT is the temperature difference between the extremes of the module. On the other hand, different approaches can be used to calculate the power obtained in the load. Each of them will provide different final power uncertainty. The two equations considered to calculate power in this project are:

$$P = VI \tag{22}$$

$$P = I^2 R \tag{23}$$

3.2.1.1 Seebeck voltage equation

The Seebeck voltage uncertainty propagation calculation for equation (21) looks like:

$$u_\alpha^2 = \Delta T^2 u_v^2 + V^2 u_{\Delta T}^2 \tag{24}$$

Or,

$$\frac{{u_\alpha}^2}{\alpha^2} = \left(\frac{u_V}{V}\right)^2 + \left(\frac{u_{\Delta T}}{\Delta T}\right)^2 \tag{25}$$

In which, u_α is the Seebeck coefficient uncertainty, u_V is the voltage uncertainty, and $u_{\Delta T}$ is the temperature difference uncertainty. The final inaccuracy varies greatly depending on the voltage and temperature values measured. In the case of this test, low voltage values are used, which will prompt a higher error. Both temperature and voltage have the same sensibility on the final Seebeck coefficient.

3.2.1.2 Power equation

The power uncertainty propagation calculation for equation (22) looks like,

$${u_P}^2 = (2RI)^2 u_I^2 + I^2 u_R^2 \tag{26}$$

And for equation (23),

$${u_P}^2 = I^2 u_V^2 + V^2 u_I^2 \tag{27}$$

We can see that the current uncertainty effect is four times bigger in Equation (26).

3.2.2 Quantitative uncertainty analysis

Quantitative analysis provides the expected final deviation from the real values. It is the final test set-up trustfulness assessment. In this section, only the systematic errors are taken into account, as they are the only ones that can be estimated prior to the test.

3.2.2.1 Seebeck coefficient uncertainty

The final Seebeck voltage uncertainty depends on the uncertainty of the temperature difference and the voltage measured. This sub-section is divided into the uncertainty of temperature measurements with a discussion about its calibration, the uncertainty of voltage measurements and the final uncertainty of the Seebeck coefficient.

Temperature uncertainty

The uncertainty equation for the temperature difference is equal to:

$$b_{\Delta T}^2 = \left(\frac{\partial \Delta T}{\partial T_1}\right)^2 b_{T_1}^2 + \left(\frac{\partial \Delta T}{\partial T_2}\right)^2 b_{T_2}^2 + 2\left(\frac{\partial \Delta T}{\partial T_1}\right)\left(\frac{\partial \Delta T}{\partial T_2}\right) b_{T_1 T_2} = b_{T_1}^2 + b_{T_2}^2 - 2b_{T_1 T_2} \tag{28}$$

To estimate uncertainty we need to identify all possible error sources. The identified sources and their inaccuracy are presented in the following table, and follow the classification found in Appendix D, section D.1.1.

Elemental error sources	$\boldsymbol{b}\ [\boldsymbol{T_1}\ \&\ \boldsymbol{T_2}]$§
1. Calibration – Thermometer specification	$0.05\ \%\ reading + 0.5\ ºC$
2. Calibration – Thermocouple standard	$1.5\ ºC$
3. Conceptual – Thermal contact resistance	$0.003\ ºC$
4. Conceptual – Spatial variation	$0.032\ ºC$
5. Conceptual – TEG Non-uniform Temp	Included in 4
6. Data reduction errors – Last digit	$0.05\ ºC$

Table 6 Elemental error sources for temperature measurement.

The first two systematic errors represent the data acquisition instruments errors. Both are eliminated thanks to calibration and to the nature of the temperature measurement difference. The calibration measures the temperature difference from the two thermocouples that are going to be used, when they are both inserted in the same hole in the aluminium plate. Thermal paste is also used in the hole to guarantee a better thermal conduction. The calibration uncertainty analysis can be found in Appendix G.

Numbered error sources 3 to 5 are conceptual errors due to the limitations of the test design. The thermal contact resistance between the aluminium plates and the thermoelectric module create a temperature jump in the interface. The impossibility of placing the thermocouples at the exact location of the thermoelectric extremes generates an error in the measurement and also, the temperature in the thermoelectric generator is not uniform so the voltage obtained is an average of the whole module. The three errors are detailed and estimated in Appendix H. In addition, the data reduction error of the thermometer is considered to be equal to $\pm\frac{1}{2}$ of the last digit. (Coleman and Steele 2009).

Conceptual corrections

The conceptual errors provided in Table 6 are used to correct the measurements. These errors are always present, with an inaccuracy, and they provide a closer value to reality. The temperature difference equation is modified to take these effects into account,

§ The following uncertainties are considered to encompass a level of confidence of 95 %, almost 2σ.

$$\Delta T^* = T_2 - T_1 - k(\bar{T}) - c_{sd} - c_{cr} \tag{29}$$

In which $k(\bar{T})$ is a constant obtained from the calibration of the thermocouples, c_{sd} is a constant that contemplates the effect of the spatial placement of the thermocouples and c_{cr} is a constant that contemplates the effect of the thermal contact resistance. All parameters have inaccuracy values as they have been presented previously.

The value for $k(\bar{T})$ is specified in the test results section. For c_{sd} a total value of $0.016\ ºC$ is used with an uncertainty equal to $b_{c_{sd}} = 0.016\ ºC$. The thermal contact resistance constant is negligible if thermal paste is used. However, if the thermal paste were absent c_{cr} would be $0.28\ ºC$ with an uncertainty equal to $b_{c_{cr}} = 0.24\ ºC$ for 4-bolted-junctions. These values have been calculated in Appendix H. All the temperatures presented in this chapter will have already been corrected with the calibration correction factor, k, and the spatial variation correction factor, c_{sd}.

Final temperature inaccuracy

The final inaccuracy of the temperature difference measurement only takes into account errors 3, 4 and 6 due to the calibration. The following equations represent the different steps needed for the final inaccuracy of the temperature difference. The inaccuracy for the bolted set-up would be $b_{\Delta T} = \sqrt{2b_{T_1}^2} = 0.34\ ºC$ and then for the system with thermal paste is:

$$b_{T_1} = b_{T_2} = \sqrt{0.016^2 + +0.05^2} = 0.05\ ºC$$

$$b_{\Delta T} = \sqrt{2b_{T_1}^2} = 0.075\ ºC$$

That provides a voltage uncertainty of $4.5\ mV$ if a Seebeck coefficient of $60\ mV$ is used. It is clear that the most accurate system is the one that works relying on thermal paste instead of on the pressure provided by 4-bolts.

Open voltage uncertainty

The elemental error sources identified for the open voltage can be found in the following table:

Elemental error sources	$\boldsymbol{b[V_{oc}]}$
1. Calibration – Oscilloscope specification	$3\ \%\ of\ full\ scale + 0.2\ mV$
2. Data reduction errors – Last digit	$10^{-5}\ mV$

Table 7 Elemental error sources identified for the voltage open-circuit measurements.

Taking into account all the error sources for a measurement of around $120\ mV$, we obtain $b_{V_{oc}} = 6.2\ mV$ for the TEG and $b_{V_{oc}} = 3.2\ mV$ for the TEC

Final Seebeck Voltage uncertainty

The Seebeck voltage uncertainty equation used is,

$$b_\alpha^2 = \left(\frac{\partial \alpha}{\partial V_{oc}}\right)^2 b_{V_{oc}}^2 + \left(\frac{\partial \alpha}{\partial \Delta T}\right)^2 b_{\Delta T}^2 + 2\left(\frac{\partial \alpha}{\partial V_{oc}}\right)\left(\frac{\partial \alpha}{\partial \Delta T}\right) b_{V_{oc}\Delta T} = \left(\frac{1}{\Delta T}\right)^2 b_{V_{oc}}^2 + \left(\frac{-V_{oc}}{\Delta T^2}\right)^2 b_{\Delta T}^2 \tag{30}$$

Taking into account that $b_{V_{oc}\Delta T} = 0$ the dependency between the errors can be seen. Both errors are affected by the measurements themselves. Uncertainty changes with the region of the space being measured. The following relative uncertainty equation is obtained if equation (30) is divided by the square of the Seebeck coefficient,

$$\frac{b_{\alpha}^2}{\alpha^2} = \frac{b_{V_{oc}}^2}{V_{oc}^{\ 2}} + \frac{b_{\Delta T}^2}{\Delta T^2} \tag{31}$$

With a temperature difference of $2\ ºC$ you obtain an uncertainty of $b_{\alpha} = 7.66\ mV$ for the TGP-651 and an uncertainty of $b_{\alpha} = 1.85\ mV$ for the ET20,68.

3.2.2.2 Load Power uncertainty

The final load-power uncertainty depends on the uncertainty of the resistance, current and voltage measurements. It has been identified that their uncertainty only depends on the inaccuracies provided by the measuring systems found in Appendix F. The final systematic uncertainty for power will depend on the value measured, due to the same dependency of voltage, current and resistance measurements. The final systematic uncertainty power values will be directly considered in Section 3.3.3.

Voltage uncertainty

Voltage measurement uncertainty has already been calculated in the previous section. A total systematic uncertainty of $3.2\ mV$ for a $100\ mV$ range and $1.7\ mV$ for a $50\ mV$ range can be estimated.

Current uncertainty

The error sources identified for current measurements are presented in the following table,

Elemental error sources	$\boldsymbol{b_I}$
1. Calibration – Multimeter specification	$0.05\ \% + 0.02\ \%^*$
2. Data reduction errors – Last digit	$10^{-4}\ mA$

Table 8 Elemental error sources identified for current measurements. *(% of reading + % of range)

The final current systematic uncertainty will depend on the value measured.

Resistance uncertainty

The error sources identified for resistive measurements are presented in the following table

Elemental error sources	$\boldsymbol{b_I}$
1. Calibration – Multimeter specification	$0.01\ \% + 0.004\ \%^*$
2. Data reduction errors – Last digit (1 $k\Omega$ range)	$10^{-2}\ \Omega$
2. Data reduction errors – Last digit (1 Ω range)	$10^{-3}\ \Omega$

Table 9 Elemental error sources identified for resistance measurements. *(% of reading + % of range)

The final resistance systematic uncertainty will depend on the value measured.

3.2.3 Model uncertainty

Experimental values are compared to a model. However, simulated results are also susceptible to errors, to uncertainty. The model suffers from errors in the simulation input values and they will affect the result. In the following analysis no error is considered for modelling assumptions or approximations, errors that can also be added up to model uncertainty. Only the errors of the measurements are added to the model simulation input values.

3.2.3.1 Seebeck coefficient model uncertainty

There is no proper model used for the calculation of the Seebeck coefficient. The Seebeck coefficient is obtained from the values in the datasheet of the manufacturers.

3.2.3.2 Load power model uncertainty

The model that is used to obtain the power in a load is represented by the next two equations,

$$P_{load} = P_{load}(\Delta T, R_{load}, R_{int}, R_{test}) \tag{32}$$

$$P_{load} = \left(\frac{\alpha \Delta T}{R_{load} + R_{int} + R_{test}}\right)^2 R_{load} \tag{33}$$

In which, R_{load} is the resistance of the load, R_{int} is the internal resistance of the thermoelectric module and R_{test} is the resistance present in the test set-up.

The most important input uncertainties are considered to be the temperature difference and the total resistance present in the test set-up. The inaccuracy of R_{load} is considered negligible due to the high accuracy provided by the multimeter. The final power inaccuracy for the model can be obtained with the following equation,

$$\varepsilon^2_{P_{load}} = \left(\left(\frac{\alpha}{R_{load} + R_{int} + R_{test}}\right)^2 2\Delta T * R_{load} * \varepsilon_{\Delta T}\right)^2 + \left(\frac{2R_{load}(\alpha \Delta T)^2}{(R_{load} + R_{int} + R_{test})^3} * \varepsilon_R\right)^2 \tag{34}$$

The model inaccuracies for the voltage in the load can be calculated with the following equation,

$$\varepsilon^2_{V_{out}} = \left(\frac{\alpha R_{load}}{R_{load} + R_{int} + R_{test}} * \varepsilon_{\Delta T}\right)^2 + \left(\frac{-R_{load}\alpha \Delta T}{(R_{load} + R_{int} + R_{test})^2} * \varepsilon_R\right)^2 \tag{35}$$

And for the uncertainty of the current going through the load, the following equation can be used,

$$\varepsilon^2_{I_{out}} = \left(\frac{\alpha}{R_{load} + R_{int} + R_{test}} * \varepsilon_{\Delta T}\right)^2 + \left(\frac{-\alpha \Delta T}{(R_{load} + R_{int} + R_{test})^2} * \varepsilon_R\right)^2 \tag{36}$$

3.3 Thermoelectric characterization results

The following section presents the measured results for the different tests. The two thermoelectric modules are tested for obtaining both the open-circuit voltage of the module and the electrical conditions on the loads. In addition, the calibration results of the thermocouples are presented. All values are presented with their average and range of certainty following the theory developed in Appendix D.

All sets of data in this section will use a t-distribution, Student's distribution, due to the limited number of measuring points and also as the statistical distribution is unknown. In addition, they will all use the Gaubert's criterion to statistically reject outliers.

3.3.1 Calibration results

We present the results found in the calibration process. The data points were obtained each 3 seconds and for a total period of 30 minutes, obtaining 915 data points. A level of confidence of 95 % for the following calibration correction factor is obtained to be,

$$k = -0{,}036 \pm 0{,}004\ ºC$$

The following results depend on the hypothesis, used in this thesis, which states that the calibration correction is constant through the whole range of temperatures tested or that the change is negligible for the calculations.

3.3.2 Seebeck coefficient results

A series of tests have been done to calculate the Seebeck coefficient of the thermoelectric module. This guarantees reproducibility and better statistical results.

3.3.2.1 Thermoelectric generator (TGP-651)

The following two tables represent the results of eight tests for the TGP-651 module. All these tests have been done on several different days to guarantee reproducibility of the way the test is conducted.

Test ref.number	*#TEG-1*	*#TEG-2*	*#TEG-3*	*#TEG-4*
Voltage (mV)	110.7	120.1	122.8	133.7
Temperature difference	1.87	1.88	2.04	2.15
Seebeck coefficient (mV/K)	59.2	63.8	60.1	62.3
Datasheet TGP-651 Seebeck (mV/K)	60			

Table 10 First set of results for the TGP-651 open circuit test.

Test ref.number	*#TEG-5*	*#TEG-6*	*#TEG-7*	*#TEG-8*
Voltage (mV)	118.1	130.0	110.7	120.1
Temperature difference	2.01	2.06	1.87	1.88
Seebeck coefficient (mV/K)	58.8	63.1	59.2	63.8
Datasheet TGP-651 Seebeck (mV/K)	60			

Table 11 Second set of results for the TGP-651 open circuit test.

The final value obtained for the Seebeck coefficient, with $t_{95}(\upsilon = 7) = 2.365$, $s_\alpha = 3.2$, $N = 8$, $b_\alpha = 7.66$, is equal to:

$$\alpha_{95} = 60.2 \pm 18.3\ mV/K$$

3.3.2.2 Thermoelectric cooler (ET20-68)

The following two tables represent the results of eight tests for the ET20-68 module.

Test ref.number	*#TEC-1*	*#TEC-2*	*#TEC-3*	*#TEC-4*
Voltage (mV)	50.9	49.7	49.4	52.6
Temperature difference	2.02	1.94	1.96	2.05
Seebeck coefficient (mV/K)	25.2	25.6	25.2	25.6
Datasheet ET20-68 Seebeck (mV/K)	25.5			

Table 12 First set of results for the ET20-68 open circuit test.

Test ref.number	*#TEC-5*	*#TEC-6*	*#TEC-7*	*#TEC-8*
Voltage (mV)	51.1	49.9	110.7	120.1
Temperature difference	2.00	1.97	1.87	1.88
Seebeck coefficient (mV/K)	25.6	25.3	59.2	63.8
Datasheet ET20-68 Seebeck (mV/K)			25.5	

Table 13 Second set of results for the ET20-68 open circuit test.

The final value obtained for the Seebeck coefficient, with $t_{95}(\upsilon = 5) = 2.571$, $s_\alpha = 0.2$, $N = 6$, $b_\alpha = 1.85$, is equal to:

$$\alpha_{95} = 25.4 \pm 4.76 \; mV/K$$

3.3.3 Power load results

A series of tests have been done to calculate the power consumed by the load connected to the thermoelectric modules. This guarantees reproducibility and better statistical results. To reduce model uncertainty for low-level measurements it is paramount to keep an account of the parasitic resistances present in the test set-up. The total resistance of the closed circuit is divided in three components, R_{load} the resistance of the load that is used to characterize the TEG, R_{int} the internal resistance of the TEG, and R_{test}, the resistance of the test set-up.

The test set-up resistance encompasses the resistance of wires and contacts and the shunt resistor of the Multimeter for current measurement, which equals $5\ \Omega$. The total measuring cables are estimated to account for around $1\ \Omega$ and the cables for connection to the TGP-651 account for $0.7\ \Omega$, being negligible for the ET20-68. In the end, a value of $R_{test} = 6.7\ \Omega$ is used for the TGP-651 and $R_{test} = 6.0\ \Omega$ for the ET20-68. All these values could also be framed as conceptual systematic uncertainties, as presented previously, as the resistances are not perfectly the ones wanted.

3.3.3.1 Thermoelectric generator (TGP-651)

The following table represents the values expected for the test, the model values. The values are presented with the model uncertainty caused by the temperature difference and the resistance of the test set-up. The temperature uncertainty is estimated as $0.05\ ºC$, from the deviation of the total of the 16 measurements and the resistance uncertainty is estimated as $1.0\ \Omega$. All the uncertainty values obtained follow equations (34) (35) (36).

Model Values (TGP-651)			
Load Resistance (model)	Voltage (mV)	Current (mA)	Power (μW)
14.9	9.4 ± 0.2	0.47 ± 0.012	4.5 ± 0.2
98.3	36.7 ± 0.9	0.35 ± 0.009	13.0 ± 0.6
217.3	58.1 ± 1.4	0.26 ± 0.007	15.2 ± 0.8
552.7	83.7 ± 2.1	0.15 ± 0.004	12.6 ± 0.6

Table 14 Values for the different load cases expected from the TGP-651 characterization test.

All the measured values with the respective uncertainty are presented in Table 15.

Test Values (TGP-651)			
Load Resistance (test)	Voltage (mV)	Current (mA)	Power (μW)
14.9	7.2 ± 5.3	0.45 ± 0.02	3.3 ± 0.8
98.3	34.4 ± 5.8	0.35 ± 0.03	12.0 ± 0.6
217.3	55.4 ± 12.8	0.25 ± 0.04	14.0 ± 0.8
552.7	83.2 ± 13.2	0.15 ± 0.02	12.6 ± 0.5

Table 15 Voltage, current and power measured for the different load resistance conditions of the TGP-651 characterization test.

A graphical comparison of model and test values is presented in Figure 16.

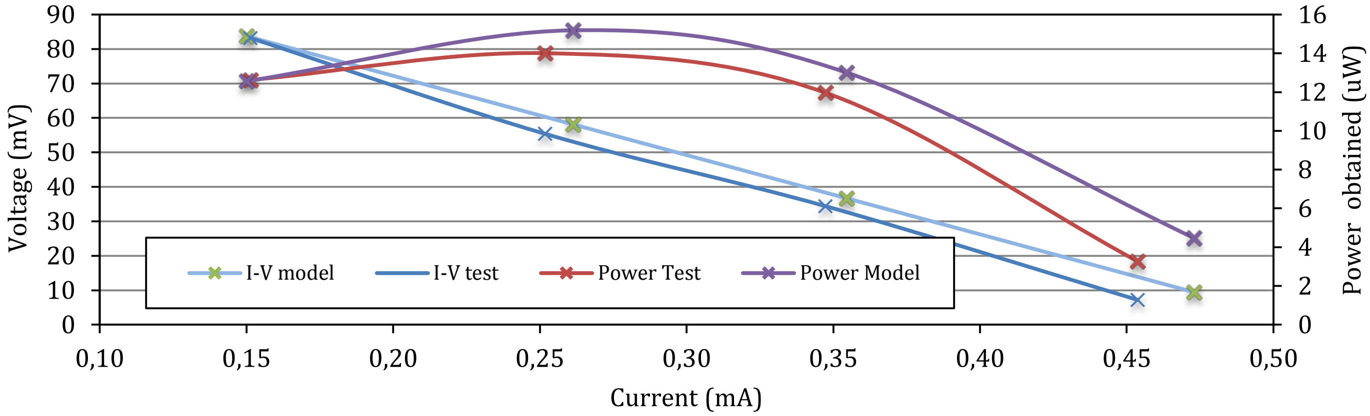

Fig. 16 Comparison of voltage, current and power of model and test for the TGP-651.

3.3.3.2 Thermoelectric cooler (ET20-68)

The following table represents the values expected for the test. The values are presented with the model uncertainty caused by the temperature difference and the resistance of the test set-up. The temperature uncertainty is estimated as $0.05\ ºC$, from the deviation of the total of the 16 measurements and the resistance uncertainty is estimated as $1.0\ \Omega$.

Model Values (ET20-68)			
Load Resistance	Voltage (mV)	Current (mA)	Power (μW)
2.02	18.3 ± 3.3	9.09 ± 1.65	166.5 ± 60.4
3.32	24.5 ± 3.6	7.36 ± 1.09	180.0 ± 53.2
9.9	37.2 ± 2.9	3.76 ± 0.3	140.1 ± 22.0
17.93	42.2 ± 2.2	2.36 ± 0.12	99.5 ± 10.5

Table 16 Model values for the different load cases done in the ET20-68 characterization test.

Test Values (ET20-68)			
Load Resistance	Voltage (mV)	Current (mA)	Power (μW)
2.02	18.1 ± 4.3	8.98 ± 2.13	162.6 ± 76.6
3.32	24.0 ± 3.3	7.23 ± 1.0	173.6 ± 50.4
9.9	37.78 ± 3.0	3.82 ± 0.31	144.2 ± 26.8
17.93	44.08 ± 2.46	2.46 ± 0.06	108.4 ± 12.9

Table 17 Voltage, current and power measured for the different load resistance conditions of the TGP-651 characterization test.

All these values are obtained with an average temperature difference of $1.96\ K$. The uncertainty values are worse than the ones obtained with the TGP-651. This worsening of the values is due to the way that the current value is obtained. In this last case the current is calculated and not measured. It needs to be calculated because the use of the multimeter in series to measure current adds 5 Ω to the total circuit. As the ET20-68 has a small resistance $3.55\ \Omega$ the peak of the power curve would have not been obtained from the test.. The comparison between model values and test values can be seen in Figure 17.

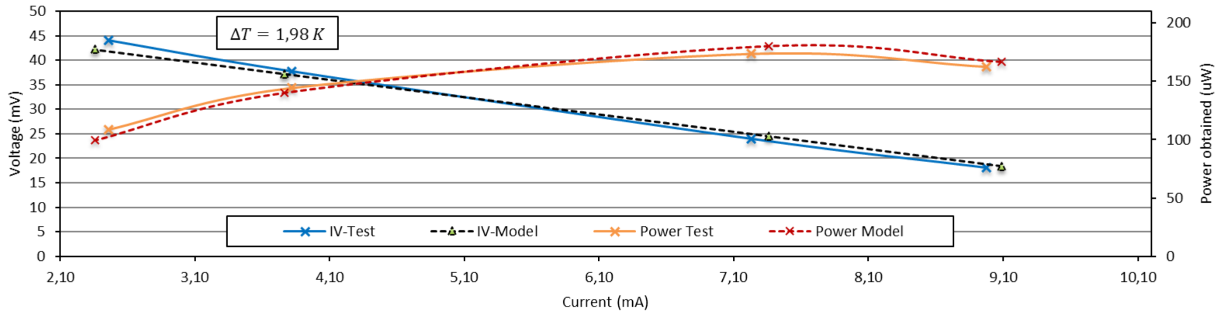

Fig. 17. Comparison of voltage, current and power of model and test values for the thermoelectric module ET20-68.

3.4 Conclusions and recommendations

This section presents conclusions for both the results and the test procedure.

3.4.1 Conclusions on the results

The measurement of voltage, current and temperature difference has allowed to successfully assess the capabilities of the two thermoelectric modules. The TGP-651, merchandised as a thermoelectric generator, provides the highest values of voltage but the lowest of power for the same loads and temperature difference. While the ET20-68 is merchandised as a thermoelectric cooler, it provides the highest values of power but lower voltage. The internal resistance increases the power losses in the TGP-651 while the lowest Seebeck coefficient decreases the voltage output of the ET20-68. Both modules behave following a linear I-V curve and they provide a maximum power when the load connected is equal to their internal resistance.

Both previous results provide the foundation for their application. The thermoelectric module needs to provide sufficient voltage to start-up the component connected to it. The ET20-68 will have trouble following this aspect. And the module needs to provide enough power so the final load has an application, an aspect in which the TGP-651 will suffer. Taking into account that power management COTS components are the ones to be connected to the modules, their input resistance has an impact on which of the modules is more convenient. Both modules need to try to operate in the peak of the power curve, when their internal resistance and the load resistance is matched.

The module that will be used for the rest of the project is the ET20,68. The ET20,68 is able to provide $20\ mV$ input for $\Delta T = 2.0$ for a power converter with an internal resistance of less than $10\ \Omega$. In addition, it is able to provide an input current that, with efficiencies of 20% for the power converter, would still create enough current to be used to charge the storage capacitor. The TGP-651 cannot guarantee this performance for such low temperature differences.

3.4.2 Conclusions on the test procedure

The high value of the voltage systematic uncertainty is a problem. For the power measurements, this problem has been counteracted with the use of the resistance measurement instead, but there is no other solution than measuring voltage for the calculation of the Seebeck coefficient.

The way the test set-up is designed has a big influence in the final uncertainty. Several set-ups have been analysed to narrow the uncertainty of the results. Before the tests, the thermal contact resistance was found to be the main source of uncertainty. To reduce it, the use of thermal paste was found to be a successful option.

There are other important aspects of uncertainty associated to the temperature difference measurements. The thermal non-uniformity of the thermoelectric generator is the less well-known and studied error source. Therefore it may provide the biggest discrepancy to the results. The tests can be done guaranteeing a better lateral isolation using a better system. This process has not been done in the thesis due to a lack of time, and giving preference to other aspects of the MSc thesis. In addition, the calibration has not been done through a range of temperatures. To be more certain of the results the calibration should be dependent on the temperatures used for testing.

Chapter 4 Power Converter Characterization Test

4.1 Introduction

The end system design uses a power converter that provides $4.1\ V$ of output. However, that decision was made at the final phases of the project. The first prototype was going to use a power converter that would provide an output voltage of $3.3\ V$. That first design of the converter is the one presented in this chapter. The values obtained are expected to be similar to the ones obtained for other output voltages as seen in the datasheet of the voltage converter chip. In addition, this chapter presents the difference of power efficiency between a tuned design in a PCB and a testing protoboard showing the importance of reducing losses with the design. To summarise, even though the results do not correspond directly with the final expected product to be used in the end-to-end prototype, the test provides important conclusions and it was a vital step for the MSc thesis.

This chapter presents the power converter characterization test. This chapter starts by presenting the objectives and test set-up for the power management characterization test. Then, to assess if the test set-up can answer the main questions satisfactorily, section 4.2 presents the systematic uncertainty analysis. After that, in Section 4.3, the obtained results and the uncertainty for each value are presented. The end of the chapter, Section 4.4, gives the final conclusions on the results and on the test design and procedure.

4.1.1 Test objectives

The test evaluates the performance of the power converter module design, presented previously. The main objective of this test is to determine the minimum input voltage that can be converted into useful powering values. In addition, it is important to know how much energy is lost in the process. For the test, the emulation of the thermoelectric harvester and the BLE is paramount, as it allows testing the specific future-operating framework. The objectives that have been identified are the following:

PM-O-1: Obtain the discharging and charging time of the capacitor and represent the discharging and charging curves.
PM-O-2: Obtain the power efficiency of the module for the required operating conditions.
PM-O-3: Obtain the conditions (output capacitor values, load duty cycle) to withstand the peak power consumption of the BLE load.

4.1.2 Test Set-up

The test set-up requires emulating the power generator, the TEG, and the load, the Bluetooth module with internal microcontroller and temperature sensor. The TEG conditions are achieved with a tuneable power supply connected to a resistance with a value representing the internal resistance of the thermoelectric generator, of $5\ \Omega$. The load is emulated with two resistances, one representing the active mode and the other one representing sleep mode, and a control-switch system. The Power converter module output connects to a resistance of $2\ M\Omega$ that generates a non-stopping current of around $1\ \mu A$, for the lowest input voltage[**], $2.0\ V$, to represent the current required for sleep mode. The Power converter module is also connected to a resistance of $100\ \Omega$ used to create the powering current of the BLE, $18.3\ mA$, for the lowest input voltage, $2.0\ V$. To emulate the duty cycle of the Bluetooth module the connection is switched with a MOSFET, and activated with an Arduino UNO controller. The Arduino's output pin has a parasitic capacitance that avoids the active mode time of the test to be the time specified in the Arduino IDE, due to the time constraint of charging that parasitic capacitor.

[**] Providing a constant current is not a priority. Providing the current for the required lowest input voltage provides a conservative test result.

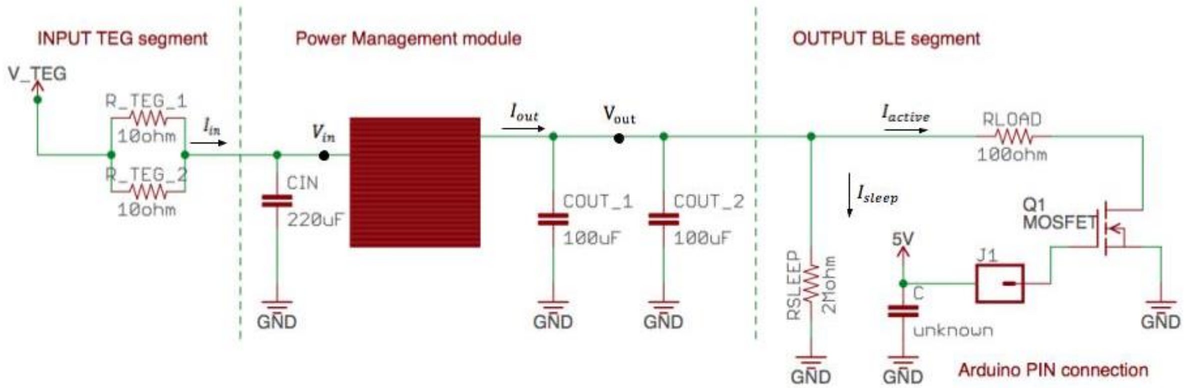

Fig. 18 Test set-up sketch for the power management module characterization test.

From the test set-up sketch, V_{out} is the voltage obtained in the output pin of the power converter chip, I_{out} is the current coming out of the power converter and used for charging the output capacitors, V_{in} is the voltage entering the power converter, I_{in} is the current entering the power converter chip, I_{sleep} is the current that the BLE consumes in sleep mode and I_{active} is the current that the BLE consumes when transmitting.

The input voltage and current are the control conditions of the test. Both remain constant during the test, and are measured prior to the output values. The voltage across the output capacitors, or output voltage is measured with an oscilloscope. The total output capacitance is equal to $220\ \mu F$ and there is a leakage capacitance current of $4\ \mu A$. The current obtained from the power management module for the charging period is measured. In addition, the current through both loads, used to emulate the BLE, is measured. It has to be taken into account that the Multimeter has a parasitic resistance of 5Ω for current measurements for a range of $100 - 10\ mA$, so the test set-up values for resistance are modified while measuring current. Furthermore, the signal provided by the control pin of the voltage converter is measured.

The discharging process starts when the control circuit is closed by providing more voltage to the G-S of the MOSFET than the D-S. The discharging occurs in $6\ ms$ so it requires a fine time sensibility of the Multimeter used. With a time resolution of 1 ms, only 256 measurements can be obtained. Therefore, only the data of the peak is obtained. The specifications of the test instruments can be found in Appendix F.

The selected output voltage of the power converter module is equal to 3.3 V. It can be seen that this is not the specified output voltage in chapter 2 or the one that is used at the end of this document for the final end-to-end prototype, in chapter 4.

4.2 Uncertainty Analysis

The test up validity needs to be assessed before starting with the measurements. The uncertainty analysis is conducted to give veracity to the test results. The analysis measures quantitatively the range in which the result is guaranteed within a certain level of confidence. The following chapter is based on the theory developed in and previously applied in Section 1.2.

4.2.1 Qualitative uncertainty analysis

The qualitative uncertainty analysis will provide the equations for the calculation of the power efficiency uncertainty. The uncertainty is defined with the following equation,

$$\eta_{PM} = \frac{V_{out} * I_{out}}{V_{in} * I_{in}} * 100\% \tag{37}$$

The efficiency uncertainty calculation follows from equation (37) and looks like,

$$u_{\eta_{PM}}^2 = \left(100\frac{I_{out}}{V_{in} * I_{in}}\right)^2 u_{V_{out}}^2 + \left(100\frac{\mathrm{V_{out}}}{V_{in} * I_{in}}\right)^2 u_{I_{out}}^2 + \left(100\frac{\mathrm{V_{out}} * I_{out}}{-{V_{in}}^2 * I_{in}}\right)^2 u_{V_{in}}^2 + \left(100\frac{\mathrm{V_{out}} * I_{out}}{V_{in} * -{I_{in}}^2}\right)^2 u \quad (38)$$

In which, $u_{V_{out}}$ is the output voltage uncertainty, $u_{V_{in}}$ is the input voltage uncertainty, $u_{I_{out}}$ is the output current uncertainty, and $u_{I_{out}}$ is the input current uncertainty. In the case of this test, low voltage values are used, which will prompt a higher error.

4.2.2 Quantitative uncertainty analysis

The quantitative analysis provides the systematic uncertainty of the different measurements and also of the final efficiency. It has been identified that their uncertainty only depends on the inaccuracies provided by the measuring systems found in Table 42 of the Appendix F. The tables with the error sources of voltage and current have already been presented in the uncertainty analysis section of the thermoelectric module characterization. However, the Multimeter is also used for voltage measurements, in this test. Therefore, the following table presents the different error sources measuring voltage with the Multimeter:

Elemental error sources	$\boldsymbol{b[V_{in}]}$
1. Calibration – Multimeter specification	$0.005\ \% + 0.0035\ \%$
2. Data reduction errors – Last digit	$10^{-5}\ mV$

Table 18 Elemental error sources identified for the input voltage measurements by the Multimeter.

With all this information already presented, the different expected systematic errors can be calculated, and they are presented in the following table:

Expected systematic errors	$\boldsymbol{b}$
V_{in} ($\sim 30.0\ mV$)	$6.2\ \mu V$
V_{out} ($\sim 3.3\ V$)	$0.15\ V$
I_{in} ($\sim 5.0\ mA$)	$10.5\ \mu A$
I_{out} ($\sim 15.0\ \mu A$)	$2.0\ \mu A$
R_{in} ($\sim 5.0\ \Omega$)	$4.5\ m\Omega$

Table 19 Expected systematic errors to be obtained for the electrical test conditions of the Power converter module characterization test.

Using equation (38) and the values obtained with Table 19. we can obtain a final relative efficiency uncertainty of $u_{\eta_{PM}} = 4.4$ %.Taking into account an infinite amount of measurements, the total amount of deviation expected would be $U_{\eta_{PM}} = \pm$ 8.6 %, for a level of confidence of 95 %. Compared to an expected efficiency of the 30 % the relative inaccuracy would be of the 28 %. The uncertainty obtained in this step of the MSc thesis is considered acceptable as a future test will be done seeking a smaller uncertainty. The final test of the end-to-end system will also require to test the behaviour of the power converter.

4.3 Power management Characterization Results

The following section presents the results for the test set-up verification, specifically the TEG and BLE emulation. In addition, the results clarify the operating conditions of the Power converter module and its applications.

All values are presented with their average and range of certainty. All sets of data in this section use a t-distribution, Student’s distribution, due to the limited number of measuring points and also as the statistical distribution is unknown. In addition, they will all use the Gaubert's criterion to statistically reject outliers. A brief explanation of both concepts can be found in Appendix D and Appendix I.

4.3.1 Verification of emulated segments

The Power converter module test set-up includes the emulation of the powering and load module. The emulation should comply with the operating conditions that are expected for the complete interconnected system. The values of data expected have already been presented in section 4.1.2, while presenting the test set-up. The emulated conditions are successfully verified with conservative results.

The next subsections 4.3.1.1 and 4.3.1.2 are named as verification of the load and verification of the powering component. Both subsections in reality represent the verification of the TEG module and the verification of the emulation of the BLE113 load.

4.3.1.1 Verification of the powering component

The powering conditions for the test emulate the performance of the thermoelectric generator. The testing point corresponds to the temperature gradient conditions, two-degree difference, already tested in the previous chapter. A difference of two degrees was analysed to be sufficient to power the power management module. The V_{TEG}, the voltage values provided by the emulated TEG, V_{in} and I_{in}, calculated with $I_{in} = \frac{V_{TEG}-V_{in}}{R_{in}}$, are presented in the following table.

Test ref.number	*#PM-1*	*#PM-2*	*#PM-3*	*#PM-4*
TEG Voltage $(mV)^*$	55.5 ± 0.01	55.4 ± 0.01	55.0 ± 0.01	55.2 ± 0.01
Input Voltage $(mV)^*$	28.1 ± 0.01	28.1 ± 0.01	30.3 ± 0.01	30.5 ± 0.01
Input Current (mA)	5.6 ± 0.4	5.6 ± 0.4	5.0 ± 0.4	5.0 ± 0.4
Input Power (μW)	157.1 ± 12.0	156.4 ± 12.0	152.7 ± 13.0	153.6 ± 13.0

Table 20 Powering input measurements of the Power converter module characterization test.

As it is shown with the data in the next subsections, these values are sufficient to create a full operating system, and they correspond with the desired powering values of the TEG.

4.3.1.2 Verification of the load

The BLE module powering requirements are divided in two: sleeping and active mode. Sleeping mode is considered to consume 1 μA. Active mode is considered to operate for $5 ms$, consuming $19\ mA$. All these values are considered as the load is characterized after the Power converter module as explain in the methodology subsection in the introduction.

Sleeping mode:

The load still consumes power when it is in the sleep mode. To guarantee that this attribute is correctly emulated with the test set-up, the current going through R_{sleep} is measured. The values measured vary from $1.0\ mA$ to $1.6\ mA$, depending on the output voltage. The values obtained guarantee the conservative emulation of the sleeping mode power consumption of the load, as the test set-up operates with higher values than required.

Active mode:

The active mode needs to guarantee that the electrical values provided to the load are sufficient for the active mode for a specific length of time. The following table presents the data of the 4 different tests carried out to measure the Active mode operation.

Test ref.number	*#PM-1*	*#PM-2*	*#PM-3*	*#PM-4*	*Average*
Active Load time (ms)	6.0 ± 0.5	5.0 ± 0.5	6.0 ± 0.5	6.0 ± 0.5	5.74 ± 0.5
Active load current - Max (mA)	31.0	30.0	30.0	31.0	30.5 ± 0.03
Active load current - Min (mA)	21.0	22.0	20.0	21.0	21 ± 0.03
Total energy emulated (μJ)	413	344	397	413	392

Table 21 Active mode parameters

With a total output capacitance of $220\ \mu F$, a total energy of $392\ \mu J$ can be emulated. It has to be taken into account that the power profile of the BLE operation is more complex than the one averaged here, including an active mode, a periodic transmission in different channels and intermediate power consumption states to save power. Therefore the current values used in this simulation are conservative but the time required for the active time may be bigger than expected.

4.3.2 Test performance results

The most important results of the test provide information about the operating capabilities of the system. The comparison of the charging and discharging times of the output capacitors provide information about the possible duty cycle. And the efficiency that can be calculated with the measured parameters provide a quality assessment of the concept.

4.3.2.1 Duty cycle capabilities

The charging current varies as the voltage of the capacitor changes. The output voltage that is generated reaches the $3.3\ V$ value, and while discharging, it reaches a value close to $2.15\ V$, the limiting operating voltage of the BLE is $2.0\ V$. The following figure provides the characteristic curve obtained for the output voltage and output current.

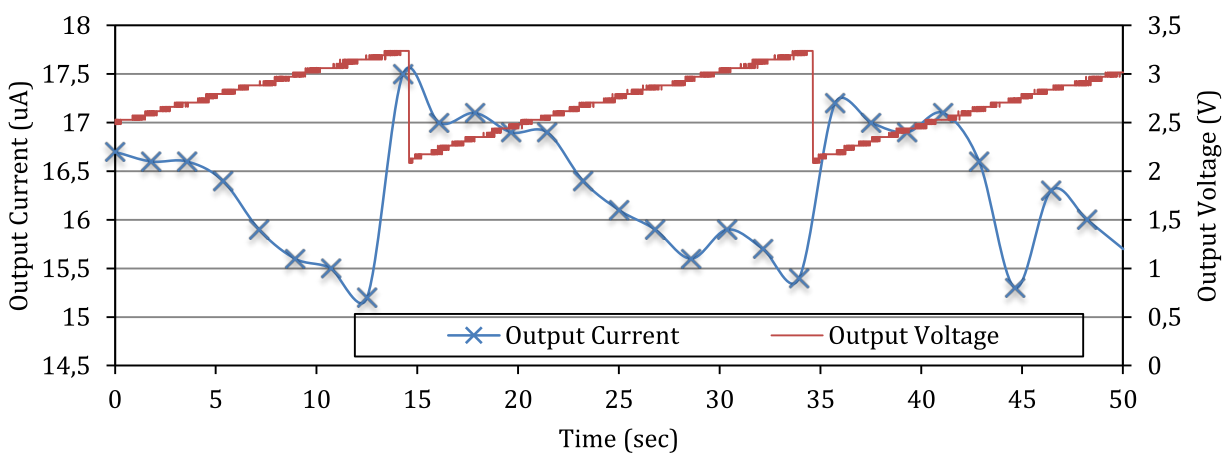

Fig. 19 Representation of the Sleep current and the output voltage in time.

The output voltage clearly represents the fast discharge of energy to the load and the charging time of the storage system. Also the output current represents the effect that current has with capacitors; it decreases as the capacitor stores energy. The output current measurements have a time resolution several orders of magnitude lower than the output voltage. The charging time required is 20.0 ± 0.01 seconds. The discharging time is equal to $5.74 \pm 0.5\ ms$, as presented previously. With these two values the duty cycle of the load for the conditions tested, and the design used, is equal to $0.03\ \%$.

4.3.2.2 Power Management efficiency

We can estimate the values of the efficiency of the module. Efficiency in this section takes into account the power management chip only. It considers the quality of the converter as well as the manufacturing of the PCB, the design of the PCB, and the test set-up. The following table includes the input and output values measured and also the final value obtained of efficiency for the different 4 tests.

Test ref.number	*#PM-1*	*#PM-2*	*#PM-3*	*#PM-4*
Input Power (μW)	157.1 ± 12.0	156.4 ± 12.0	152.7 ± 13.0	153.6 ± 13.0
Output Current 2 V (μA)	16.2 ± 4.0	16.3 ± 4.0	16.1 ± 4.0	16.3 ± 4.0
Output Current 3.3 V (μA)	14.9 ± 4.0	15.1 ± 4.0	14.3 ± 4.0	15.2 ± 4.0
Output Power 2 V (μW)	34.8 ± 9.6	34.8 ± 9.6	34.4 ± 9.6	35 ± 9.6
Output Power 3.3 V (μW)	49.2 ± 14.0	49.8 ± 14.0	47.2 ± 13.9	50.2 ± 14.0
Efficiency	$[0.22 - 0.31]$	$[022 - 0.32]$	$[0.23 - 0.31]$	$[0.23 - 0.33]$

Table 22 Values obtained from the Power converter module characterization test. These values are used to obtain the final values of the Power converter module efficiency.

The final value obtained for the efficiency of the system for 2.0 V, with $t_{95}(\upsilon = 4) = 2.776$, $s_\alpha = 0.002$, $N = 4$, $b_\alpha = 0.027$, is equal to:

$$\eta_{PM_{2V}} = 22.4 \pm 7.6\ \%$$

And for 3.3 V with $t_{95}(\upsilon = 4) = 2.776$, $s_\alpha = 0.002$, $N = 4$, $b_\alpha = 0.045$, is equal to:

$$\eta_{PM_{3.3V}} = 31.7 \pm 12.4\ \%$$

4.3.3 Load mode control

This section characterizes the signal that can be sent directly by the power management module, by the ultra-low power converter, to the BLE to communicate the availability of energy present in the output capacitor. The PGD pin of the LTC3108 is pulled up when V_{out} reaches below 7.5 % of its programmed value, and then it will go low when V_{out} value drops to 9.5% below of its programmed value. The reached value allows the activation of the advertising events from the BLE module. In addition, the oscillating signal allows advertising events sequentially, if the energy is still enough.

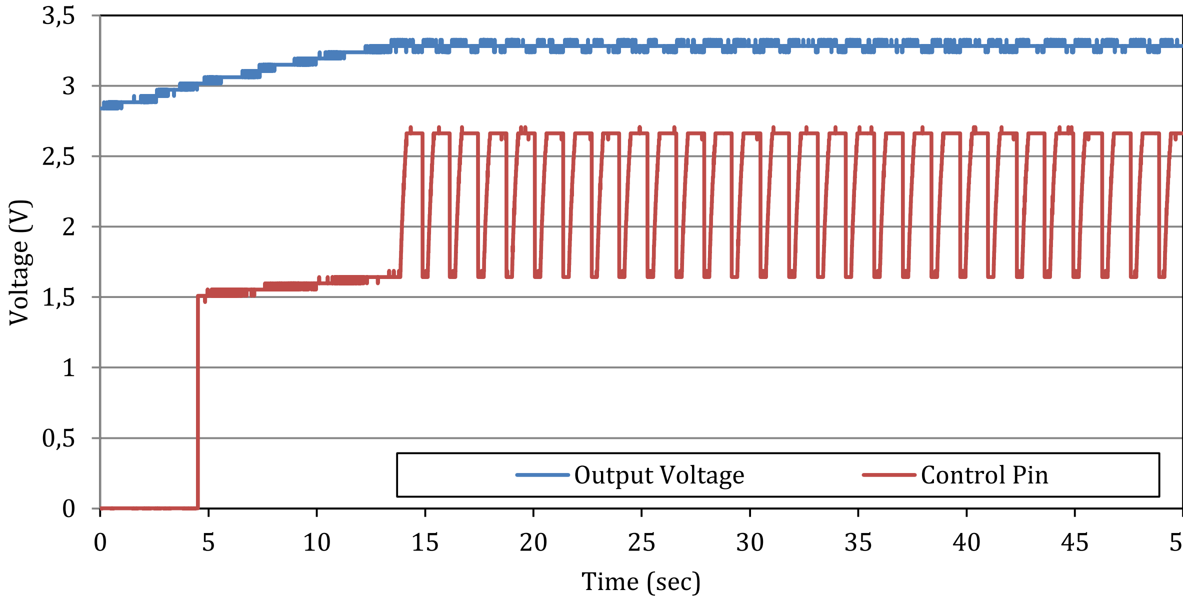

Fig. 20 Representation of the output voltage and the PGD pin voltage from the power converter characterization test.

In Figure 20 the signal of the control pin compared to the output voltage signal can be appreciated. It can be seen that when the output voltage reaches a value of around $3.3\,V$ the control signal starts oscillating to provide a control mechanism to an external module. In addition it can be seen how the control pin suffers a substantial increase in its voltage when the output voltage reaches $3\,V$. This effect could create extra power consumption to the system as power would be drained through the wake-up pin of the BLE module.

4.3.4 Minimum voltage for output charging

The system has been tested with an input voltage of as low as $27\,mV$ to obtain the generation of power. However there is a difference between the starting voltage and the minimum operating voltage. After powering with $27\,mV$ the module can be powered with an input voltage of not less than $20\,mV$. However the behaviour of the system has not been tested with this powering condition.

4.4 TEG module and PM module interface test

The thermoelectric harvester and power management modules are connected together. The test set-up resembles the Power converter module characterization test set-up without emulating the power source, but with the TEG characterization test set-up. The values measured are the input voltage, the output voltage, the charging time of the output capacitor and the temperature difference during the test.

Parameter	*Average values*
Temperature difference (K)	2.0
Input Voltage (mV)	26.8
Charging time $(seconds)$	26.3

Table 23 Measurements obtained from the test that connects the TEG and the Power converter module.

The uncertainty of these values was approved in the previous characterization tests. The uncertainty of each of the values presented in the table is equal to the final uncertainty values of their respective characterization test chapters. The values obtained guarantee the proper operation of the connection of the TEG module with the Power converter module. The values for charging are increased due to the slight decrease of the input Voltage used compared to the one used in the Power converter module characterization test.

4.5 Conclusions and Recommendations

This section presents conclusions for both the results and the test procedure.

4.5.1 Conclusions on the results

The Power Management module can be used to power the BLE with the TEG, with a temperature difference of 2ºC, for a charging time of 20 seconds and a transmission consuming an average of $26\,mA$ during $6\,ms$. These favourable values illustrate the performance of the module and its feasible inclusion in the full system. Successful and similar results are also obtained by connecting the thermoelectric generator instead of the power source.

The output capacitor conditions the performance of the module, maximum energy to be supplied, and charging and discharging times. The charging speed depends on the leakage current of the capacitors and its capacitance. The total output leakage current is equal to $4\,\mu A$, which corresponds to $1/3$ of the total output current that is being obtained. Other capacitors, for example, with the same total capacitance, have only a leakage current of $0.5\,\mu A$, speeding up the charging. Several capacitors can be placed in parallel to augment the total capacitance. However, more capacitance increases the charging time. An addition of several capacitors also increases the leakage current.

The results presented are obtained by testing the smaller PCB presented before. However, previous results were obtained with a protoboard. The results obtained from the two test differ, the one with the PCB being better. This concludes that the design of the circuit has an impact on the performance. It is considered that the presence of parasitic resistance reduces the efficiency while the presence of parasitic capacitance reduces the required start up voltage. The results from the previous tests with the Protoboard are presented in Appendix B. The Power converter module can still suffer several modifications, a better assembling of the circuit, the use of components with fewer losses, and the adaptation for the space to be used in.

The control signal obtained from the power converter seems promising for the purpose of indicating the Bluetooth module when to sense data and advertise it. However, the initial step in voltage will create a current through the activation pin of the Bluetooth module. This won't allow the storage capacitor to reach its maximum voltage potential. Therefore, other methods are considered as the use of a tuned comparator that just suffers a rise in the vicinity of the maximum voltage that can be obtained through the storage capacitor.

To summarise, the power converter successfully transforms ultra-low voltage values, from small temperature differences (2 K), into high voltages and it is able to charge a storage capacitor as long as the leakage currents do not outweigh the output current.

4.5.1 Conclusions on the test procedure

The high inaccuracy of the charging current measurements provides a high inaccuracy to the efficiency of the module. To reduce the uncertainty one source of uncertainty should be diminished. The biggest source of efficiency uncertainty is the output current $\left(100\frac{\mathrm{V_{out}}}{V_{in}*I_{in}}\right)^2 u_{I_{out}}^2$. This uncertainty only can diminish if we reduce the uncertainty of the measuring of the current, as the other values are fixed. The systematic uncertainty of I_{out} is equal to $(0{,}05\% * I_{out} + 0{,}02\% * 10mA)$ and it gives a systematic uncertainty of $u_{I_{out}} = 2\,\mu A$.

The test results, due to the I_{out} inaccuracy would need to be repeated. However, a similar experiment can be done for the final end-to-end system prototype. At the time of completion of this chapter and tests the results were enough to continue with the design of the whole system. The need to obtain a final end-to-end system was considered to be more important than the big uncertainty obtained. In addition, the values were expected to be rechecked in the final test.

Chapter 5 BLE module characterization test

5.1 Introduction

The chapter starts presenting the objectives of the BLE characterization test. Then, the test set-up with the principal sources of power leakage and the most important characteristics of the Bluetooth controller are presented. Then, Section 5.2, presents the systematic uncertainty analysis of the test. After, Section 5.3 contains the obtained results and the uncertainty for each value. The end of the chapter, Section 5.4 gives the final conclusions on the results and on the test design and procedure.

5.1.1 Test objectives

The overall objective of the test is to verify the performance of the BLE module. The characterization of the BLE module allows the sizing of the power management module, specifically the storage component. In addition, it is expected to test the module with the lowest power consumption for an operational BLE for the full system. The objectives of the test are the following:

T-O-5: Identify the different sources of the increase of the BLE113 power consumption through hardware and software modification.

T-O-6: Obtain the current consumption profile of the BLE113. The current profile should encompass the initialization, the sleep mode, and several advertising events.

T-O-7: Calculate the amount of energy required for the operation of the BLE113. The sleep power and the advertisement required energy need to be calculated.

T-O-8: Verify that data packets can be received with the lowest power consumption profile reached.

5.1.2 Test set-up

The test set-up requires both measuring the power consumption of the module and the reception of the advertisement packets. The BLE113 is connected to a constant $3.3\,V$ source. In addition, with an Arduino output pin, the advertisement is activated by a computer command. This allows emulating the activation expected by the LTC3108 when it reaches the $3.3\,V$ level. To obtain the current consumption, the voltage through a shunt resistor is measured. Both the initialization event and the advertisement events are measured. An advertising event, for the rest of the chapter, is considered to encompass all the processes done by the whole set of controller, Bluetooth and temperature sensor.

The characteristic measuring time of an advertisement event is in the order of $10\,ms$. Therefore, the test uses an oscilloscope, for those voltage measurements, with high time resolution, $25\,\mu s/S$. Multimeters used before have only a resolution of $1\,ms$ for current measurements. The shunt resistance used is equal to $15\,\Omega$, a compromise between current measurement sensibility and the total voltage drop through the resistance. The payload data of the advertising frame consists of 8 bytes, which is expected for a float number following the standards of the IEEE 754. In addition, the transmission power used is $1dBm$, the maximum that the Bluetooth module can achieve. The maximum power transmission is used as it will provide the best possible reception in any environment and the difference in energy consumption with one power level or the other does not hinder the overall performance of the system.

The advertisement data is obtained by a Bluetooth USB dongle by the same manufacturer of the module, the BLE121LR. This dongle allows emulating the operation of a BLE113 as a receiver or transmitter through a computer program. Figure 21 presents a sketch-up of the test set-up that has been just described.

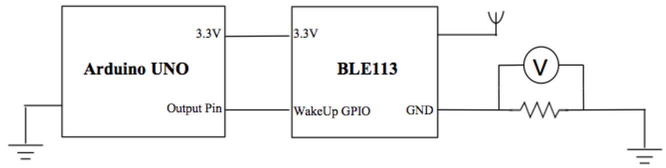

Fig. 21 Summarised sketch-up of the BLE113 Characterization test.

5.1.3 Test Preparation

The BLE113 should be prepared for the test. Possible sources of power loss should be eliminated and the module should guarantee different functionalities that are required for the final operation of the full system.

5.1.3.1 Power Leakage sources

The test does not have any validity if the power consumption of the BLE has not been minimized. The different sources of unintended power leakage identified from the BLE113 are detailed. The sources are:

Breakout Board : The breakout board is an important source of losses. The breakout board design should guarantee that there is not an extra component with no functionality in the final application that draws current. As an example, the breakout board presented previously, BB_LED, has a LED connected always to the power source. A LED increases the power consumption of the system and it is not necessary apart from debugging.

Floating Pins : Most pins of the module draw current whilst kept floating. By pulling the pins down the consumption has been reduced.

Slowing internal clock: The system clock can be slowed from 32MHz to 250 kHz when radio is active to reduce the power consumption of RF transmission. If the system clock is slowed then it will compromise high speed UART communications. When using UART communication the slow internal clock should not be used. In this project UART is not needed.

Advertising channel selection: Bluetooth devices by default scan and send data in three channels: channel 37, 38 and 39. The total time for advertising in all of the channels is equal to around $1\ ms$. This project sends the data through the three channels but a single channel can be used, for both the advertiser and the scanner, to reduce power consumption.

Sleep power mode selection: The selection of the sleeping power mode should be carefully evaluated. Lower power consumption modes lose functionalities that in the long run can compromise the advertising event power consumption. For this module Power Mode 3 consumes half of the power of Power Mode 2. Therefore Power Mode 3 requires less time to charge the capacitor. However, in Power mode 3 the voltage regulator to the digital core is off, and the oscillators are not running. (Texas Instruments). After coming from sleep mode the firmware does not allow to go back to sleep mode until the module stabilizes. Extra time increases the time in an active state making the peak average consumption higher. In the end PM3 requires more energy for the load than in PM2, even though it will charge faster. Power Mode 2 has been selected for this project. The power consumption of each of the sleep Power modes has been calculated and is presented in Appendix A.

Transmission power: The transmission power can be modified by software. The TX power can go from $0\ dBm$ to around $-25\ dBm$. The current consumption for example is affected by this change. The following table presents current consumption values for some TX power values.

TX power (selectable)	*Current consumption (mA)*
$0\ dBm$	20.7
$-6\ dBm$	18.8
$-14\ dBm$	18.3

Table 24 Current consumption compared to transmission power for the BLE113.

The first power leakage source is dependent on Hardware, while the other sources are dependent on how the internal controller is programmed. The code used for the operation of the module is paramount for correct performance.

5.1.3.2 Software Capabilities

The code used provides the functionalities required for the test set-up and the final use for the prototype. In addition, it enables the reduction of power leakage sources, for example PLs-4. The different functionalities activated on the module are listed. A more in detail explanation of the capabilities is presented in Appendix B with the code that enables them.

- GPIO activation for external wake-up
- Single advertising per wake-up call
- Channel transmission selection
- Internal temperature measurement

The first two capabilities reduce the total power consumption by allowing sleep mode operation and reducing active mode operation. Then, the selection of a single use channel will reduce the power consumption and as previously stated, a temperature measurement is necessary for having an end-to-end system.

5.2 Uncertainty Analysis

The test up validity needs to be assessed before starting with the measurements. The uncertainty analysis is conducted to give veracity to the test results. The analysis measures quantitatively the range in which the result is guaranteed within a certain level of confidence. The following chapter is based on the theory developed inAppendix D and previously applied in previous chapters.

5.2.1 Qualitative uncertainty analysis

The energy required for the advertising event, the average power consumption of the advertising and the current through the load need equations to represent their systematic uncertainty, as they are all obtained with the manipulation of measured variables. The power consumption uncertainty equation has already been presented in previous test chapters. The power consumption is calculated with the voltage going through the BLE113m and the current obtained through the shunt resistor measurement.

The current consumption is obtained by measuring the voltage through a shunt resistor. Therefore the equation used for the current is equal to,

$$I_{BLE} = \frac{\mathrm{V_{shunt}}}{\mathrm{R_{shunt}}} \qquad (39)$$

In which I_{BLE} is the current that goes through the Bluetooth module, $\mathrm{R_{shunt}}$ is the resistance where the voltage is measured, and $\mathrm{V_{shunt}}$ is the voltage measured at the resistance. The current uncertainty calculation follows from equation (39) and looks like:

$$u_{\mathrm{I_{BLE}}}^2 = \left(\frac{1}{R_{shunt}}\right)^2 u_{V_{shunt}}^2 + \left(\frac{\mathrm{V_{shunt}}}{\mathrm{R_{shunt}^2}}\right)^2 u_{\mathrm{R_{shunt}}}^2 \eta_{PM} = \frac{\mathrm{V_{out}} * I_{out}}{V_{in} * I_{in}} * 100\% \quad (40)$$

In which, $u_{V_{shunt}}$ is the shunt voltage uncertainty, $u_{R_{shunt}}$ is the resistance shunt uncertainty, $u_{I_{BLE}}$ is the current through the Bluetooth module uncertainty. The selection of the shunt resistance is of importance as a higher value reduces the current uncertainty. However a higher value creates a higher voltage drop through the shunt. The total energy required is obtained through the following equation,

$$\mathrm{E_{req}} = \mathrm{W_{out}} * t_{adv} = (3.3V - V_{shunt}) I_{BLE} t_{adv} \quad (41)$$

In which, $\mathrm{E_{req}}$ is the total energy required for an advertising event. $\mathrm{W_{out}}$ is the average power required in an advertising event, and t_{adv} is the time required for an advertising event. The uncertainty equation for the total energy required is,

$$u_{\mathrm{E_{req}}}^2 = (\mathrm{W_{out}})^2 u_{t_{adv}}^2 + (t_{adv})^2 u_{\mathrm{W_{out}}}^2 \quad (42)$$

In which, $u_{\mathrm{E_{req}}}$ is the energy required uncertainty, $u_{t_{adv}}$ is the advertising time uncertainty, $u_{\mathrm{W_{out}}}$ is the BLE113m average power consumption through advertising uncertainty.

5.2.2 Quantitative uncertainty analysis

The quantitative analysis provides an estimated value of the final systematic uncertainty obtained for the final current and other measurements. With all the instrumentation measuring accuracy values presented, the different expected systematic errors can be calculated, and they are presented in the following table:

Expected systematic errors	***b***
V_{shunt}	$3.2\ mV$
R_{shunt}	$0.01\ \% + 0.004\ \%^*$

Table 25 Expected systematic errors to be obtained for the electrical test conditions of the Bluetooth module characterization test. *(% of reading + % of range) for 1 Year accuracy specification.

The effect of the resistance on the overall uncertainty needs to be assessed. The current uncertainty for the lowest power state of the active state, the active mode with $6.8\ mA$, provides the highest relative uncertainty of the current profile. Therefore its relative uncertainty is calculated for different values of shunt resistance. These values are presented in the following table,

$R_{shunt}\ (\Omega)$	$V_{shunt}\ (mV)$	$Max.\ V_{shunt}\ (mV)$	*Total uncertainty* $u_{I_{BLE}}$	*Relative uncertainty*
10	67	300	0,102	1,529
15	101	450	0,046	0,679
30	201	900	0,011	0,170
60	402	1800	0,003	0,042

Table 26 Expected systematic errors to be obtained for the electrical test conditions of the Bluetooth module characterization test.

The previous values guarantee that the oscilloscope with the shunt resistance allows profiling the current in the order of the μs with an acceptable uncertainty. However, this method cannot be used for sleep mode power consumption measurements. Values of $1.0\ \mu A$ are expected and the uncertainty is several times the value to be measured. The use of the Multimeter allows the measurement of the value with a systematic uncertainty of $\pm\ 2.0\ \mu A$.

5.3 Test Results

Measuring the total energy that is being consumed during the whole operation of the Bluetooth module is the main requirement of this chapter. For this purpose, the current and voltage need to be measured. The current consumption varies greatly depending on the state of the Bluetooth module. This variability will also make the input voltage vary due to the voltage drop obtained in the shunt resistance. In addition, knowing the exact profile of the advertising event allows analysing if more actions should be taken to reduce the power consumption.

5.3.1 Current profile of the BLE113m

The current profile is presented in the following figure. Reproducibility is obtained from the repetition of different advertisement packets. In addition the same test has been carried out several times to guarantee a reproducible measurement of the advertising events and the initialization energy.

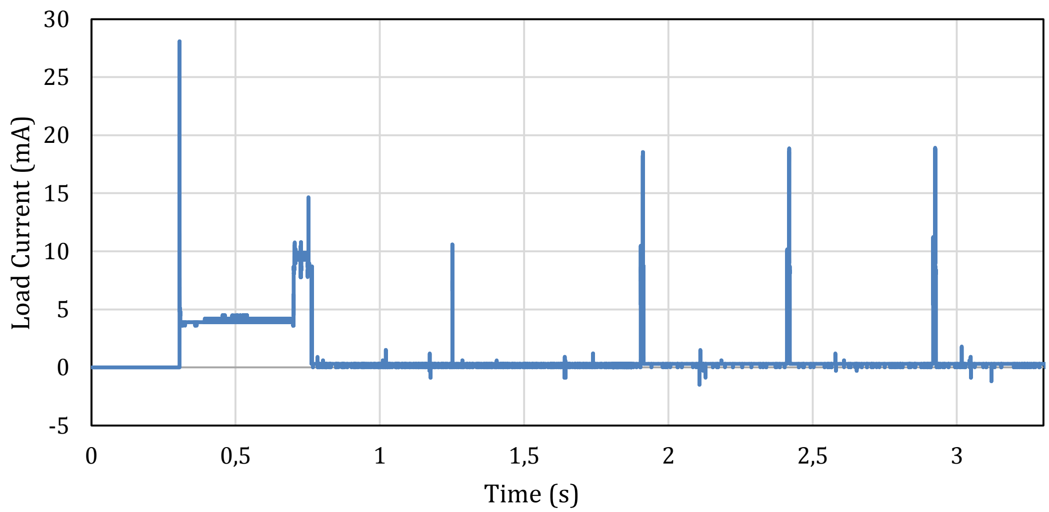

Fig. 22 BLE113 operation current profile

In the previous figure, three advertising events can be seen. In addition, there is an surge of current that represents the start of the initialization of the BLE module.

5.3.2 Current profile of the Advertising event

The current profile of the advertising event is presented in detail and by sections to understand the performance of the module. The advertising event can be divided in, as it can be seen in Fig. 18:

A. Initialization.
B. Active mode. Module wake-up time and Temperature measurement.
C. Radio Frequency communication. The three peaks correspond with the transmission in 3 channels.
D. Module power-off time.

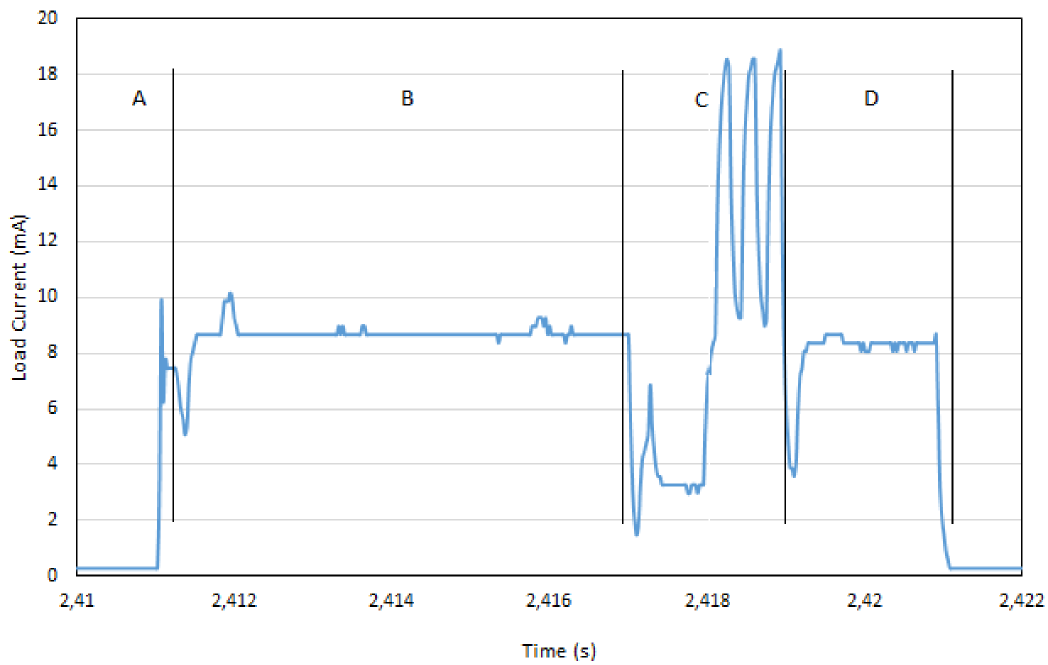

Fig. 23 Advertising event current profile of the BLE113 module with both the advertising and the internal temperature measurement.

First, a start-up peak is observed that leads to the wake-up of the module. Section B represents the stabilization time of certain internal components needed to start with the communication. In addition, Section B includes the temperature measurement process. After that, in Section C, there are three peaks that correspond with the communication on the three channels, requiring a total time of around $1\ ms$ as considered in previous chapters. Section D corresponds with the functions required to put the module into sleep and wait for a wake-up call.

5.3.3 Power consumption

The energy required for the measurement and communication of the data is calculated. It is needed as input for the capacitor sizing. For this purpose the power obtained is integrated through time. The following table presents the values obtained in the test

Test ref.number	*#BLEm-1*	*# BLEm-2*	*# BLEm-3*	*Average*
Average Power $(mW)^*$	26.4	26.35	26.7	26.5 ± 0.8
Advertising event time (ms)	10.05	10.07	9.82	10.0 ± 0.5
Total Energy required (μJ)	265.6	265.5	262.0	264.4 ± 9.0

Table 27 The table presents the values of power consumption for the Bluetooth module with 8 bytes, and for final prototype operation. The systematic uncertainty used for the single measurement events is equal to, 0.14 to power, 0.01 for time and 1.4 for the total energy required.

The sleep current, measured with the multimeter, is also presented in the following table.

Test ref.number	*# BLEm-1*	*# BLEm-2*	*# BLEm-3*
Sleep current (μA)	1.2 ± 2.0	1.3 ± 2.0	1.1 ± 2.0

Table 28 Sleep current measured in three different tests.

It is also important to stablish a relation between energy required and size of the data sent. The maximum size of the data packet is 31 bytes, the full potential of advertising communication. The energy required for advertising 1 byte and 31 bytes, this time without measuring the temperature, is presented in the following tables and later compared to establish conclusions.

Test ref.number	*# BLEm31-1*	*# BLEm31-2*	*# BLEm31-3*	*Average*
Average Power $(mW)^*$	29.4	29.0	28.6	29.0 ± 1.4
Advertising event time (ms)	7.0	7.07	7.27	7.27 ± 0.5
Total Energy required (μJ)	205.6	205.4	208.2	208.3 ± 6.7

Table 29 Values of power consumption of the BLE113m for an advertising payload of 31 bytes. The systematic uncertainty used for the single measurement events is equal to, 0.14 to power, 0.01 for time and 1.0 for the total energy required.

Test ref.number	*# BLEm1-1*	*# BLEm1-2*	*# BLEm1-3*	*Average*
Average Power $(mW)^*$	26.3	24.3	26.0	25.6 ± 3.6
Advertising event time (ms)	6.3	7.22	6.3	6.6 ± 1.7
Total Energy required (μJ)	165.7	175.9	164.5	168.7 ± 20.8

Table 30 Values of power consumption of the BLE113m for an advertising payload of 1 bytes. The systematic uncertainty used for the single measurement events is equal to, 0.14 to power, 0.01 for time and 0.9 for the total energy required.

The total energy required for 1 bytes is less than for 31 bytes. The difference of energy is equal to $39.6 \pm 3.6\ \mu J$. That means a total of $1.3\ \mu J/byte$ is required. The energy difference comes from the time it is required to send the data. In Appendix B, the difference of the time used for transmitting can be seen graphically.

5.3.4 Scanning of advertising data

The scanner should be able to receive the advertising data. This sub-section presents an example of the data received and also assesses the reception performance of the scanner. The scanner is not able to receive all the advertising events. The scanner receives around $60\ \%$ of the total advertising events with a signal loaded environment, specifically 7 extra signals were sensed. In addition, the same experiment was done without extra signals obtaining a $70\ \%$ of the total advertising events.

Apart from the temperature data several information is sent over while advertising. An example of the raw advertising data is presented in the following list, with the conversion to decimal values and the meaning of it:

Type of data	*Hex value received*	*Decimal value*	*Information of the data*
RSSI value	$0xffffffc7$	-57	$-$
Packet type	$0x02$	2	Data packet
MAC address	$0xffffffffff$	$ff{:}ff{:}ff{:}ff{:}ff$	$-$
Address type	$0x0$	0	Public address type
Bond status	$0xff$	255	$255\ =$ No bond
Length of data payload	$0x04$	4	$-$
Data payload	$0x0000001c$	28	Degrees (Integer)

Table 31 Partitioning of a data packet example. The type of data for each division is also used and the hexadecimal values are transformed to decimals. The hex values are placed in order of reception.

The data payload consists of 8 bytes as specified before, for a float number. However, the temperature data has been saved as an integer for this test.

5.3.5 Initialization energy

Apart from the expected internal capacitors of the breakout board and the module itself, other actions should occur for the proper start-up of the module. Registers, functions, and non-volatile memory are initialized. In addition, some components need to be calibrated and wait for a stabilization time, for example, internal clocks. In this case, the 32.768-kHz crystal oscillator seems to be the reason of most of the time required, as $0.4\ s$ are required to start it up.(Texas Instruments). This initialization process costs energy, and in the BLE113 module this energy exceeds the energy required for sending data. The following figure presents the initialization current profile of the BLE113.

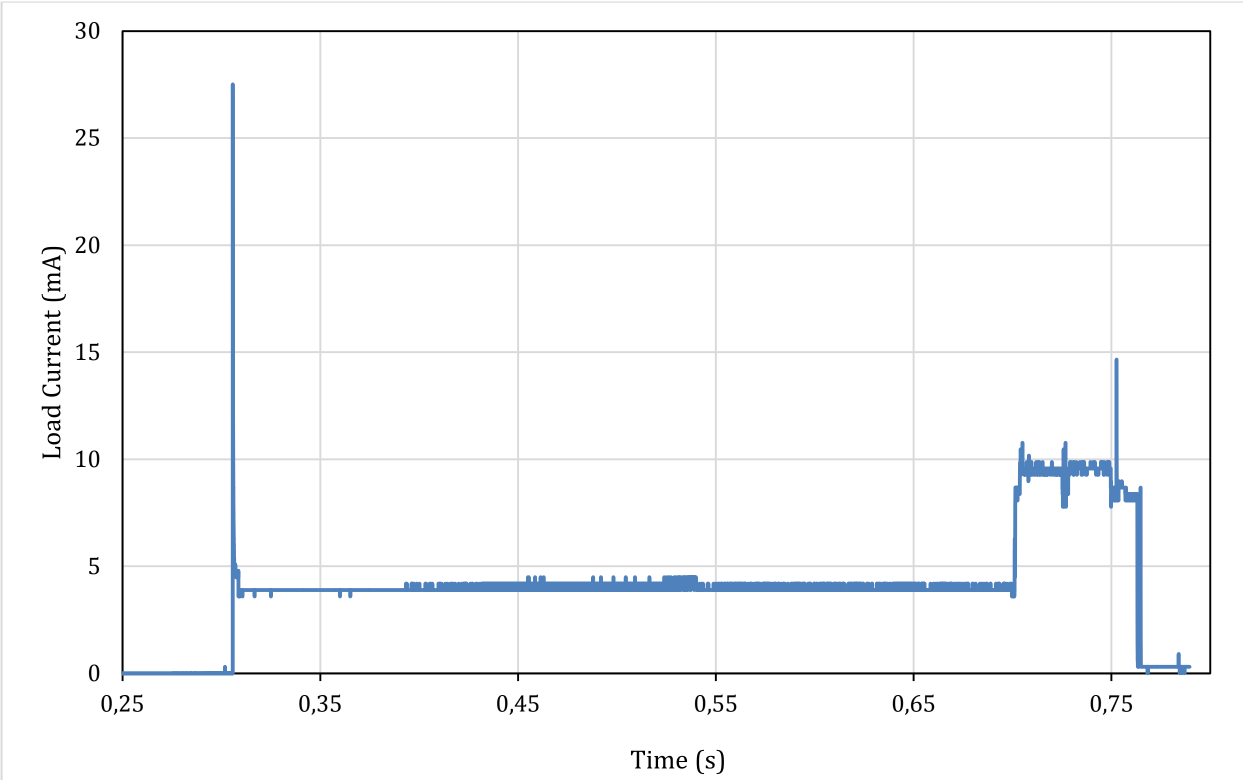

Fig. 24 Current profile of the initialization/start-up process of the BLE113 module.

To solve this problem the use of a super capacitor is required. The required energy for the initialization process is represented in the following table. In addition, the capacitance required for providing with the initialization energy from the voltage limits of $3.3\ V$ to $2.0\ V$ is presented.

Parameter	*Value*
Required initialization energy $(mJ)^*$	6.9
Required capacitance (mF)	2.33
COTS Dimensions of super capacitor with required capacitance (μJ)	$15.0 * 12.0 * 2.2\ mm^3$

Table 32 Values obtained of the initialization process of the BLE module.

5.4 Test Conclusions

This section presents conclusions for both the results and the test procedure of the tests done for characterizing the BLE113 module.

5.4.1 Conclusions on the Test Results

Measuring a controller internal temperature and transmitting it with BLE through advertising requires a total of $262.0\ \mu J$, taking into account a payload of 8 bytes. A capacitor with a $220.0\ \mu F$ capacitance, and charged by the Power converter module should be enough to power the advertising event. Advertising with the module is also reliable with bigger data payloads up to a maximum of 31 bytes. If the module is used as a scanner, for actuator functionality, the same profile but without the temperature measurement and with lower RF activity power consumption is expected to be obtained.

In contrast, the initialization energy of the BLE113 module requires a factor X larger capacitor, compared to the advertising events. It was considered that the communication operation was the limiting factor for the communications subsystem but the total initialization energy required exceeded what was expected. For future designs it is recommended to pay close attention to this power consumption and to seek modules with as low as possible initialization energy. Nevertheless, the values obtained still guarantee the viability of the performance for advertising events and the charging times of the capacitors. The total initialization energy required exceeded what was expected. To sum it up, it is concluded that for the BLE selection the initialization energy should be one limiting design factor due to its need for a bigger storage component and the consequential bigger sensor.

5.4.2 Conclusions on the Test Set-up

Not all the advertising packets of data are received by the scanner. Several stray signals are scanned during the test. It is considered that these unintended signals avoid the scanner to sense the advertising signal. It has to be considered that these are part of the limitations of the system. This problem is meant to be reduced when used in the satellite. In addition, scanners work with a scanning window and a scanning period, creating moments in which the scanner is not scanning for data. The use of a future scanner with a characterized performance and the proper analysis of the parameters to use will provide a better percentage of packet reception.

The problem of non-compatibility of signals would need to be addressed for future development of this technology, as several autonomous sensors could be installed in the same satellite. This will need statistical analysis for assessing the best scanning times and intervals to lose the minimum amount of data. And also it would need to have a more complex power management system that does not activate the advertising directly when the capacitor is charged but when it is charged and it is convenient for the whole system.

Chapter 6 Final end-to-end system test

6.1 Introduction

The chapter presents the values obtained for the final test of the whole system. This test chapter is briefer than previous ones mainly because it uses a lot of information already presented. This test chapter encompasses all the previous tested subsystems and it adds the final part of the power management subsystem, the logic control segment.

6.1.1 Test objectives

The overall objective of the test is to verify that the prototype is operational. Also, the conditions in which the prototype is working are obtained. In addition, the test is used to verify that the control design will act accordingly. The objectives of the test are the following:

EtoE-R-1: Obtain the real performance values of the control subsystem\

EtoE-R-2:Guarantee that the initialization process and the advertising process are started as required with the control subsystem.

EtoE-R-3: Obtain the final temperature difference required to have an operating system

6.1.2 Test set-up

The test set-up requires measuring several values. First, the voltage values in which the different operational amplifier modules provide a positive signal. Then, the total output current obtained from the power converter needs to be measured. There are not any important considerations for this test set-up, everything should be connected as it is expected for the final system. A super capacitor of $22\ mF$, with a leakage current of $5\mu A$, is used as a conservative way to be able to characterize the powering of the system and then use the information for sizing. Through the whole experiment, data packets should be received. The following figure represents the circuit of the control subsystem for the test.

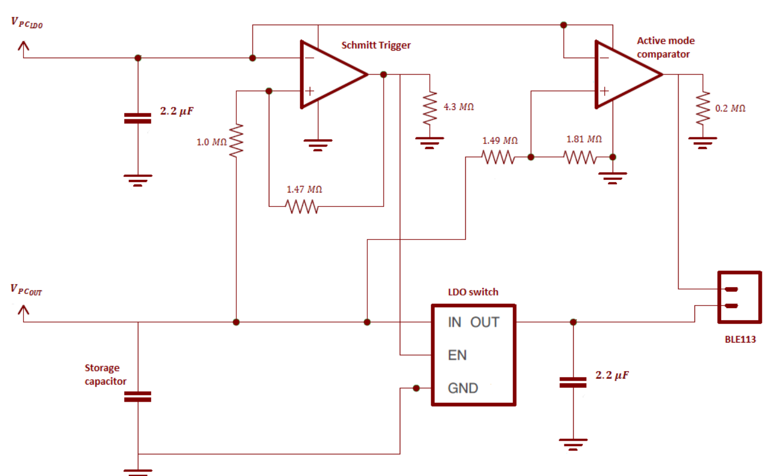

Fig. 25 Control subsystem for the final test.

The resistances used for the two comparators are of high value to provide a low current drain from the storage capacitor. The turning point of the Active mode comparator is equal to $4.0\ V$ and the Schmitt trigger activates at $3.7\ V$. These values do not correspond with the ideal design but allow obtaining the required characteristics of the design. It is important to remark again that the system should be design in a way that the signal change of the Schmitt trigger occurs for a voltage lower than the one of the Active mode comparator. Both outputs are also connected through ground with high value resistances avoiding a floating state output that may consume extra current or will cause a misbehaviour of the comparators. The power converter module used is the protoboard design, from Figure 10, as the PCB designs were both designed for 3.3 V of output voltage.

6.2 Uncertainty Analysis

The uncertainty analysis of this section follows the uncertainty of past chapters. In the end, one of the benefits of modularity testing is that for the final testing all the methods are already developed. Therefore, this chapter needs less clarification.

6.3 Test Results

Several results are presented in this section. First, the Schmitt trigger activation process is presented. Then the active mode comparator is presented with the amount of power that is consumed in the wake up call of the Bluetooth module. In the end, the conditions presented by the TEG module are compared to the charging performance of the system, represented by its charging time.

6.3.1 Schmitt trigger activation

The Schmitt trigger is designed to activate itself at $3.7\ V$. However, the obtained results determine that the trigger is produced when $3.8\ V$ is obtained, the use of a protoboard for the testing may be the reason of this difference in values. The following figure represents both the initialization process of the Bluetooth module and the Schmitt output voltage.

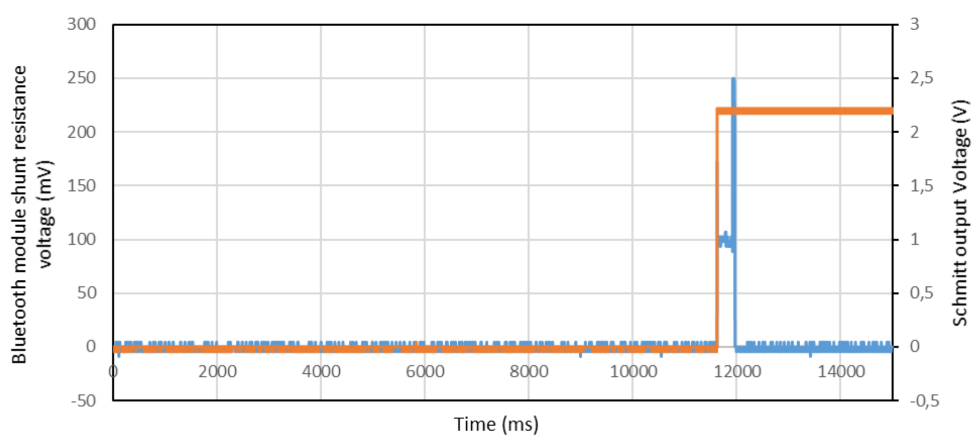

Fig. 26 Schmitt trigger test representation.

In the previous figure it can be observed how at the moment that the Schmitt trigger changes its output to $2.2\ V$, the reference voltage, the advertising event occurs. After the advertising occurs the Schmitt trigger stays closed allowing the provision of power for the Bluetooth module sleep mode.

6.3.2 Active mode comparator

The Active mode comparator provides a positive output voltage when the input voltage reaches $4.02\ V$ close from the designated value, $4.01\ V$. The process of wake-up requires power consumption through the GPIO pin of the Bluetooth module. An optimal design would require knowing this energy as it will need to be added to the advertising energy required. The following figure represents the current through the shunt resistor, $10\ \Omega$, used to measure the current through the wake-up pin.

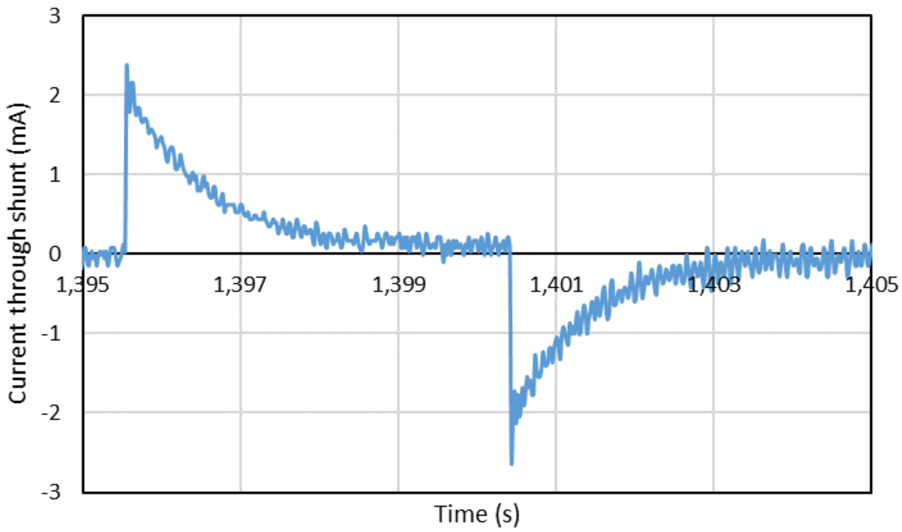

Fig. 27 Current consumed in wake-up process of the Bluetooth module.

It can be seen that current flows first into the Bluetooth module and then outside of the Bluetooth module. The current that goes outside the Bluetooth module is considered to be part of the energy already measured in the active mode of the Bluetooth module. However, the positive current needs to be considered as additional required energy. The energy required is equal to $0.023\ \mu J$.

6.3.3 Active mode with TEG

The conditions of operation can be measured after charging can be observed in the storage capacitor. The powering conditions are represented in the following table that includes the temperature difference tested and the voltage that comes directly out of the generator and to the power converter.

Test ref.number	*#EtoE-1*		*# EtoE -2*		*# EtoE -3*		*Average*
Temperature difference	2.38		2.3		2.26		2.31 ± 0.25
Input Voltage (mV)	35.9	35.7	35.4	35.4	35.4	35.4	35.55 ± 4.37

Table 33 Input powering conditions for the end-to-end test.

With the previous values the expected thermoelectric generated voltage and the current entering the input of the power converter can be calculated using the previous average values. These calculated values are presented in the following table.

Test ref.number	*Average values*
Thermoelectric voltage generated (mV)	58.9
Input current (mA)	6.58
Input power (μW)	234.0

Table 34 Input powering conditions calculated with the measured values of the end-to-end test.

The output current of the power converter is obtained with the multimeter. The final value of output current is obtained, with $t_{95}(\upsilon = 102) = 1.99$, $s_\alpha = 0.44$, $N = 103$, $b_\alpha = 2.01$, is equal to:

$$I_{out_{pc}} = 19.24 \pm 4.0\ \mu A$$

The uncertainty is big in the same order as the values obtained in Chapter 4 for the charging current, output current of the power converter. No other method was able to be used. High values of shunt resistance are required if the current is obtained by the measure of voltage through a shunt resistor. These high values will reduce the amount of power that the capacitor obtains. Therefore the current measured will be reduced from the one obtained for the expected final design. Taking into account that the previous output current has been obtained for $4.0\ V$ then the total efficiency obtained is equal to $35\ \%$. This output current minus the current losses present in the system is the one that produces the charging of the capacitor. The charging times measured are presented in Table 35.

Test ref.number	*#EtoE-1*	*# EtoE -2*	*# EtoE -3*	*Average*
Charging time (s)	15.7	15.4	16.0	16.2 ± 0.63

Table 35 Storage capacitor charging time measurements for the end-to-end test.

The charging time allows calculating the duty cycle of the system. Taking into account the average value of the charging time with the value obtained in Chapter 4 of the active required time, $10\ ms$, the duty cycle can be obtained. A duty cycle of $0.06\ \%$ is obtained with a temperature difference of $2.31\ K$.

6.4 Conclusions

Charging is able to be achieved with low values of temperature difference, $2.31\ K$. In addition a total period of 16.2 seconds can be obtained for operation. The values obtained in this test do not provide the exact minimum temperature difference that is needed for the operation of the system. The use of a slightly higher temperature difference allowed to complete the tests faster. Due to time constraints in the project the decision to not guarantee the exact minimum temperature difference was taken. In addition, the minimum temperature difference would increase the time require of the test to infinite, as the charging current, equal to the power converter output current minus the current losses, would be close to zero, making unnecessarily long experiments.

Additional effort is required to measure better ultra-low currents. The output current values obtained still maintain relative values of uncertainty of 20 %.This limitation did not allowed to measure in detail current losses occurring through other paths and caused by other components.

Chapter 7 Conclusions and Recommendations

This chapter starts presenting the conclusions of the MSc thesis while answering the research questions and giving a general assessment of the completion of the research objective. In addition a summary of the results obtained is presented. The next subsection, the discussion subsection, presents the different causes and consequences of the results, the impact of this research in the whole body of knowledge, and the limitations of the research. In the final subsection, the recommendations subsection, the possible lines of future research, to follow-up with the project, are presented.

7.1 Conclusions

The project provides a feasibility assessment, by testing of the use of a self-powering autonomous temperature sensor in a small satellite due to its small tested temperature difference required. The sensor was powered with a thermoelectric generator, it sends data with a Bluetooth Low Energy module with internal microcontroller and temperature sensor, and it gathers the data with that temperature sensor. In addition, the prototype has a power management subsystem for interfacing and controlling the different components. The sensor has been tested for a temperature difference of $2.4\ K$, not the minimal feasible. However, this is considered to be close to the minimal temperature difference required. The temperature difference is considered small enough to be obtained in a small satellite. In addition, literature identified $3.5\ K$ as the maximum temperature difference that can be obtained in a specific university satellite. However, this temperature differences would need to be tested in space to be able to provide a complete question to answer if this conditions can be achieved in a small satellite.

In addition, the prototype is based on COTS components with only a PCB needed to be manufactured and design. Having said that, the final design size is not adequate for its implementation in PocketQubes, as a useful replacement of its wired counterpart because the reduction in wiring is relatively small compared to the increase in size of the wireless sensor. The size is limited by the actual technology available, some technology development is needed to get a substantial decrease in size. However, the implementation in bigger satellites is feasible and may provide substantial advantages after placed remotely and/or at locations where wiring is difficult to integrate. Furthermore, it can be implemented for an on-space technology demonstration mission in a PocketQube.

Moreover, the project allows establishing certain performance figures that can be used in future research and implementation. The most important characteristics are presented to allow a quick overview of the performance that can be obtained. The values obtained for the testing of the thermoelectric generator and the power converter only are presented first. Then the Bluetooth module performance results are presented. In the end, the control subsystem and the final test results are presented.

Thermoelectric generator and power converter

The system departs from a specified temperature difference. The smallest difference required by the power conversion device has been sought. This value is ultimately needed for its final implementation in a specific satellite. The input voltage and current, and the output current represent the efficiency of the power conversion device.

Parameter	*Value*
Temperature difference (K)	2.0
Input Voltage (mV)	30.0
Input Current (mA)	5.0
Output Current (μA)*	15.0

Table 36 Summary of values obtained with the project prototype. *Current measured for a programmed $\mathbf{3.3\ V}$ output.

The low values of output current highlight the necessity of using COTS components with low leakage current. The storage capacitor used in the project causes one third of the total output current to be lost due to its leakage current values. Later, the values of leakage current in capacitors are commented in the discussion subsection. From the previous results relative performance values can be obtained. These values are presented in Table 37.

Parameter	*Value*
Output current / Temperature difference ($\mu A/K$)	7.5
Input Voltage / Temperature difference (mV/K)	15.0

Table 37 Relative parameters to represent the extent of the prototype design for different applications. of internal resistance of the different components with temperature.

All these values consider that most of the characteristics of the design remain constant. However, the efficiency of the power converter changes with the input voltage due to the transformer transformation ratio used. For expected higher temperature differences and therefore for expected higher input voltages the transformation ration should be decreased. It should be considered that the prototype requires at least 2K of temperature difference as well.

Communications module and storage component

The Communication module presents unforeseen issues which turned out to be a major design driver for the overall system. Mainly, the initialization energy was not considered as it was thought that the RF communication process would be the driving energy factor. However, the Bluetooth module used here, even though it may potentially be changed to one with lower initialization energy, has been characterized and can be used as a conservative baseline for future designs. The energy required for each of the different modes, active mode and initialization mode, are presented in Table 38 and Table 39. In addition, the required storage capacitances needed, taking into account a voltage decrease between $4.1\ V$ and $3.3\ V$, are presented.

Parameter	*Value*
Energy for advertising event* (μJ)	265.0
Capacitor needed for advertising event (μF)	89.6

Table 38 Values obtained for advertising event with the BLE113 communications module and for measuring the internal temperature of the module. 8 byte of useful data are sent through the advertising event.

Parameter	*Value*
Energy for advertising event* (mJ)	6.9
Capacitor needed for advertising event (mF)	2.33

Table 39 Initialization energy results.

The biggest value of capacitance is needed in the final system design. In the case of this project a different capacitor is used than the one presented in the previous tables. The capacitance used is equal to $22\ mF$, and it is used as the standard for testing processes.

Power control

The power control is able to guarantee a successful automatic control of the switch to power the Bluetooth module. First the Schmitt trigger used in the project is able to open for initialization when the storage reaches 3.8 V, and the advertising comparator allows sending the advertising signal when the voltage reaches 4.01 V. These components have not been optimized for the best limit cases of switching as presented in Chapter 2.

Final end to end prototype

The final end to end prototype comprises all the subsystems together. The final values obtained are presented in the following table. The values presented do not correspond with the exact minimum requirements. The test was carried out with slightly higher values to be able to obtain faster results.

Parameter	*Value*
Temperature difference (K)	2.4
Storage charging time (sec)	16.0

Table 40 Final end to end test measured values.

The values provide successful conclusions as a low temperature difference is obtained, and the duty cycle could be used for housekeeping applications. However, the values presented here

The volume required for the autonomous system is as important as the performance values and the environmental working characteristics for the thermoelectric harvester. The size for the different subsystems or modules of the system are presented in Table 41, both the Bluetooth module and the power convertir with power control sizes have been optimized for the expected final circuit. The comparison between the autonomous system volume and the volume of the old Delfti-n3xt temperature sensor is presented in table 43.

Parameter	*Value*
Thermoelectric generator (mm)	$13.2\ x\ 13.2\ x\ 2.2$
Bluetooth module (mm)	$28.0\ x\ 23.0\ x\ 3.9$
Power converter with power control (mm)	$32.0\ x\ 30.0\ x\ 6.0$
Storage capacitor (mm)	$20.0\ x\ 15.0\ x\ 2.3$

Table 41 Size values of the different subsystems of the autonomous thermoelectrically-powered temperature sensor.

Dimensions of	*Value*
Complete autonomous temperature sensor (mm)	$32.0\ x\ 30.0\ x\ 14.4$
Reference wired sensor (mm)	$20.0\ x\ 20.0\ x\ 10.9$ + wires

Table 42 comparison between the autonomous temperature sensor of this project and the temperature sensor used in Delfi-N3xt.

It can be seen that the size of the autonomous temperature sensor is considerably higher. Therefore, its use cannot be accepted due to size reduction but with its possible integration improvement. It has to be taken into account that the height of the autonomous temperature sensor could be decreased 2.3 mm of height if the initialization energy would not drive the capacitor design.

7.2 Discussion

The discussion analyses the results in more detail and provides a general observation of the implications of the project. This section starts presenting the implications for the state of the art of this technology in satellites and then it discusses the effects that several decisions done during the project have in the final outcome and in the results.

Implications on the literature

The conclusions of the project provide the foundation for a discussion on its applicability and the effect that thermoelectric harvesting for autonomous sensors can have in small satellites. This work is the first one to provide an end-to-end prototype of an autonomous thermoelectrically-powered sensor designed for small satellites. It can be compared to other works in which the feasibility was done by analysis instead of testing (Takacs, Aubert et al. 2012) and (von Lukowicz, Abbe et al. 2016). The obtainment of a working hardware allows to be used as a comparison to wired temperature sensors for researches in which they analyse the reasons for the change to wireless systems in satellites.

The low temperature difference that has been obtained, 2.4 degrees, is able to complete the research done in (von Lukowicz, Abbe et al. 2016), in which they state that 3.5 degrees is the minimum temperature difference that could be obtained in their own CubeSat. However, they only provide an analytical solution in which they do not determine if it is possible with the current technology state of the extra components needed. In addition, the temperature gradients have not yet been characterized for this purpose in-orbit. The expected and tested temperature differences still have a high uncertainty for real practice application. It is recommended to test this on-board of the satellite. In principle, a flight model of the prototype presented in this study, could be used to characterize the thermal gradients by simply recording and analysing the time intervals between sensing and communication events. therefore still have a high uncertainty for real practice applications.

Use and Integration

The present project presents one of the simplest possible sensors, which eliminates the wires with its corresponding benefits but not a specific application with a big improvement in the design has been properly analysed. The research done in this project is considered as an enabler for future concepts. As an example of the benefits of using energy harvesting for a specific application, researchers identified that the use of electromagnetic harvesting can be used to harvest undesirable micro-jitters in mechanical moving parts to measure its disturbances with an autonomous low-power accelerometer (Kwon and Oh 2016). Another possible example is the use of energy harvesting for active thermal control by power electrochromic devices (ECD) that change the optical characteristics depending on the energy applied (von Lukowicz, Abbe et al. 2016).

In addition to all these technologies presented by other researchers, several general applications can be pitched. The first clear advantage would be to use this technology for difficultly accessible locations, through-hole access. For example, the need of having sensors inside a propellant tank would need to provide a hole through to communicate the interior with the exterior. However an autonomous sensor, with several modifications to withstand the environmental conditions of the location, can be introduced inside the tank to provide inside data. Also, so far the only applications that have been foreseen consist of a periodic use, a singular use does not need the complexity of the system when a storage component, a battery, could be used. However, if the action is activated after a long time, for example for the end of life of the satellite or for de-orbiting, then the constant scan for an activation packet may require a huge battery component. In this case, the use of energy harvesting may be a possible alternative. This allows the use of actuators in addition to sensors with the possible creation of sensor/actuator network of ADCS as envisioned in (Amini, Aalbers et al. 2006, Amini, Gill et al. 2007, Zheng and Armstrong 2010).

Size

Literature documentation presents that the use of autonomous sensors will allow the reduction of mass and volume in satellites and it is used as the main reason for the start of this research (Amini, Gill et al. 2007). These statements are backed up by the big influence that any kind of harness, and all harness-related components, has in the total mass budget of the satellite. With this project primal rough values can be given to compare if the use of the harness and its connectors is really lower than the connexion with wires. The total size obtained is equal to, 9.1 cm^3 The size may be reduced by optimizing the Power converter module PCB design and the BLE113 breakout board design. It has to be taken into account that the full module can be divided to fit easily. For example the temperature sensor can be further away from the thermoelectric generator However, the comparison with the Delfi-N3xt temperature sensor show that the benefits of this technology is not a reduction in size.

Limitations and design modifications

The final design had several on-going modifications during the research to adapt the work with the different problems that have appeared and the time constraint of the thesis. Some components have not been optimized to the final values wanted, as the proof of concept was already obtained and all the important conclusions concerting self-powering were obtained. For example, the control components were not taken to behave for the optimized extreme voltages required and presented previously in Chapter 2, in the time scheme of the control subsystem.

As another example, the storage capacitor is oversized in capacitance terms, even though its leakage current is among the smallest found. The problem with optimizing the capacitor is that there is not a perfect in all terms COTS component available. The storage capacitor should be able to work at certain voltage levels, have low leakage current, and also should have small size with its specified exact required capacitance. It has been found that super capacitors have big amounts of capacitance for small leakage currents. However, for the available super capacitors, their size is considerably bigger than other capacitors. And then, tantalum capacitors have small sizes and can obtain the required capacitances needed in this project but their leakage current is considerable higher as it depends on the voltage levels and capacitance. Due to the high capacitances needed for the initialization energy this last type of capacitors cannot be possibly use. In the end, the capacitor selection is a trade-off between leakage current and then higher required temperature differences or size and less space to fit into small satellites.

7.3 Recommendations

It is recommended to optimize the design of the sensor. The main areas to improve are the communications subsystem and also the integration and tuning of the whole electronics into a unique PCB. However, the most important considerations come from the ways to develop the knowledge of this technology in small satellites. As any research will improve the optimization of the design as a natural consequence

The application of a temperature sensor with thermoelectric harvesting has been seen as feasible. As seen, the size of the system hinders its possible implementations so finding an application that could benefit more with the concept would be a favourable asset for the technology. Therefore, the technology could be taken a step further. A possible area is the investigation on the use of actuators with a Bluetooth ‘scanning’ mode, following a similar arquitecture than the one presented in this thesis. The system will have a similar working mechanism but instead of advertise data it will scan for an order. Then, it will do the specific ordered action. The research would allow the evaluation of the possibilities of using a network of autonomous sensors and actuators. The coexistence of all these autonomous systems and the data transmission between them and a central computer would be an interesting area of research.

The most important limitation of the design is the initialization energy required by the selected Bluetooth low energy module. This project departs from the research done in intra-spacecraft communication in small satellites, having selected a specific module due to its benefit in wireless communication, with a lower level of importance in the energy requirements (Schoemaker). However, self-powering sensors have different requirements for their communication module as reducing all sources of energy consumption is paramount. The initialization energy was not considered as a limiting factor of the design but it should be considered for future development and implementation. Information on the initialization energy required requires intensive search compared to the easy availability of information on the energy required for normal operation of the module. A comparison of the energy requirements, including initialization energy, of different modules has already been done by (Marcel Meli 2014) and can be used as a reference for future selection. For example the use of a module based on the SoC nRF51822 compared to the CC254X could provide an initialization energy decrease of 20 %.

The thesis guarantees the feasibility of introducing thermoelectric harvesting for self-powering an autonomous temperature sensor when there are benefits with the implementation. However, another energy harvesting technology was identified and can be researched. It was identified that RF harvesting could provide benefits to the whole small satellite system. The whole concept will rely on a dedicated RF source close to the main battery of the satellite and a net of sensors with rectennas tuned to receive the energy of the specific RF source. The testing of a wireless energy transfer system, with a dedicated source, was going to be tested in this project but time and workload constraints required the cancellation of that branch of the thesis. As presented previously, work has already been done in different research but taking into account the harvesting of ambient signals (Takacs, Aubert et al. 2012) and the use of dedicated RF sources was already researched on-ground (Visser 2012). However, special attention would need to be carried out in the possible adverse effects that adding a dedicated RF sources has in the other subsystems of the whole satellite. In addition, the power consumption of a dedicated RF source needs to be investigated to assess its feasibility in the overall small satellite system concept.

Chapter 8 References

- "Delfi-PQ Mission http://www.delfispace.nl." Retrieved 9th October, 2016.

- Admasu, B. T., X. B. Luo, J. W. Yao and T. Z. Ming (2013). Effects of Non-Uniform Hot Junction Temperature Distribution on the Outputs of Thermoelectric Power Generation System. Applied Mechanics and Materials, Trans Tech Publ.

- Amini, R. (2016). Wireless Communication onboard Spacecraft PhD, Technische Universiteit Delft.

- Amini, R., G. Aalbers, R. Hamann, W. Jongkind and P. Beethuizen (2006). New generations of spacecraft data handling systems: Less harness, more reliability. Proceedings of 57th International Astronautical Congress.

- Amini, R., E. Gill and G. Gaydadjiev (2007). The challenges of intra-spacecraft wireless data interfacing. 57th International Astronautical Congress.

- Bouwmeester, J., G. Aalbers and W. Ubbels (2008). Preliminary mission results and project evaluation of the Delfi-C3 nano-satellite. Proceedings of 4S Symposium.

- Coleman, H. W. and W. G. Steele (2009). Experimentation, validation, and uncertainty analysis for engineers, John Wiley & Sons.

- De Boom, C., J. Leijtens, L. Duivenbode and N. van der Heiden (2004). Micro digital sun sensor: System in a package. MEMS, NANO and Smart Systems, 2004. ICMENS 2004. Proceedings. 2004 International Conference on, IEEE.

- Denker, R. and A. Muhtaroğlu (2013). "Feasibility analysis and proof of concept for thermoelectric energy harvesting in mobile computers." Journal of Renewable and Sustainable Energy **5**(2): 023103.

- FischerElektronik WLPK thermal paste datasheet.

- Gill, E., G. Monna, J. Scherpen and C. Verhoeven (2007). Misat: Designing a series of powerful small satellites based upon micro systems technology. 58th International Astronautical Congress.

- IAC, I. E. C. IEC584 Class 1.

- Instruments, T. CC2541 datasheet.

- KeysightTechnologies Keysight 34401A datasheet.

- Kwon, S.-C. and H.-U. Oh (2016). "Experimental validation of satellite micro-jitter management strategy in energy harvesting and vibration isolation." Sensors and Actuators A: Physical **249**: 172-185.

- Lindh, J. (2016). Bluetooth Low Energy Beacons. Application Report. SWRA475A. T. Instruments.

- LinearTechnology LTC3108 datasheet.

- Ultralow Voltage Step-Up Converter and Power Manage. http://cds.linear.com/docs/en/datasheet/31081fb.pdf.

- M. T. Penella, M. G. (2007). A Review of Commercial Energy Harvesters for Autonomous Sensors. Instrumentation and Measurement Technology Conference - IMTC 2007. Warsaw, Poland.

- Madhusudana, C. V. Thermal contact conductance, Springer.

- Marcel Meli, J. B. (2014). Comparing the energy requirements of current Bluetooth Smart solutions. Embedded World 2014. Nuremberg.

- MicroPelt TGP-651 Thermogenerator-Package (TGP) Preliminary datasheet. http://www.micropelt.com/downloads/datasheet_thermogenerator_package.pdf.

- PicoTechnology PicoScope 2000 Series datasheet.

- RS-Components Data Sheet RS-1316. K.J.E.T.R.S.N. Data-Logger Thermometer.

- Sandau, R., K. Brieß and M. D'Errico (2010). "Small satellites for global coverage: Potential and limits." ISPRS Journal of photogrammetry and Remote Sensing **65**(6): 492-504.

- Schoemaker, R. Robust and Flexible Command and Data Handling on Board The Delffi Formation Flying Mission. MSc of Science in Space Engineering, Delft University of Technology.

- Stephen Beeby, N. W. (2010). Energy Harvesting for Autonomous systems.

- Straub, J. (2012). Cubesats: A low-cost, very high-return space technology. AIAA Reinventing Space Conference 2012.

- Takacs, A., H. Aubert, M. Bafleur, J.-M. Dilhac, F. Courtade, S. Fredon, L. Despoisse, C. Vanhecke and G. Cluzet (2012). Energy harvesting for powering wireless sensor networks on-board geostationary broadcasting satellites. 2012 IEEE International Conference on Green Computing and Communications, IEEE.

- Takacs, A., H. Aubert, L. Despoisse and S. Fredon (2013). "Microwave energy harvesting for satellite applications." Electronics Letters **49**(11): 1.

- Takacs, A., H. Aubert, S. Fredon, L. Despoisse and H. Blondeaux (2014). "Microwave power harvesting for satellite health monitoring." Microwave Theory and Techniques, IEEE Transactions on **62**(4): 1090-1098.

- Visser, H. J. (2012). "Indoor wireless RF energy transfer for powering wireless sensors." Radioengineering **21**(4): 963-973.

- von Lukowicz, M., E. Abbe, T. Schmiel and M. Tajmar (2016). "Thermoelectric Generators on Satellites—An Approach for Waste Heat Recovery in Space." Energies **9**(7): 541.

- Yeh, C., C. Wen, Y. Chen, S. Yeh and C. Wu (2001). "An experimental investigation of thermal contact conductance across bolted joints." Experimental thermal and fluid science **25**(6): 349-357.

- Zheng, W. H. and J. T. Armstrong (2010). "Wireless intra-spacecraft communication: the benefits and the challenges."

APPENDIX-A Criteria for energy harvesting technologies

Different concepts have been rejected or accepted following conditions that provide the best outcome for the project. The following list presents the requirements that are needed for an self-powering-concept to be developed.

[R-1] Potential for integration improvement, the concept shall be able to provide an enhancement in the way to integrate sensors in a small satellite.

[R-2] Development of small satellite technology, the concept shall provide with an innovative use of a self-powering technology focusing on the enhancement of the small satellite state-of the art.

[R-3] Continuous powering, the concept shall be an energy harvesting related topic, as this is the main aim of the thesis.

[R-4] Achievable research, the concept shall be able to be tested and developed in the time span of a master thesis and with the available resources of the university.

[R-5] In-orbit mission functionality, the concept shall provide an enhancement in small satellite technology in-orbit.

APPENDIX-B PCB board Layouts

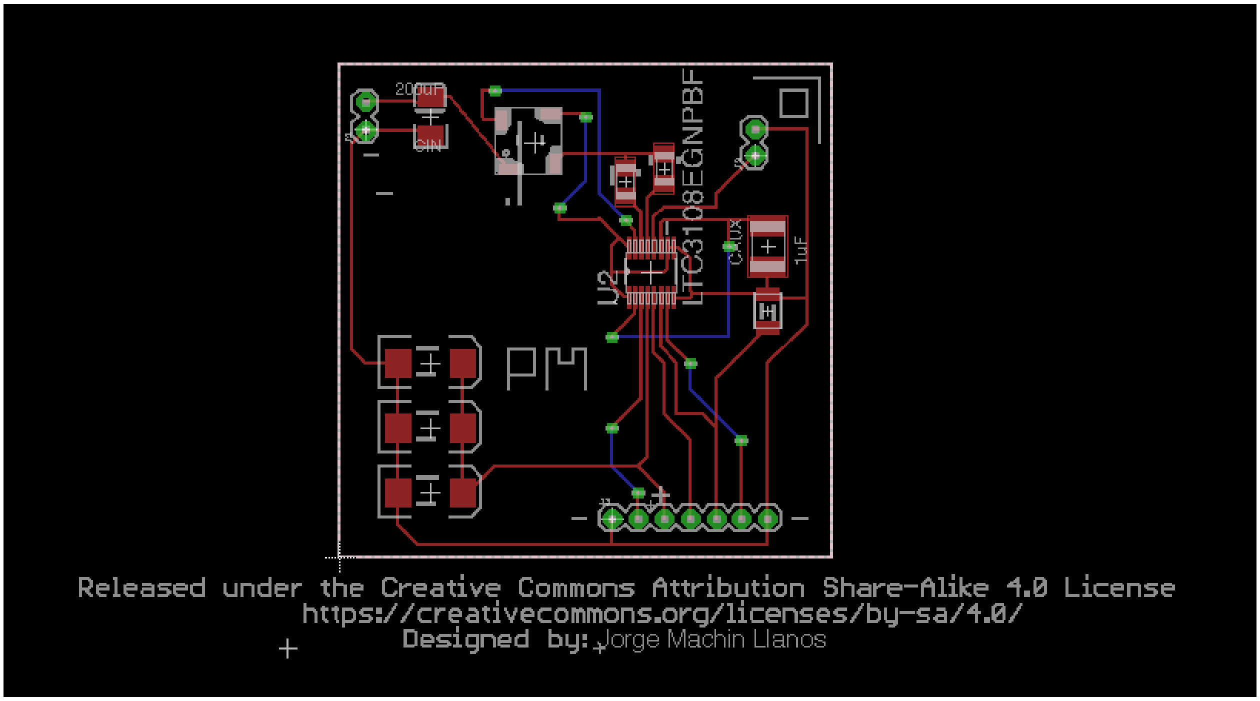

Fig. 28 Board Layout for PCB called PCB-big

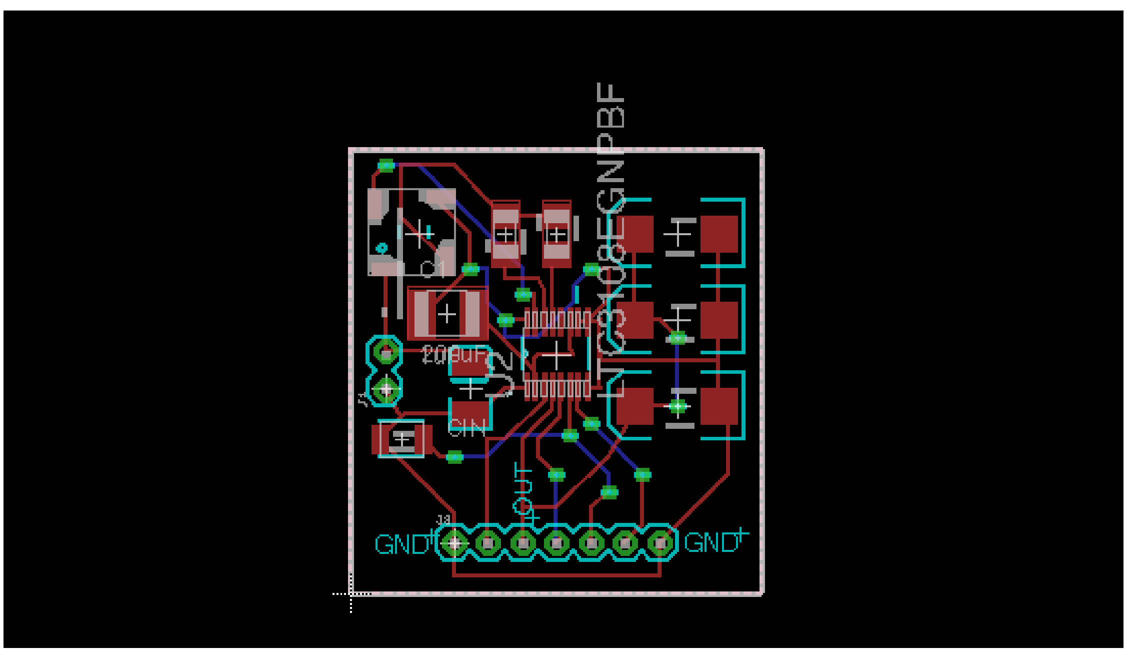

Fig. 29 Board Layout for PCB called PCB-PM

APPENDIX-C PCB Schematics

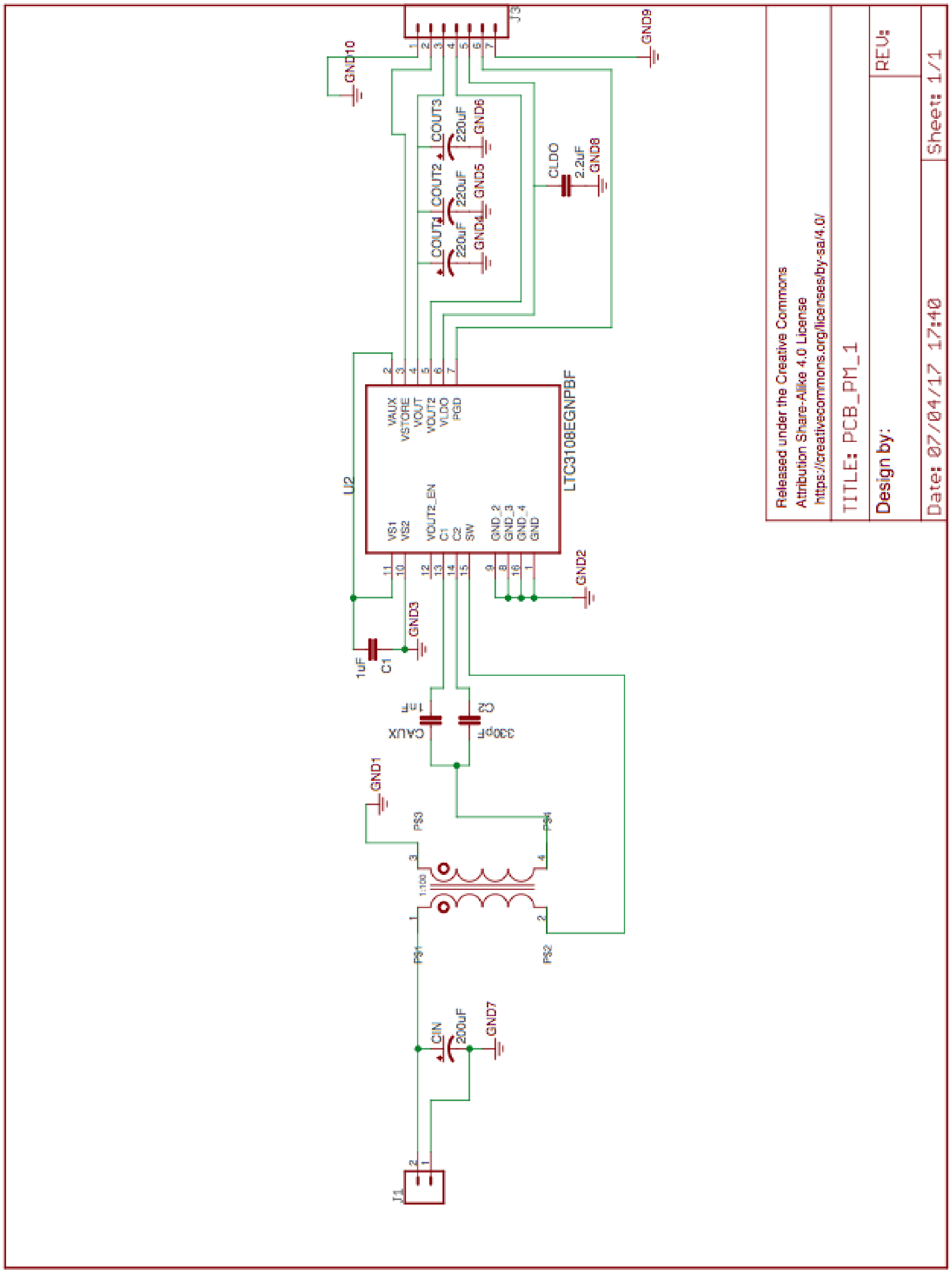

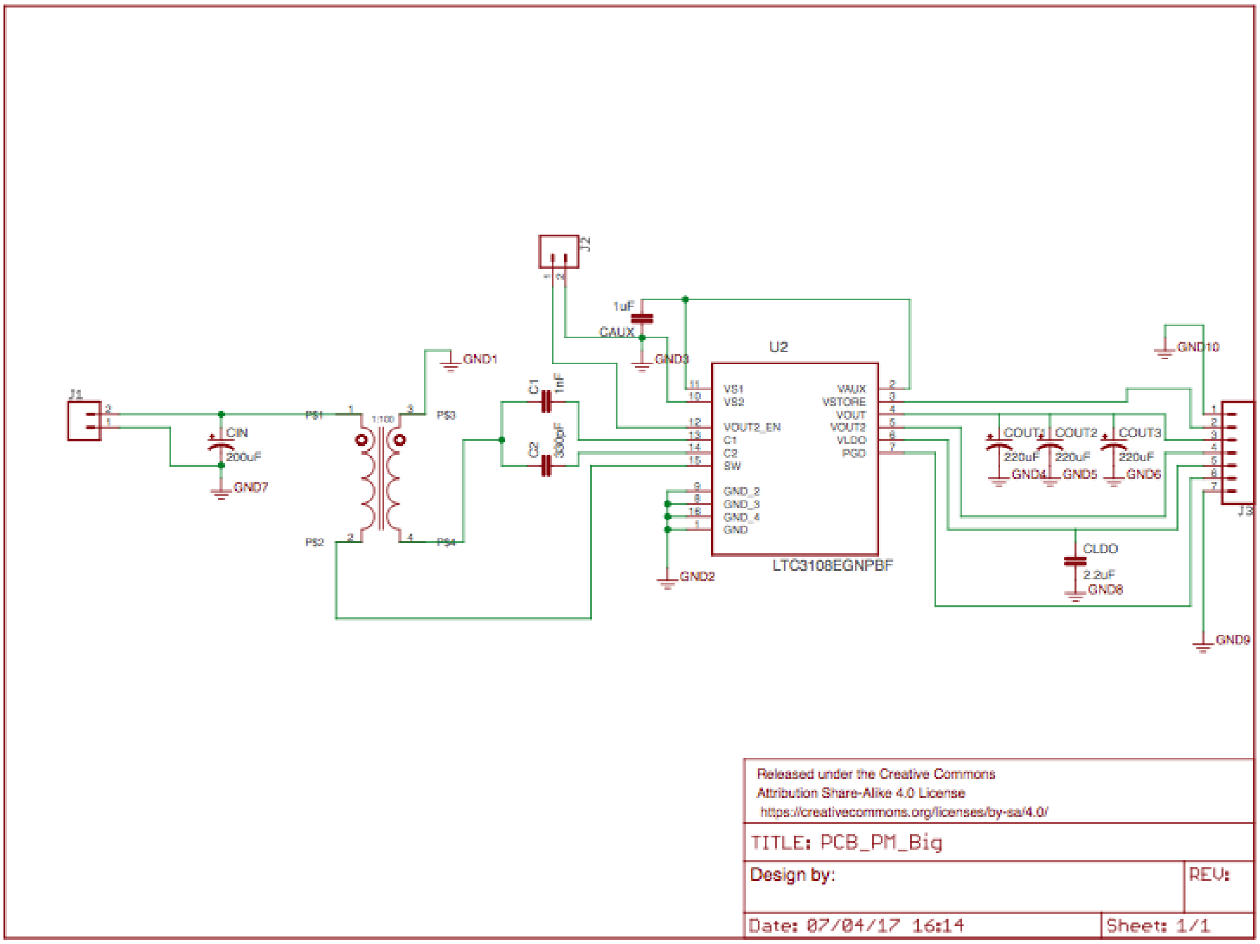
J1
J2
J3
CIN
200uF
GND7
GND1
GND2
GND3
GND9
GND10
1uF
CAUX
1:100
C1
1nF
C2
330pF
U2
VS1
VS2
VOUT2_EN
C1
C2
SW
GND_2
GND_3
GND_4
GND
VAUX
VSTORE
VOUT
VOUT2
VLDO
PGD
LTC3108EGNPBF
COUT1
COUT2
COUT3
220uF
220uF
220uF
GND4
GND5
GND6
CLDO
2.2uF
GND8
Released under the Creative Commons
Attribution Share-Alike 4.0 License
https://creativecommons.org/licenses/by-sa/4.0/
TITLE: PCB_PM_Big
Design by:
REV:
Date: 07/04/17 16:14
Sheet: 1/1

APPENDIX-D Uncertainty analysis theory

The uncertainty analysis is conducted to give veracity to the test results. The analysis measures quantitatively the range in which the result is guaranteed within a certain level of confidence. In addition, to support the uncertainty analysis, a sensitivity analysis is needed. The sensitivity analysis investigates the importance that an input error has in the final outcome. The results expose the effect certain variables have in a test set-up or model. Apart from clarifying any possible difference between tested values and estimated model values.

D.1 Theory and notation

The following section presents the notation and equations that will be used related to uncertainty analysis.

D.1.1 Error types

We can consider two types of errors, systematic and random errors. Random errors are related to precision, and calibration has no effect on it. Its uncertainty can be estimated by multiple point measurements. Systematic errors provide consistent inaccuracies. They are related to accuracy and their inaccuracy cannot be estimated with a multiple point measurement. They are inherent to the measuring process.

D.1.2 Systematic uncertainty

Among the possible error sources of systematic uncertainty we will consider the following (Coleman and Steele 2009):

- *Calibration errors*, based on the calibration process and imperfections in the standard.
- *Data reduction errors*, errors due to computational resolution, or using regression curves
- *Conceptual errors*, using measured values in a model that do not match theoretically. For example, the use of a one-point intake pressure measurement in an equation that requires average inlet pressure.
- *Data acquisition errors*, errors due to the system and environment of the data intake.
- *As-delivered by the manufacturer*, inherent uncertainty determined by the provider of the component or instrument.

D.1.3 Random uncertainty

Random errors are difficult to discover and quantify analytically. They require quantification after a multiple point measurement. Multiple point measurements should take into account different time scales and how they will affect the final outcome. An extra-fast data system won't be able to fulfil the function if it does not scan values for long test periods. And therefore, does not represent random errors present in long time scales. The method that is going to be used in this section for the random uncertainty is the direct method. The direct method random uncertainty estimation follows (Coleman and Steele 2009):

$$(s_r)_{direct} = \left[\frac{1}{M-1}\sum_{i=1}^{M}(r_i - \bar{r})^2\right]^{1/2} \tag{43}$$

in which, M is the number of measurements, r_i is a one-point measured value, $\bar{r}$ is the average of all the measured values.

D.1.4 Multiple variable equation

The propagation of uncertainty is important when obtaining a variable with an equation of measured values. To estimate the propagation of uncertainties the Taylor Series Method is used. For the following final variable, r, calculated with two variables X, Y the following uncertainty is obtained (Coleman and Steele 2009):

$$r = r(X, Y) \tag{44}$$

$$u_r^2 = \left(\frac{\partial r}{\partial X}\right)^2 b_X^2 + \left(\frac{\partial r}{\partial Y}\right)^2 b_Y^2 + (s_r)^2{}_{direct} + 2\left(\frac{\partial r}{\partial X}\right)\left(\frac{\partial r}{\partial Y}\right) b_{XY} \tag{45}$$

In which, u_r is the uncertainty of r, b_X is the systematic uncertainty of variable X, b_Y is the systematic uncertainty of variable Y, s_X is the random uncertainty of variable X, s_Y is the random uncertainty of variable Y and b_{XY} is the correlated systematic uncertainty. The uncertainties that are considered for these equations comprise a level of confidence of 95%.

The last term of both equations presents the correlated errors. These errors are dependent to more than a variable and can improve or damage the final uncertainty. Among the possible errors that can be found are variables measured with the same instrument and variables calibrated in the same standard. The equation used for correlated systematic errors is (Coleman and Steele 2009):

$$b_{ik} = \sum_{w=1}^{L} b_{iw}\, b_{kw} \tag{46}$$

in which, b_{ik} corresponds to the correlated systematic error between variable i and variable k, and L corresponds to the number of fundamental error sources. The previous equation provides an absolute uncertainty, but it is convenient to also present it with a relative, non-dimensional result. The non-dimensional equation for the uncertainty is equal to,

$$\frac{u_r^2}{r^2} = \left(\frac{X}{r}\frac{\partial r}{\partial X}\right)^2 \frac{b_X^2}{X^2} + \left(\frac{Y}{r}\frac{\partial r}{\partial Y}\right)^2 \frac{b_Y^2}{Y^2} + \frac{s_r^2}{\bar{r}^2} \tag{47}$$

The previous results have been presented for only two variables. The original Taylor series method for uncertainty analysis covers multiple variables as represented with the following equations,

$$r = r(X_1, \dots, X_N)$$

$$\frac{{U_r}^2}{r^2} = \left(\frac{X_1}{r}\frac{\partial r}{\partial X_1}\right)^2 \left(\frac{U_{X_1}}{X_1}\right)^2 + \cdots + \left(\frac{X_j}{r}\frac{\partial r}{\partial X_j}\right)^2 \left(\frac{U_{X_j}}{X_j}\right)^2$$

D.1.5 Confidence interval

When using a limited size population an estimate is obtained for the true value. Therefore, a frequency is needed on how often this estimate, or interval, complies with the true value. This is the level of confidence for a certain confidence interval.

The previous equations always take into account that the standard deviation is not known, but calculated. Therefore the values measured resembled a t-distribution or Student's distribution instead of a Normal distribution. The confidence intervals that are going to be used are the following:

$$X_i - U_{\%} \le \mu \le X_i + U_{\%} \tag{48}$$

$$U_{\%} = t_{\%}(s_x^2 + b_k^2)^2 \tag{49}$$

While for using the average value obtained the following two equations are used:

$$\bar{X} - \bar{U}_{\%} \le \mu \le \bar{X} + \bar{U}_{\%} \tag{50}$$

$$\bar{U}_{\%} = t_{\%}\left(\frac{s_x^2}{N} + b_k^2\right)^{1/2} \tag{51}$$

In which X_i is an independent measurement, $\bar{X}$ is the average of all measurements, N is the number of measurements and $t_{\%}$ is the parameter use to represent a level of confidence of % in the interval, $U_{\%}$ is the confidence interval for a certain frequency % when using X_i, $\bar{U}_{\%}$ is the confidence interval for a certain frequency % when using $\bar{X}$, and s_x^2 is the random error and b_k^2 takes into account the systematic errors. The systematic errors are not reduced by a factor of $\sqrt{N}$ while using the average values. The values for $t_{\%}$ are obtained from a t-distribution table as it has been presented in Figure 30.

	C				
ν	0.900	0.950	0.990	0.995	0.999
1	6.314	12.706	63.657	127.321	636.619
2	2.920	4.303	9.925	14.089	31.598
3	2.353	3.182	5.841	7.453	12.924
4	2.132	2.776	4.604	5.598	8.610
5	2.015	2.571	4.032	4.773	6.869
6	1.943	2.447	3.707	4.317	5.959
7	1.895	2.365	3.499	4.029	5.408
8	1.860	2.306	3.355	3.833	5.041
9	1.833	2.262	3.250	3.690	4.781
10	1.812	2.228	3.169	3.581	4.587
11	1.796	2.201	3.106	3.497	4.437
12	1.782	2.179	3.055	3.428	4.318
13	1.771	2.160	3.012	3.372	4.221

Fig. 30 Student's distribution values table. (Coleman and Steele 2009)

D.2 Qualitative uncertainty analysis

The qualitative analysis identifies the most important sources of uncertainty and how they propagate through the equation chain. It can also be considered as a sensitivity analysis. It is executed by an analysis of the absolute sensitivity coefficients,

$$\theta = {}^{\partial r}/_{\partial X_i} \tag{52}$$

In which θ is the absolute sensitivity coefficient. A qualitative uncertainty analysis is important prior to any test. The equation chains and the values needed to be measured, to obtain the lowest uncertainty on the desired value, can be selected from the qualitative uncertainty analysis.

APPENDIX-E Images of the Thermoelectric Characterization Test

The following appendix presents graphically some important aspects of the test set-up.

Assembly of the test set-up:

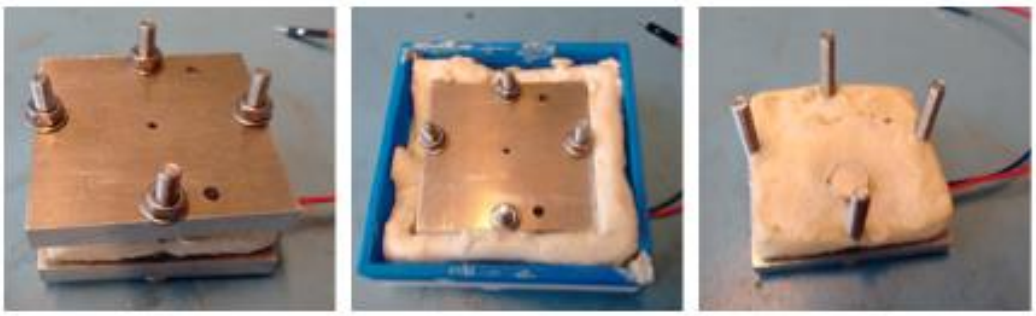

Fig. 31 Three photos of the assembly of the test set-up.

Use of thermal paste:

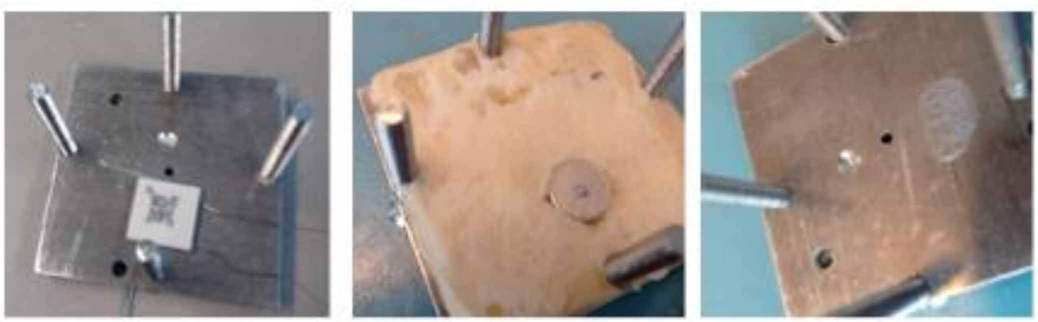

Fig. 32 Three photos of the application of thermal paste. The two photos on the left show the way the paste is applied and the photo on the right shows the footmark after detaching the thermoelectric module

Thermocouple holes:

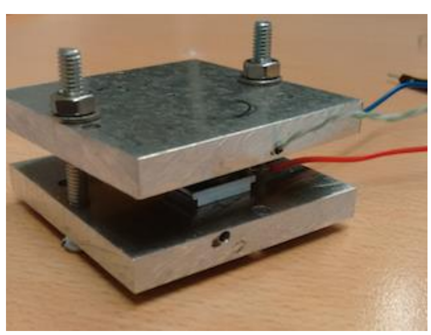

Fig. 33 Photo of the thermocouple, green/white wire inserted into its measurement hole.

APPENDIX-F Instrumentation Specifications

The different measuring systems and their accuracies for the measured variables are presented in the following table (KeysightTechnologies) (PicoTechnology) (IAC) (RS-Components):

Type of instrument	*Product*
Multimeter	Hewlett Packard 34401A
Oscilloscope	PicoScope 2204
Thermometer	RS-1316 [ITS-90]
Thermocouple	K-type thermocouple [IEC584 Class-1]

Table 43 Product name of the data acquisition systems used for the thermoelectric characterization test.

F.1 Data acquisition errors

The instrument/transducers introduce an inaccuracy into the system. The following table presents the inaccuracies for the instruments used in this test.

Measured variable [Range]	*Transducer used*	*Accuracy* $[\pm]$
Resistance $[100\ \Omega$ or $1\ k\Omega]$	Multimeter	$0.01\ \% + 0.004\ \%^*$
Voltage $[100\ mV]$	Oscilloscope	$3\ \%\ full\ scale + 200\ \mu V$
Voltage $[5\ V]$	Oscilloscope	$3\ \%\ full\ scale + 200\ \mu V$
Voltage $[100\ mV]$	Multimeter	$0.005\ \% + 0.0035\ \%^*$
Current $[10\ mA]$	Multimeter	$0.05\ \% + 0.02\ \%^*$
Current $[100\ mA]$	Multimeter	$0.05\ \% + 0.005\ \%^*$
Temperature	Thermometer	$0.05\ \% + 0.5\ ºC$
	K-type thermocouple	$1.5\ ºC$

Table 44 Measurement accuracies, with the instruments presented, for the variables needed in the test. *(% of reading + % of range) for 1 Year accuracy specification.

In addition for the total error added by the instrument the display resolution should be taken into account. We will consider the magnitude of the error to be equal to $\pm\frac{1}{2}$ of the last digit. (Coleman and Steele 2009). The display resolution values of the different instruments are presented in Table 45.

Measured variable [Range]	*Transducer used*	*Display resolution*
Resistance $[1\ \Omega]$	Multimeter	$10^{-3}\ \Omega$
Resistance $[1\ k\Omega]$	Multimeter	$10^{-2}\ \Omega$
Voltage $[100\ mV]$	Oscilloscope	$10^{-5}\ mV$
Voltage $[5\ V]$	Oscilloscope	10^{-5}
Current $[10\ mA]$	Multimeter	$10^{-4}\ mA$
Temperature	Thermometer. RS-1316	$0.1\ ºC$

Table 45 Display resolution of the different transducers used in the testing.

APPENDIX-G Thermocouple calibration for the thermoelectric characterization test

This appendix will expand on the numbers behind the calibration of the thermocouples and why it is beneficial for the final uncertainty of the test.

Uncertainty without calibration

For easier calculations, the $0.05\ \%$ value in error 1, from Table 6, is transformed to $1.3\ ºC$, for a measurement at around $25\ ºC$. The uncertainty equation for the temperature difference is equal to:

$$b_{\Delta T}^2 = \left(\frac{\partial \Delta T}{\partial T_1}\right)^2 b_{T_1}^2 + \left(\frac{\partial \Delta T}{\partial T_2}\right)^2 b_{T_2}^2 + 2\left(\frac{\partial \Delta T}{\partial T_1}\right)\left(\frac{\partial \Delta T}{\partial T_2}\right) b_{T_1T_2} = b_{T_1}^2 + b_{T_2}^2 - 2b_{T_1T_2} \quad (53)$$

In addition, all the error sources have been incorporated into the calculus, even though errors 3,4 and 5 are almost negligible compared to errors 1 and 2. The unfolding of the uncertainty equation is:

$$b_{T_1}^2 = b_{T_2}^2 = 1.8^2 + 1.5^2 + 0.1^2 + 0.1^2 + 0.05^2 \quad (54)$$

Obtaining,

$$b_{T_1} = b_{T_2} = 2.34\ ºC$$

Without calibration and taking into account that the measurements are done with the same thermometer but through different channels. And the thermocouple standard elemental error cannot be used as a correlated error because we cannot guarantee that both thermocouples were in the same batch for calibration. Then the correlated systematic error is zero.

$$b_{T_1T_2} = 0$$

And therefore,

$$b_{\Delta T} = 3.3\ ºC$$

Calibration procedure

Now, the benefit of the calibration procedure can be analysed quantitatively and compared to the non-calibration results. The calibration involvement can be model as

$$\Delta T^* = T_2 - T_1 - k(\bar{T}) \quad (55)$$

In which, ΔT^* is the adapted temperature difference due to the calibration and $k(\bar{T})$ represents the calibration constant. And it is also represented as

$$\mathrm{k} = T_2{}' - T_1{}' \quad (56)$$

$$\Delta T^* = T_2 - T_1 - k = T_2 - T_1 - (T_2{}' - T_1{}') \quad (57)$$

In which $T_2{}'$ and $T_1{}'$ are the temperatures of the thermocouples while calibrating.

The nature of the temperature difference equation allows eliminating the systematic errors present in the calibration and test measurement. Subtracting the same quantity of error eliminates the error. Proof will be provided using the general equation of inaccuracy analysis. For that purpose the analysis only needs the error generated by the thermocouple standard.

$$b_{T_1} = b_{T_2} = b_{T_1'} = b_{T_2'} = 1.5$$

We should take into account that the correlated terms, T_1 and $T_1{}'$ suffer the same error, and T_2 and $T_2{}'$ suffer the same error. Taking into account the derivatives, we find that the total correlated term for the final temperature difference uncertainty is:

$$b_{correlated} = 2\left(\frac{\partial \Delta T^*}{\partial T_1}\right)\left(\frac{\partial \Delta T^*}{\partial T_1{}'}\right) b_{T_1 T_1{}'} + 2\left(\frac{\partial \Delta T^*}{\partial T_2{}'}\right)\left(\frac{\partial \Delta T^*}{\partial T_2}\right) b_{T_2{}' T_2} \tag{58}$$

$$b_{correlated} = -2b_{T_1 T_1{}'} - 2b_{T_2{}' T_2}$$

With

$$b_{T_1 T_1{}'} = b_{T_2{}' T_2} = (1.5)^2$$

Adding all these terms into the general uncertainty equation of the modified temperature difference we obtain that the thermocouple standard calibration uncertainty is eliminated.

$$b_{\Delta T^*}^2 = 4b_{T_1}^2 + b_{correlated} = 0$$

It needs to be remarked, again, that this happens with every systematic error that is present in both calibration and test. Therefore, both calibration error sources 1 and 2 are eliminated from the calculus. However, as two measuring processes are present for the final obtainment of the temperature difference, we have to take into account two times the random error of measuring the temperature difference.

APPENDIX-H Thermal uncertainties in the thermoelectric characterization test.

There are three identified conceptual uncertainties that affect the thermal difference measurements. The following appendix presents the uncertainties and provides with the rationale for their estimation.

H.1.1 Thermal contact conductance error

Imperfections on the surface of solids increase the resistance to heat transfer. Heat transfer is produced through contact with conduction and through void volumes with radiation and convection. The contact heat transfer resistance produces an uncertainty for the test set-up. Specifically in the thermocouple and the thermoelectric generator contact with the plates. The final aim for the designer of the test is to reduce these thermal contact resistances apart from estimating its final uncertainty.

Two methods are identified to decrease the thermal contact resistance. First, pressure application increases the contact area of the interface. Second, thermal paste fills the gaps of the interface. For pressure application the set-up will use bolts. Two bolts are not enough because they don't provide a distribute pressure in all the heat transfer area, so four bolts are needed. However, in the end, when thermal paste is applied, the bolts function is to keep the system together. To calculate the thermal contact conductance we will use the heat transfer equation, (Madhusudana)

$$h = \frac{Q/A}{\Delta T} \tag{59}$$

In which, h is the before-mentioned thermal contact conductance, Q is the total heat flow, A is the nominal contact area and ΔT is the temperature difference in the contact interface. The thermal conductance used for a bolted contact of two aluminum plates is taken from (Yeh, Wen et al. 2001) and it covers a range of $[3 - 40\frac{kW}{m^2K}]$[††]. While the thermal conductance of a common thermal paste is equal to $450\frac{kW}{m^2K}$ (FischerElektronik). The thermal resistance for the TGP-651 is equal to $\frac{28K}{W}$ (MicroPelt), and for a temperature difference of $2\,K$ we obtain a total heat flow of $0{,}07\,W$. With this heat flow we can obtain the total temperature difference lost in both cases, as presented in the following Table.

Parameters	*Bolted-junction*	***Thermal paste***
Thermal contact conductance	$[3 - 40\frac{kW}{m^2K}]$	$450\frac{kW}{m^2K}$
Temperature difference in interface 1 ($\boldsymbol{A = 70.9\,mm^2}$)	$[0.33 - 0.025\,]\,K$	$2.2 * 10^{-3}\,K$
Temperature difference in interface 2 ($\boldsymbol{A = 130\,mm^2}$)	$[0.18 - 0.015\,]\,K$	$0.001\,K$

Table 46 Temperature difference due to thermal contact resistance for bolted-junction and thermal paste use for its application between the thermoelectric generator package and the aluminum plates.

With the values calculated, the final uncertainty of a bolted-junction set-up is estimated to be $\pm 0.5\,ºC$ while for thermal paste is equal to $\pm 0.003\,ºC$. The other thermoelectric component, ET20.68, also suffers from the same problem. Its extremes are of a certain kind of ceramic, so the values for the bolted-junction conductance differ to the ones of aluminum to aluminum. However, due to the clear advantage of the thermal paste, the uncertainty gain is not presented.

[††] The thermal conductance values of the bolted-junction are estimations. The values presented are from an experiment between aluminum alloys (6061-T6) jointed by bolts. However, our test does not follow those conditions. Despite that, as an estimation, the values can be used.

H.1.2 Thermal spatial variation error

In-situ measurements are difficult to achieve. Normally, the measurements are done close to the desired location so the measurement differs from the real value. The thermocouples are not placed exactly at the walls of the thermoelectric generator module. Therefore, the values obtained are not exactly what we require for the final calculation of the Seebeck effect. To estimate the temperature difference uncertainty we need the thermal conduction equation:

$$\Delta T = \frac{qL}{kA} \tag{60}$$

In which, q is the heat transferred through the thermoelectric package, k is the thermal conductivity of the aluminum plates, ΔT is used as the estimated temperature difference between the TEG extremes and the position of the thermocouples, and L as the distance from the extremes of the TEG to the thermocouples.

For the conductivity of the aluminum plates, as we don't know their exact composition, we will use values of $[150 - 250]\frac{W}{mK}$. However the smaller value is more conservative. The values used for the calculation are $q = 0.07\,W$, $A = 71\,mm^2$, and $L = 5\,mm$, which correspond to the heat going through the TGP-651 module, the smallest interface of the module, and a conservative distance between the thermocouple drilled hole and the extreme of the interface. With that we obtain a temperature difference of $\Delta T = 0.032\ ºC$. Multiplying that by 2 we obtain the total uncertainty caused by the two thermocouple measurements.

H.1.3 Thermal Non-Uniformity error

A thermoelectric module consists of interconnected thermoelectric pairs. These thermoelectric pairs are subject, individually, to the Seebeck effect. Therefore, each thermoelectric pair suffers a different temperature difference. Each individual voltage adds up to the whole system. The thermoelectric module is not perfectly isolated laterally. Therefore apart from the main heat path from aluminium plate to aluminium plate there is a lateral heat loss in the form of convective transfer. In addition, the aluminium plates will suffer the same effect, adding to the total non-uniformity of the thermoelectric module, due to their conductive heat transfer. The module temperature non-uniformity generates incongruences of the measured values. The measured voltage is the average of all the different temperature differences found in the module. Therefore the measured temperature difference is local.

In the end, maintaining a uniform temperature in both sides of the module provides higher output values. (Admasu, Luo et al. 2013)And maintaining a uniform temperature allows correlation with the model foreseen. To reduce this uncertainty, thermal insulation is added to the lateral walls of the system reducing lateral heat paths. The total uncertainty of this error would be considered as incorporated into the spatial variation error. This is because ultimately, the position that the thermocouple is in will provide also with the non-uniform error for the lateral measurement.

APPENDIX-I Rejection of outliers

The following appendix presents Chauvenet's criterion for statistically reject outlier data points. In addition it presents the application of this criterion in the different sets of data of the project. The Chauvenet's criterion is needed to reject data points that have a significant effect to the statistical values and they are assumed to be random in nature.

8.1.1 Chauvenet's criterion

The Chauvenet's criterion first considers that the whole data set corresponds to a normal distribution. Then the criterion specifies that all points within a probability of $1 - 1/(2N)$ should be retained. With this in mind we obtain that the maximum deviation allowed away from the mean is equal to(Coleman and Steele 2009):

$$\Delta X_{max} = s_X * \tau \tag{61}$$

In which, ΔX_{max} is the maximum deviation from the mean, s_X is the standard deviation and τ is the non-dimensional deviation, which can be obtained from a Gaussian probability table. As an example, in the calibration of the thermocouples for the temperature difference a difference of 4 ºC of temperature was obtained. It was considered spurious following the Chauvenet's criterion as its closest data points were both sentencing 0 ºC and the average temperature difference was also around 0 ºC.

APPENDIX-J Comparison of the different Power converter modules

The values obtained for the test of the Protoboard power converter module and the PCB module are presented in this Appendix.. The main aim of this Appendix is to support the statement that the manufacturing of the circuit is important for the performance of the module without overloading too much the thesis document. The protoboard module tested can be seen in the following pictures.

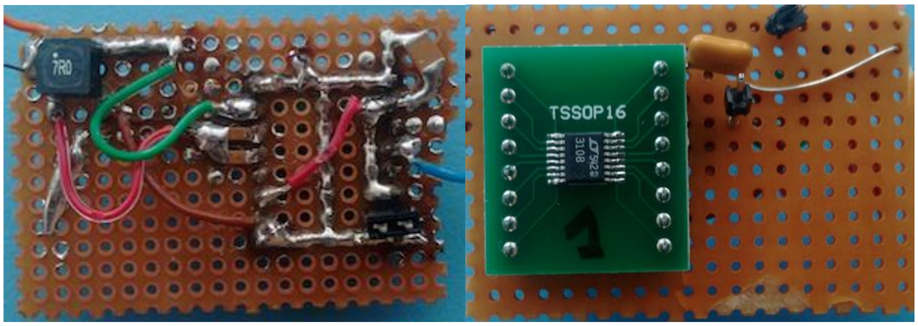

Fig. 34 Photos of the Power converter module protoboard

Three different Power Converter modules have been manufactured. The Protoboard was the first one, to assess if the module would work. After favourable results, the aim was to reduce the size of the module and to encompass all into a PCB. To reduce risk, due to the lack of experience in PCB design, two PCBs were designed and ordered. One, the smaller, with a more requiring design, and space constrained. The second one, bigger, and with a less complicated design. Both of them work but the big one was not tested in detail, due to time constraints, to evaluate what is the difference in performance. In the end, the protoboard module was used for the final test as the PCBs were designed to provide 3.3 V output values. The protoboard allows to change easily the selected output voltage. The PCBs should have been designed with a selectable interface.

J.1 Performance Values

One of the most important representations of the performance difference is the reduction of advertising events as it can be seen in the following figure.

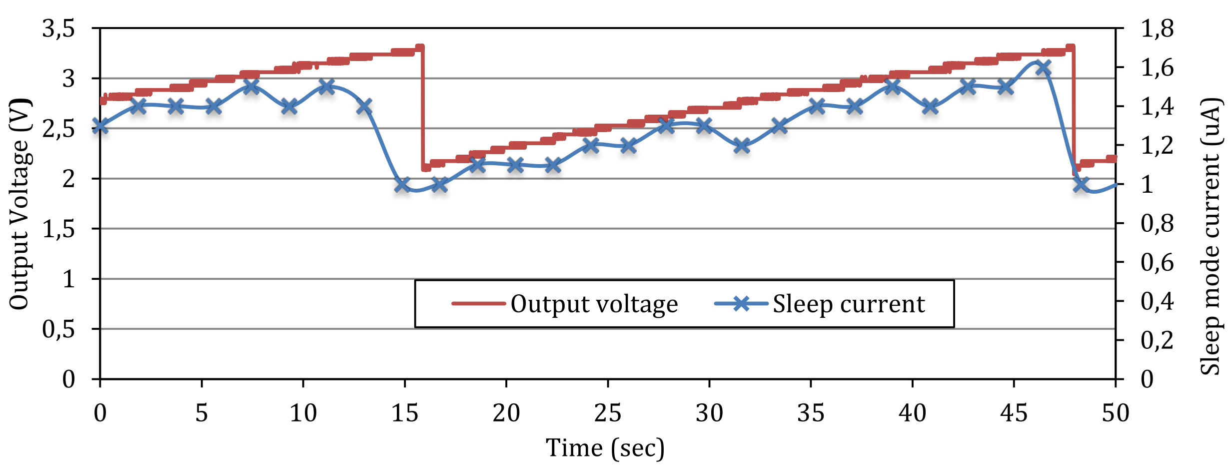

Fig. 35 Representation of the Sleep current and the output voltage in time for the Protoboard module

Two advertising events can be done in a period of 50 seconds compared to three events with the PCB. Other values can be presented alongside to the values of the PCB module to clearly see the differences of performance.

Test ref.number	*Protoboard*	*PCB*
TEG Voltage $(mV)^*$	55.6	55.2
Input Voltage $(mV)^*$	33.6	29.2
Input Current (mA)	4.4	5.3
Input Power (μW)	149.4	154.8
Output Power 2 V $(\mu$W)	23.0	34.8
Output Power 3.3 V (μW)	37.8	49.6
Efficiency	$[0.15 - 0.25]$	$[0.22 - 0.32]$

Table 47 Set of values obtained from the test of two different Power converter module's, the optimized product (PCB) and the starting and ending product (Protoboard).

Both of the modules get similar power, the PCB uses higher current and the Protoboard uses higher voltage. However, the output power is higher with the PCB. It is considered, as said in the main report that this can be because of parasitic elements in a less tuned and well manufactured design.

APPENDIX-K BLE113 Sleep modes power consumption

The current profiles for the advertising event are presented coming from different sleep power modes. All the graphs represent the same operation but with a different sleeping mode selected.

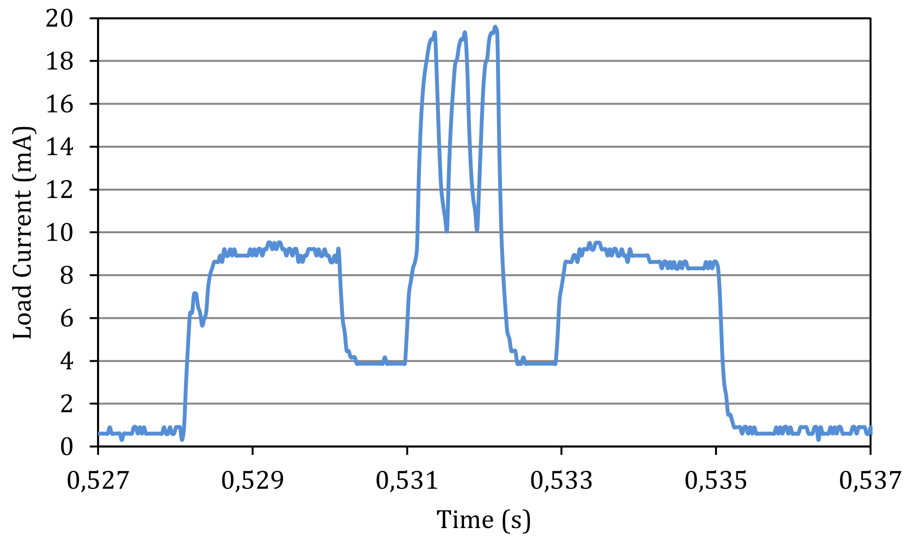

Fig. 36 Advertising event coming from Power Mode 1 (PM1)

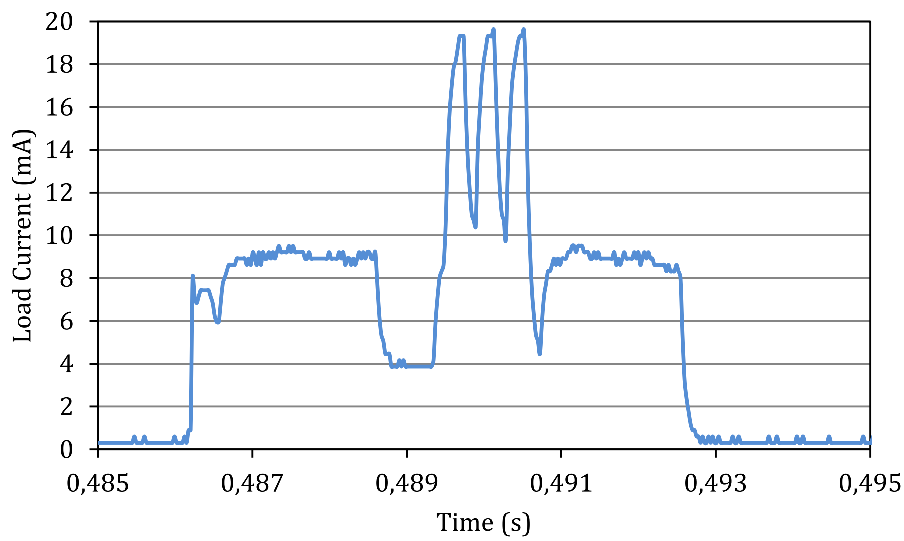

Fig. 37 Advertising event coming from Power Mode 2 (PM2), the sleep mode used for this project.

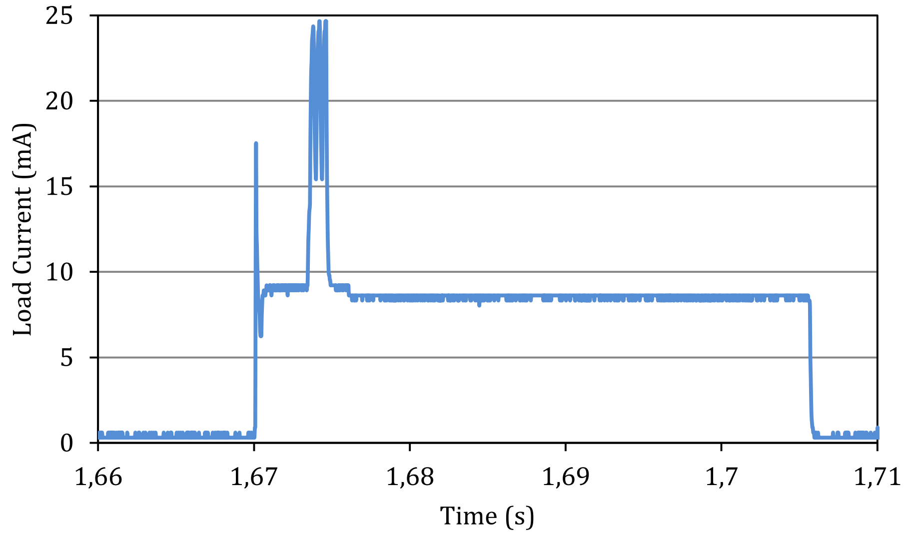

Fig. 38 Advertising event coming from Power Mode 3 (PM3)

It can be seen that the advertising profiles obtained after PM1 and PM2 sleep modes are similar. Even though, the total current consumed in sleep mode for PM1 is higher than PM2. Therefore, PM2 is selected. It can also be seen that PM3 advertising event requires more energy than PM2 advertising event. This means that a lower power consumption during sleep mode has been achieved but by requiring more energy in the active event. For this project, Power Mode 2 is selected due to its lower energy required for advertising. PM3 would only be beneficial for very small duty cycles and long periods of use in which the power source is a battery. It is expected that what is lost in the active event could not be gained in the sleep mode, in terms of time, for an application using a self-powering technique that charges a storage element.

APPENDIX-L Functionalities of the BLE113 software implemented in the module.

This Appendix presents the code used in the BLE113 module. The code enables the wake-up GPIO, the temperature measurements, and modifies parameters to achieve the lowest known power consumption to obtain the lowest known power consumption and to unable the wake up GPIO and the temperature measurement. The code is based on BGScript and event-programming scripting language used by some of the Bluetooth modules of the manufacturer.

The following code starts the module and defines the conditions of the GPIOs, and the advertising data characteristics. The event *system_boot* occurs everytime that there is a restart of the module.

```
dim celsius
dim offset
dim tmp(5)
# !!!!!!!!!!!!!!!!!!!!!!!!!!!!!!!!!!!!!!!!!!!!!!!!!!!!!!!!!!!!!!!!!!!!!!!!!!!!!!
# NOTE: the data you put in either the main advertisement packet or the scan
# response packet cannot exceed 31 bytes in length. This is a BLE protocol
# limitation. Any data that is longer than this will be truncated.
# !!!!!!!!!!!!!!!!!!!!!!!!!!!!!!!!!!!!!!!!!!!!!!!!!!!!!!!!!!!!!!!!!!!!!!!!!!!!!!

event system_boot(major, minor, patch, build, ll_version, protocol, hw)
    # ------------------------------
    # build custom advertisement data
    # ------------------------------
    # To stop the LED to blink and to reduce power leakage through GPIOs
    call hardware_io_port_config_direction(0, $0)
    call hardware_io_port_write(0, $ff, $00)
    #call hardware_io_port_config_direction(1, $3)
    call hardware_io_port_config_direction(1, $0)
    call hardware_io_port_write(1, $ff, $00)
    call hardware_io_port_config_direction(1, $3)
    call hardware_io_port_config_direction(2, $0)
    call hardware_io_port_write(2, $ff, $00)

    #GPIO interrupt code
    call hardware_io_port_config_irq(0,$4,0)
    # set custom advertisement data
    call gap_set_adv_data(0, 13, adv_data(0:13))
    # set advertisement characteristics
    call gap_set_adv_parameters(32, 32, 7)
    # timer to go to sleep mode
    call hardware_set_soft_timer($21,1,1) # 0x148 =
end
```

The next code presents two more events needed for operation. The event *hardware_io_port_status* gurantees that when there is a raising edge to the interrupt pin the module will start measuring the temperature of the controller. In addition, the *hardware_soft_timer* event guarantees that the module stops advertising and goes into a low consumption mode.

```
event hardware_io_port_status(timestamp, port, irq, state)
    # event activated when the GPIO is activated through a rising edge
    # -----
    # hardware_adc_read (14,3,X) reads the internal temperature in the CC2541
    call hardware_adc_read(14,3,0)
end

event hardware_soft_timer (handle)
    #if handle = 1 then
    call gap_set_mode(0,0)
    #end if
end
```

The following part of the code consists of the event *hardware_adc_result*, activated when an ADC measurement occurs. It adapts the result directly obtained by the module to be able to send it through the advertisement event. After that, it activates the advertising mode and sets the timer to go again to low power state mode.

```
event hardware_adc_result(input, value)
    # event activated when the internal temperature is activated
    # -----
    #ADC value is 12 MSB
    offset= -1845
    #celsius = value / 16
    celsius = value / 16
    adv_data(11:4) = celsius

    #Calculate temperature
    #ADC*V_ref/ADC_max * T_coeff + offset
    celsius = (10*celsius*1240/2047)* 10/45 + offset

    # 0 = Temperature value is on Celsius scale
    tmp(0:1)= 0

    # Convert to IEEE 11073 32-bit float
    tmp(1:4) = float(celsius, -1)
    #tmp(1:4) = celsius
    adv_data(0:4) = tmp(1:4) #

    # set custom advertisement data
    call gap_set_adv_data(0, 4, adv_data(0:4))
    # start advertising
    call gap_set_mode(gap_user_data, gap_non_connectable)
    # set timer to go to sleep mode
    call hardware_set_soft_timer($21,1,1) # 0x148 = 328; Time=10ms (32768Hz )
    # 0x50 = 80; Time=2ms (32768Hz ) #0x21=33; TIME=1ms
end
```

In addition in the *hardware.xml* document the following line should be implemented for not allowing the Bluetooth module to go to the power saving mode 3.

<sleep enable="true" max_mode="2" />

And the ports should be initialiated in the file *hardware.xml* with the following statements:

<port index="0" pull="down" tristatemask="0" />
<port index="1" pull="down" tristatemask="0" />
<port index="2" pull="down" tristatemask="0" />

APPENDIX-M Establishing the power requirements per byte of information transmitted through BLE advertising.

Two case scenarios have been considered to measure the different energy required depending on the size of the payload data. The first case sends a total of 1 byte of useful data and the second case sends 31 bytes, the maximum amount. The values have already been presented previously. This appendix presents the current profile of these two cases to graphically see the increase in transmitting time.

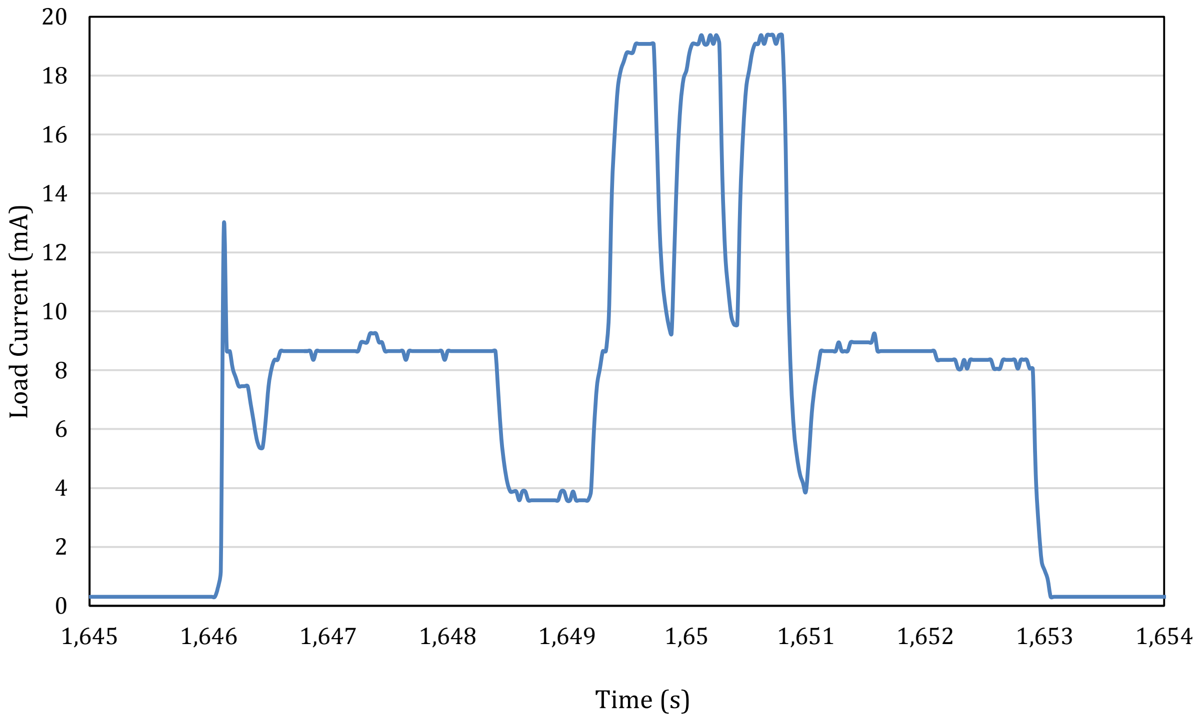

Fig. 39. Current going through the shunt resistor for the BLE113 characterization test for the case in which 31 bytes are sent via advertising. The graph represents a total time of 9ms.

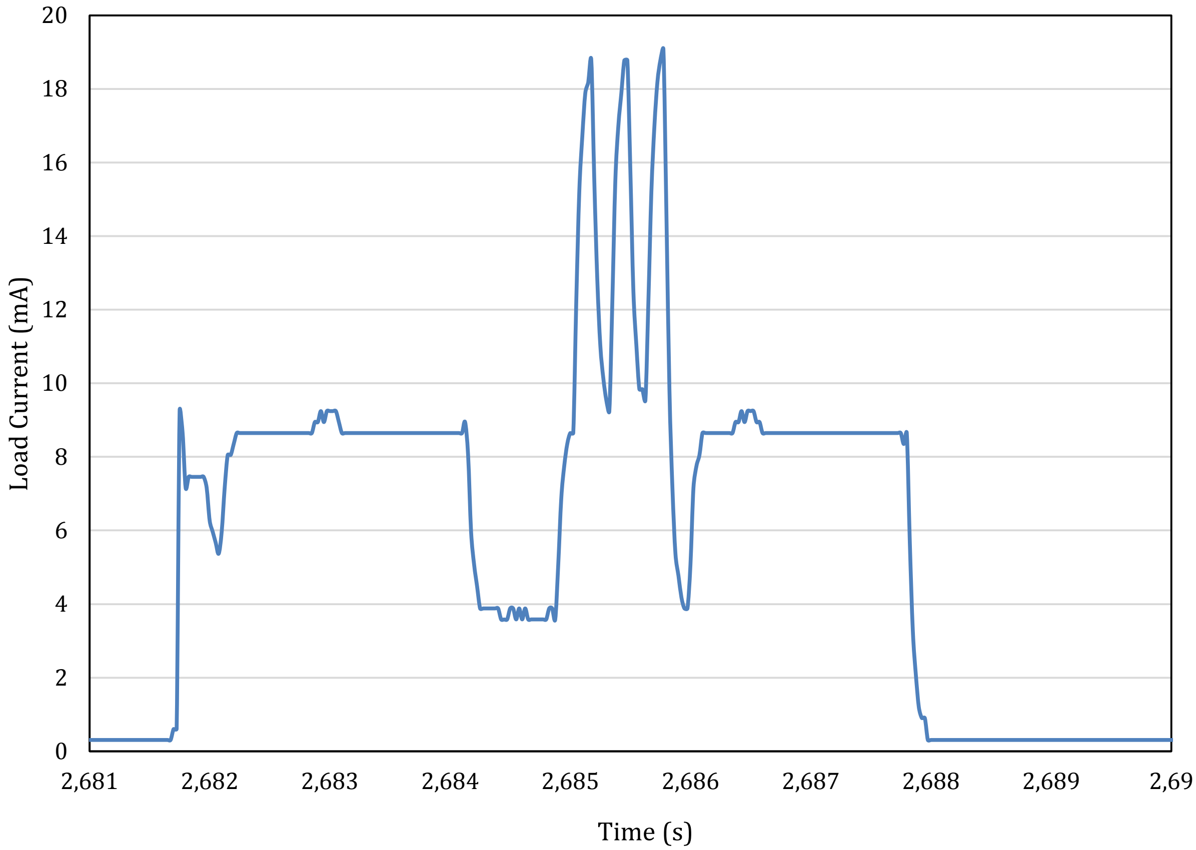

Fig. 40 Current going through the shunt resistor for the BLE113 characterization test for the case in which 31 bytes are sent via advertising. The graph represents a total time of 9 ms.

APPENDIX-N Images and dimensions of the temperature sensor used in Delfi-n3Xt

This appendix presents the pictures and dimensions of the conventional temperature sensor used as a size reference for the assessment of the final autonomous design.

The dimensions of the sensor are the following:

Parameter	*Value*
Temperature sensor PCB(mm)	$20.0\ x\ 20.0\ x\ 2.9$
I2C connector (mm)	$14.0\ x\ 5.4\ x\ 8.0$
Wires (mm)	$Dependent\ on\ location$

Table 48 Dimensions for the conventional temperature sensor used in Delfi-n3Xt.

The following images present first the PCB temperature sensor and then the integration of one of the sensors in a CubeSat wall structure. The connector can be seen in Figure 42.

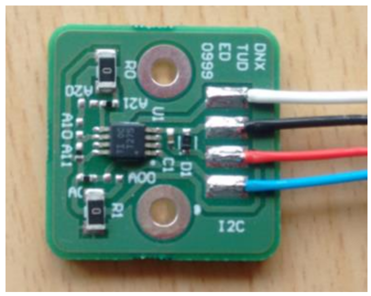

Fig. 41 Conventional temperature sensor used in Delfi-n3Xt.

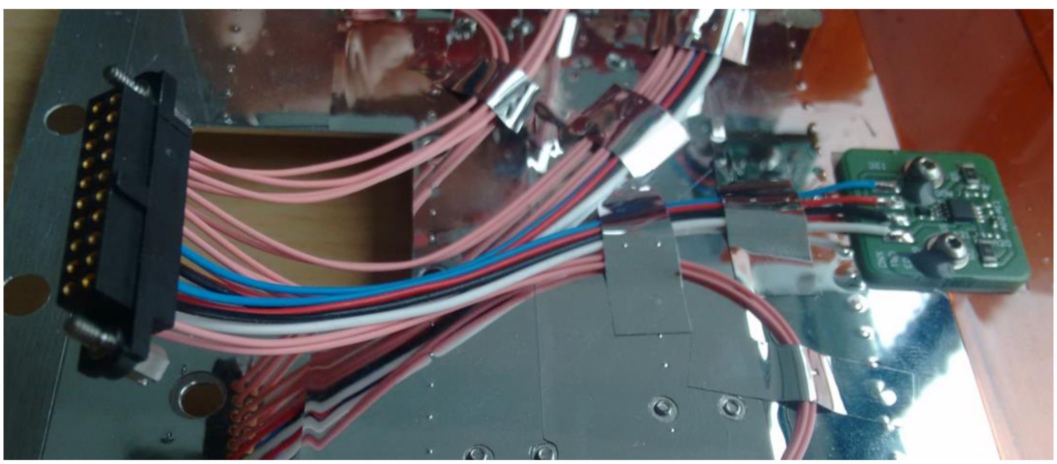

Fig. 42 Integration of the temperature sensor and connector used for data communication.

APPENDIX-O Paper Submisssion to the IAC-2017

The following pages contain the paper to be presented in the 68th International Astronautical congress 2017, the 25-29 of September and organised by the International Astronautical Federation (IAF) in Adelaide, Australia.

IAC-17,B4,6B,15,x40480

Thermoelectric harvesting for an autonomous self-powered temperature sensor in small satellites

Jorge Machin Llanos[a]*, Jasper Bouwmeester[b]

[a] *Delft University of Technology (TU Delft), The Netherlands,* J.MachinLlanos@student.tudelft.nl
[b] *Delft University of Technology (TU Delft), The Netherlands,* jasper.bouwmeester@tudelft.nl
* Corresponding Author

Abstract

There are several benefits of using autonomous sensors in spacecraft. Avoidance of wired connections reduces cost, mass, and increases the flexibility and reliability of the system. The impact of wire reduction can be significant, especially for small satellites with many sensors, like temperature and sun sensors. Previous research has already focused on wireless intra- spacecraft communications. This research tests the self-powering capabilities of a system based on a COTS thermoelectric generator connected to a Bluetooth Low energy communication system, with a built-in controller and temperature sensor, and a power management interface. The system will be considered as a candidate for an autonomous temperature sensor in a future PocketQube mission of Delft University of Technology.

Controlled temperature differences can be achieved in a test environment, allowing the measurement of the generator power capabilities. It is tested that the system requires, for operation, a minimum temperature difference of 2.31 K between the extremes of the thermoelectric generator. It generates a peak power of 234 uW for that difference. In addition, the voltage difference obtained of 35.5 mV exceeds the minimum voltage required by the power management subsystem to be used. The power management sub-system consists of an ultra-low power converter that provides an output voltage of 4.1 V and a measured power efficiency of 32 % Moreover, thanks to the management of the Blutooth sleeping modes, with the built-in controller and several operational amplifier comparators, an average power consumption of 5 uW is required during operation. The case studied would allow measuring temperature and sending the data over a Bluetooth link to the on-board computer every 16.2 seconds

It is concluded that the technology, based on COTS components, can be implemented and considered as the first step for a fully autonomous sensor with thermoelectric power generation in small satellites. Its implementation may provide substantial advantages for remote or/and locations where wiring is difficult to integrate. The tested performance values provide the foundation to develop the technology further.

Keywords: PocketQube, Thermoelectric harvesting, wireless intra-spacecraft communication, autonomous sensor

Nomenclature

α	Seebeck coefficient (mV/K)
π	Peltier coefficient (V)
ΔT	Thermoelectric generator temperature difference (K)
b	Systematic uncertainty
D	Duty cycle
I_{TEG}	Current through the TEG
t_{ON}	Time sensor is ON
T	Sensing period
T_h	Hot side temperature
R_i	Internal TEG resistance (Ω)
R_L	Load resistance (Ω)
$\dot{Q}_P$	Heat produced due to Peltier effect
V_{TEG}	TEG voltage produced

Acronyms/Abbreviations

BLE	Bluetooth Low Energy
COTS	Commercial off-the-shelf
GEO	Geostationary Orbit
LDO	Low dropout linear regulator
PM	Power Management
SoC	System on Chip
TEG	Thermoelectric generator
TU-Delft	Delft University of Technology

1. Introduction

Space missions benefit from the use of smaller, faster-to-develop, and cheaper spacecraft. A reduction in system size and an improvement in integration can be fulfilled with the use of self-powered autonomous sensors instead of wired sensors. Compared to batteries they can last for longer mission times. In addition, new technology concepts, as sensors in remote or unreachable locations, can be envisioned thanks to the elimination of wires. An autonomous sensor is characterized by its wireless intra-spacecraft communication module and its self-powering module.

Several researchers have already spotted the benefits of using wireless intra-spacecraft communication [1][2][3]. The main benefits can be summarized as a reduction in mass, space, and complexity, failure isolation, and flexibility increase. Energy harvesting is related to these benefits in the same way, as it is used to eliminate harness.

Research on the self-powering field for satellites has already been carried by companies and research institutions. Analysis has already been made on the introduction of thermoelectric harvesting and radio frequency harvesting for the exterior part of a GEO broadcasting satellite. [4] [5]. A piezoelectric harvesting design has been tested to obtain energy from the micro jitter of external components of the satellite [6]. An autonomous sun sensor was designed and tested in a Cubesat mission [7]. And TEGs will be space characterized to obtain in-space performance for a future application in a mission [8].

However, no research has focused on the design and testing of a complete internal self-powered autonomous sensor for a small satellite, using COTS components. This kind of research would identify possible showstoppers and it would be used as a reference for future analysis and applications. This research characterizes the performance of the modules required on a future thermoelectrically powered autonomous sensor for small satellites. The design aims for small design volume and for the smallest operational temperature difference.

The research focuses on its possible inclusion of a proof-of-concept in the next TU-Delft mission, the Delfi-PQ, the first PocketQube mission after a long heritage in Cubesat technology [9].

This paper starts with some theory on thermoelectric energy harvesting, in Section 2, and the presentation of the envisioned and tested system, in section 3. In section 4, the test set-ups are discussed.. Afterwards in Section 5, the results of the different characterization tests are presented. In the end, in Section 6, the conclusions and recommendations are given.

2. Thermoelectric harvesting theory

The working principle of a thermoelectric generator device is the so-called Seebeck effect, electrical power is generated when there is a temperature gradient between two in contact dissimilar conductors. The effect can be modelled as follows,

$$V_{TEG} = \alpha \Delta T \qquad (1)$$

Another thermoelectric effect needed for the heat balance equation of the module is the Peltier effect. It states that when there is a voltage difference there will always be heat generated. The effect is modelled as follows,

$$\dot{Q}_P = \pi * I_{TEG} = \alpha T_h I_{TEG} \qquad (2)$$

In addition, the current and the power provided to the load can be obtained with equation (1) and Ohm's law,

$$I_{TEG} = \frac{\alpha \Delta T}{R_L + R_i} R_L \qquad (3)$$

$$P_{out} = VI = \frac{(\alpha \Delta T)^2}{(R_L + R_i)^2} R_L \qquad (4)$$

3. Self-powered autonomous sensor design

An autonomous sensor is able to be self-powered as it stays in sleep mode most of the time. Therefore, its most important characteristic is its duty cycle, presented in (5).

$$D = \frac{t_{ON}}{T} = \frac{advertising\ time}{advertising\ time + charging\ time} \qquad (5)$$

The active time or advertising time represents the time required for sensing, controller operations and transmitting the information. The powered subsystem has three possible roles, initialization, active mode also called advertising mode, and sleep mode. The charging time is from an advertising event until the capacitor stores enough energy for another active process.

The self-powered autonomous sensor is composed of 5 subsystems. The powering subsystem (thermoelectric generator), the power management subsystem, the communications subsystem, the sensor, and the controller. The different modules are presented in Figure 1.

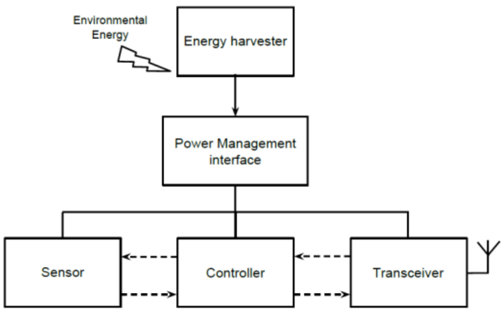

Figure 1. Sketch of the system modules.

3.1 The powering subsystem

Powering is provided by a COTS thermoelectric module. The thermoelectric module selected is the ET20,68,F1A,1313,11 from LairdTechnologies. It has been selected after a trade-off between the known-available commercial options seeking high Seebeck coefficient and low internal resistance. The TEG performance specifications are presented in Table 1.

Table 1. Specifications of the thermoelectric generator.

Specifications of TEG	Value
Internal resistance	3.55 Ω
Maximum heat generated	9.3 W
Maximum current	2.0 A
Maximum temperature gradient	67.0 K
Seebeck Coefficient	25.5 mV/K
Dimensions	13.2 x 13.2 x 2.2 mm

3.2 The communications subsystem

Previous research compared different wireless communication protocols for intra-spacecraft communication. The conclusion is that Bluetooth Low Energy has better power consumption characteristics per transmitted bit for data bus communication compared to Wi-Fi and ZigBee communication [10] . The research in this paper departs from these conclusions. Consequently, the BLE113 module is selected. It has a low average communication power and it includes a temperature sensor and a microcontroller, lowering the complexity of its integration in a system.

The method for data communication selected is the “advertising” mode of Bluetooth. In this mode, the transmitter broadcasts data to a non-specified receiver. It does not require pairing of the Bluetooth devices and the communication is only one-way. Advertising produces the lowest power consumption and the easiest implementation for data packets limited to less than 31 bytes. Its disadvantage is that one-way communication yields a less robust data link compared to communication which is checked and acknowledge for potential retransmission. The BLE module performance specifications are presented in Table 2.

Table 2. Specifications of the Bluetooth low energy module, the BLE113.

Specifications of BLE113	
TX current	18.2 mA (0 dBm)
RX current	14.3 mA
Sleep mode current	1 µA
Input voltage	2.0 – 3.3 V
Size	9.15 x 15.75 x 2.1 mm

3.3 The power management subsystem

The power management module is divided into two sections. The first section consists of a voltage step-up converter as the voltage input values required by the powered components are higher than the ones provided by the TEG. The design is based on the LTC3108 and follows the manufacturer design guidelines for the additional components needed. The full section is presented in Figure 2. The datasheet specifies that the converter design is able to generate outputs of 3.3 V with a minimum input voltage of 20 mV. Therefore, a minimum temperature difference of 2 K would be required for the voltage conversion.

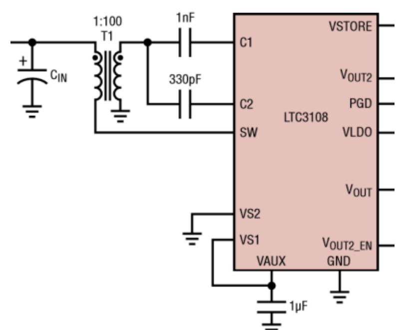

Figure 2. Recommended components connected to the LTC3108 for ultra-low input voltage levels. Image from Datasheet.

Several additional functionalities are implemented in the converter. The design uses the LDO, with an output of 2.2 V, used to provide a stable, constant, reference to the control segment of the power management subsystem.

In addition, the module requires a storage system to be able to provide energy for the power bursts. The energy used for the advertising events, peak power consumption when the sensor system should become active is provided with the energy stored in a capacitor. The capacitance used of the storage capacitor is 22 mF for testing purposes and does not represent the optimal required capacitance. The other important parameter of the output capacitor is the current leakage, as it will increase the total charging time. The current leakage value of the capacitor corresponds with the average value found in the COTS capacitors. The specifications of the power converter and the storage component are presented in Table 3.

Table 3. Specifications of the power conversion section of the power management module, mainly considering the output capacitor and the LTC3108.

Specifications of converter	
Input resistance	5 Ω
Minimum input Voltage	20 mV
Size	30.0 x 32.0 x 6.0 mm
Power Efficiency	20%-40 %
Capacitor current leakage	5 µA

The second section consists of a logic control system. The first requirement of this section is to provide a constant output voltage to the powered items. This is provided by a Low Drop-out linear regulator with a reduced quiescent current. The LDO contains also a switch that is activated when enough energy to complete the initialization mode is stored. Then, it should remain open, to sustain the sleep mode. This type of control is obtained with a non-inverting Schmitt trigger. The final functionality is to provide a signal for entering active mode. This is controlled with a non-inverting operational amplifier comparator. The circuit encompassing all these functions is presented in Figure 3.

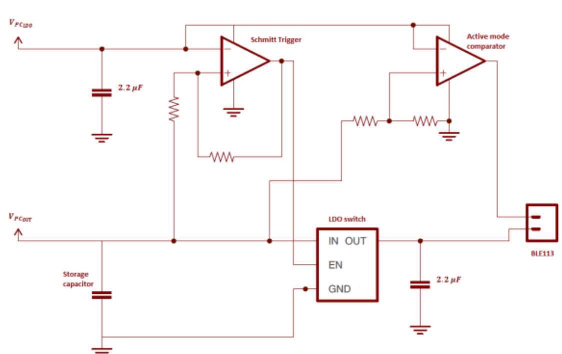

Figure 3. Circuit for the power control system.

In addition, the time diagram schematic of the system is presented in Figure 4. The initialization energy discharge is bigger than the one required for the active modes. Therefore, the Schmitt trigger should be activated before the advertising comparator because a positive signal into the BLE113 consumes enough energy to not allow to charge the storage component and so not start with the initialization process.

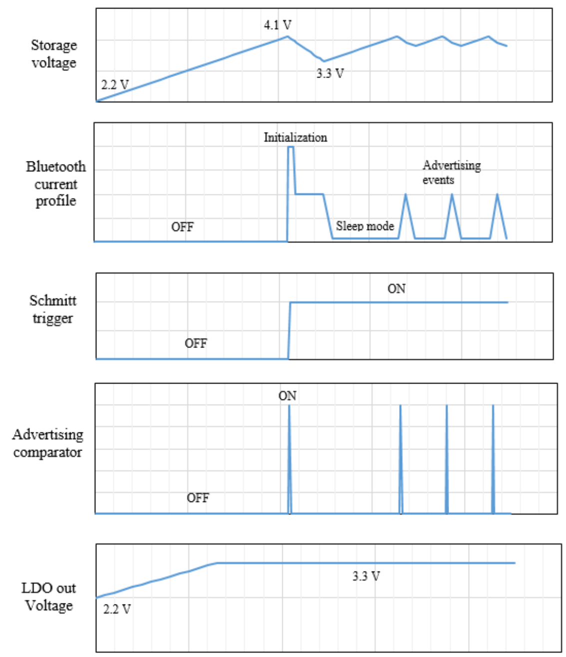

Figure 4. Time scheme of the control segment of the power management subsystem. .

3.4 The controller

The BLE113 embedded controller, the CC2541, is used as the main controller of the system. This decision simplifies the system and allows easier integration than using an external controller.

3.5 The temperature sensor

The temperature sensor used is the embedded sensor in the BLE controller, the CC2541 with an accuracy of ± 2 degrees after one-point calibration. It serves its purpose for a proof of concept application.

4. Test setup

The full system is tested in a modular fashion, each independent module is characterized first, before the connection to the full system.

4.1 Thermoelectric characterization test.

The thermoelectric generator is characterized with its IV- curve and Power curve. Power, voltage and current are measured through different load values (18Ω, 10Ω, 3.3Ω, 2Ω) for a temperature difference of 2 K. The voltage through the load is measured which allows calculating the current with Ohm's law.

Figure 5 presents a scheme of the set-up used for obtaining a known temperature gradient across the TEG. A heater is used to control the temperature difference.

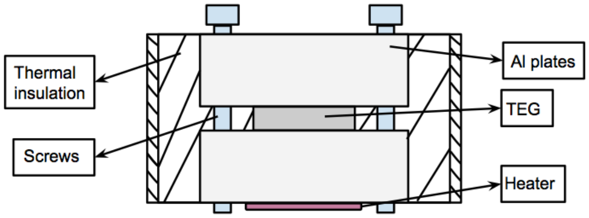

Figure 5. Thermoelectric characterization test set-up.

Thermocouples, impregnated in thermal paste, are introduced into drilled holes in both of the Al plates to measure the temperature difference. The measurement's main sources of uncertainty are presented in Table 4. They have been mitigated to guarantee successful results.

Table 4. Error sources of the measured temperatures considered as the extreme temperatures of the TEG

Elemental error sources	$b\ [T_1 \ \&\ T_2]$
1. Thermometer specification	$T * 0.05\ \% + 0.5\ ºC$
2. Thermocouple standard	$1.5\ ºC$
3. Thermal contact resistance	$0.003\ ºC$
4. Spatial variation	$0.032\ ºC$

The thermal contact conductance problem is improved with the use of thermal paste between the Al plates and the module. The non-homogeneity of the thermoelectric pairs inside the module is reduced by encircling the module with a thermal insulation foam. The spatial variation of the position of the thermocouple measurement and the real position that the TEG considers in the model is considered as part of the error sources of the test

A calibration can be done to eliminate error source 1 and 2. Both thermocouples are positioned in contact with each other and the difference of temperature is determined. This difference is taken into account for corrections of the final measured values.

4.2 Bluetooth low energy characterization test

For this test, the BLE is connected through an independent power source and a shunt resistance to measure the current consumption. The shunt resistance used is equal to 15 Ω. Lower resistance would lower the accuracy of the measurement. Higher resistances would increase the voltage difference between the powering voltage and the input voltage seen by the BLE.

4.3 End-to-end design performance test

The main goal of this test is to obtain performance measurement for the full design. The overall performance and the proof of design is obtained with the temperature difference measurement and the power obtained in the storage capacitor that ultimately is represented by the advertising period.

The test set-up consists of the connection of the full system. The thermoelectric generator is connected to the power converter with an output capacitor of 1uF. The power converter output is then connected to the storage capacitor and its LDO output to the components specified in Figure 3.

5. Test Results and Discussion

5.1 Thermoelectric characterization results

The main aim of this test is to verify the TEG model and the product parameters, in addition to obtain a controlled and accurate testing environment for temperature differences to use in future experiments with the full system.

Figure 6 compares the model values with the measured test values. The model values are obtained with equations (3) and (4). The test values correspond to the average, data points marked with a cross, of 3 different tests. It can be seen that there is a good correlation between what is expected and what is measured..

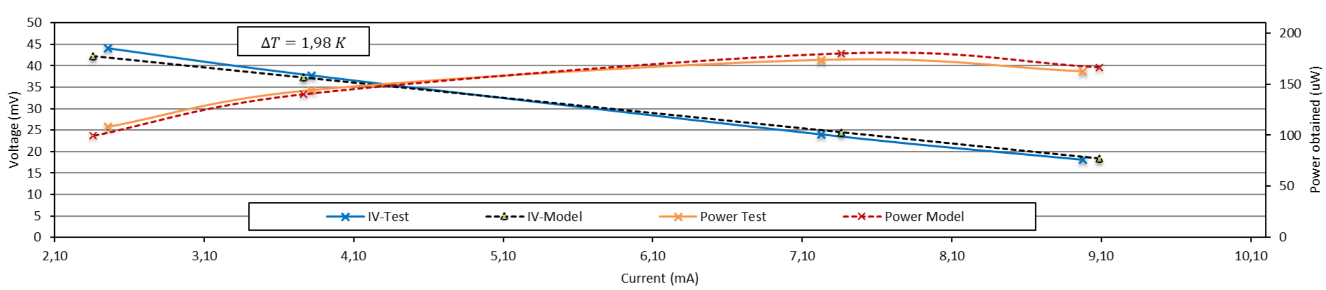

Figure 6. Thermoelectric characterization test results compared to the expected results calculated by the thermoelectric generator model.

The correlation implies that all the important error sources have been minimized

5.2 BLE characterization results

The BLE is adjusted to provide the lowest achievable power consumption. Test results have been obtained to represent the current profile by the BLE during advertising events, allowing to calculate the power consumption of the communications module to analyse what is the achievable duty cycle of the system.

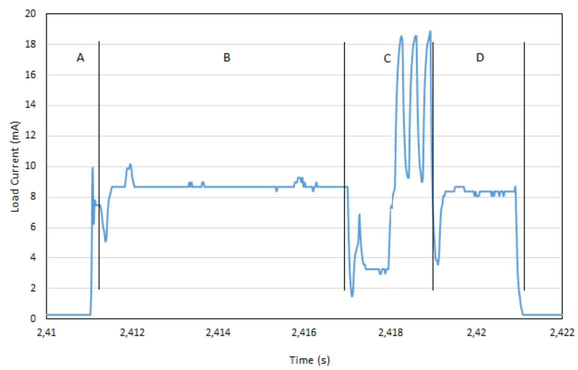

Figure 7. Current profile of the BLE113 representing a single advertising event.

The current profile for an advertising event is represented in Figure 5. Several phases can be observed in the profile. Section A represents the wake-up of the module. Section B corresponds to the temperature measurement and the stabilization of internal functions of the controller. Section C corresponds with the start of the data transmission. The three peaks correspond with the three channels used to transmit the data (Channels 37, 38 and 39). Section D represents another stabilization period embedded into the performance of the module that is required before getting into sleep mode again.

In addition, to the advertising profile, the required initialization energy needs to be measured. The current profile of the BLE module from initialization to a couple of advertising events can be seen in Figure 7.

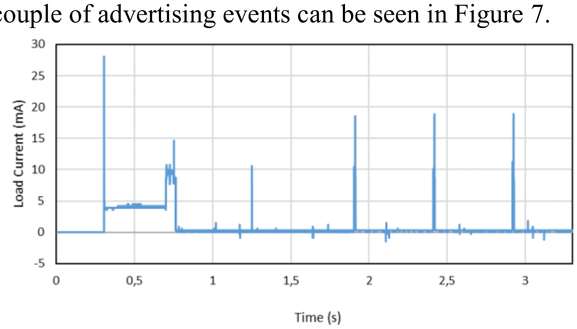

Figure 8. Current profile for the BLE module from initialization to 3 advertising events.

It can be observed that the initialization energy entails the highest amount of energy required. This initialization energy is a major design driver for the system.

Table 5. BLE113 performance values obtained in the characterization test.

BLE113 performance parameter	Value
Advertising event energy	264.4 µJ
Advertising event time	10.0 ms
Adv. Required storage capacitance	89.6 uF
Initialization energy	6.9 mJ
Initialization event time	0.4 seconds
Init. Required storage capacitance	8.2 mF

The initialization energy of the BLE113 module requires a 100 times larger capacitor, compared to a theoretical system in which initialization of the module would be ignored. It is therefore recommended for future designs to pay close attention to this power consumption and to seek for modules with as low as possible initialization energy. Nevertheless, the values obtained still guarantee the viability of the performance characterization for advertising events and the charging times of the capacitors.

This research develops a thermoelectric harvesting design based on a sensing application. However, the same design framework could be used with an actuator that scans instead of advertise. as long as a certain delay in the response of the actuator is not a problem for its application. The current consumption for receiving is different than for sensing but similar values should be expected.

5.3 End-to End design performance results

All the modules are connected together. The thermoelectric generator measured powering parameters provide the operational conditions of the system. These values are presented in Table 6.

Table 6. TEG measured powering values for the End-toend design test.

TEG input values	Value
Temperature difference	2.31 K
Input voltage	35.55 mV
Input current	6.58 mA
Peak input power	234 uW

The input current has been calculated from the input voltage and the voltage provided by the TEG due to the temperature difference measured. With these values there is a charging in the storage capacitor. The temperature difference is not the minimum feasible but it is close to the limit of the performance. The minimum temperature difference would increase the time required for the test to infinite, as the charging current, equal to the power converter output current minus the current losses, would be close to zero making unnecessarily long experiments. The values that are obtained from the power converter are presented in Table 7.

Table 7. Power converter performance values for the end-to-end design test.

TEG performance parameter	Value
Output current	19.24 µA
Output voltage	4.0 V
Output power	76.96 uW
Power efficiency	32 %

Ultra-low current values are obtained from the power converter module. Therefore, the use of low-leakage components is a major design driver. As an example of how much can be lost in a single component, the leakage current of the storage capacitor used equals around 25 % of the total output current obtained. The rest of the components are selected with low current leakages. The output voltage presented in Table 7 is the one in which the advertising event comparator provides a positive signal. Nevertheless, the power converter is designed for a maximum of 4.1V

The power control segment works as expected. The Schmitt Trigger first closes the LDO switch and then it remains closed. The comparator provides the signal for waking up the Bluetooth module at 4.0 V. The Schmitt Trigger should provide a positive signal slightly before the advertising comparator signal. If not, the comparator would drain energy and the initialization process won't ever be achieved. The final performance values that can be obtained from the whole system are presented in Table 8.

Table 8. Performance values obtained in the End-to-end design performance test.

TEG performance parameter	Value
Charging Time	16.2 seconds
Achievable duty cycle	0.06 %
Average power consumption	4.93 uW

The efficiency of the power management module is fairly low compared to higher power DC-DC converters which typically approach 80-90% efficiency. If in the future the ultra-low power management modules increase their efficiencies, the duty cycle could be increased. However, this lower efficiency is obtained for obtaining a low minimum input voltage, higher input voltages would increase the requirements of the power harvesting source.

6. Conclusions

The results given in this research provide the first power values, from generator to load, for an autonomous thermoelectrically-powered temperature sensor, designed for a small satellite, for small size and temperature difference. The system design works for 2.31 K of temperature difference providing a temperature measurement over a Bluetooth Low energy (BLE) link every 16.2 seconds.

The total BLE module initialization energy required exceeded what was expected. Therefore, it is concluded that for the BLE selection, the initialization energy should be a trade-off criterion as it may drive the size of the energy storage component and consequently the size of the entire sensor system. A communications module based on the SoC nRF51822 may provide better initialization values.

Table 9. Volume and mass values of the designed autonomous temperature sensor and the one used in the Delfi-n3Xt mission and connected by wires.

Parameter	Autonomous T. Sensor	T. Sensor
Height	14.4 mm	10.9 mm
Width	32.0 mm	20.0 mm
Length	30.0 mm	20.0 mm

With the technology available, it is concluded that this type of system will not decrease the size from a classical temperature sensor, as it can be seen in Table 9. It presents a reference temperature sensor used in the Delfi-N3xt mission. Its dimensions also consider a 4 pin, I2C, connector. The dimensions of the autonomous sensor have been optimized to not take into account the conservative sizes used to facilitate testing. In addition, 2.3 mm of height of the autonomous temperature sensor could be decreased if the initialization would not drive the capacitor design. Nevertheless, the results can be used for the development of applications for remote or unreachable locations, as a sensor or an actuator. Whereas, with the current state-of-the-art technology, self-powered wireless sensors are most suitable for large satellites or where integration of the wiring harness is relatively complex, they can be carried as technology demonstrator in a PocketQube for obtaining better conclusions that will foster the implementation of the technology.

Within this study, an end-to-end development and testing campaign have proven that powering a wireless sensor with a thermal electric generator is feasible with the stat-of-the-art technology and works with modest thermal gradients. Future developments are recommended to optimize the system further in terms of size and performance and also to demonstrate and characterize such systems in a real space environment.

References

[1] Amini, R., G. Aalbers, R. Hamann, W. Jongkind and P. Beethuizen. New generations of spacecraft data handling systems: Less harness, more reliability, 57th International Astronautical Congress, Valencia, Spain, 2006, 2-6 October.

[2] Amini, R., E. Gill and G. Gaydadjiev (2007). The challenges of intra-spacecraft wireless data interfacing. 58th International Astronautical Congress, Hyderabad, Andrhra Pradesh, India, 2007, 24 – 28 September.

[3] Zheng, W. H. and J. T. Armstrong "Wireless intra-spacecraft communication: the benefits and the challenges.", NASA/ESA Conference on Adaptive Hardware and Systems, Anaheim, CA, USA, 15 – 18 June 2010.

[4] Takacs, A., H. Aubert, M. Bafleur, J.-M. Dilhac, F. Courtade, S. Fredon, L. Despoisse, C. Vanhecke and G. Cluzet Energy harvesting for powering wireless sensor networks on-board geostationary broadcasting satellites. 2012 IEEE International Conference on Green Computing and Communications, Besancon, France, 20–23 Nov, 2012.

[5] Takacs, A., H. Aubert, S. Fredon, L. Despoisse and H. Blondeaux, Microwave power harvesting for satellite health monitoring. *IEEE Transactions on Microwave Theory and Techniques*, 2014, 62.4: 1090-1098.

[6] Kwon, Seong-Cheol; OH, Hyun-Ung. Experimental validation of satellite micro-jitter management strategy in energy harvesting and vibration isolation. *Sensors and Actuators A: Physical*, 2016, 249: 172-185.

[7] de Boom CW, van der Heiden N, Sandhu J, Hakkesteegt HC, Leijtens JL, Nicollet L et al. In-Orbit Experience of TNO Sun Sensors. 8th International ESA Conference on Guidance, Navigation and Control Systems. Noordwijk: ESA. 2011

[8] Von lukowicz, Marian, et al. Thermoelectric Generators on Satellites—An Approach for Waste Heat Recovery in Space. *Energies*, 2016, 9.7: 541

[9] Speretta, S., Soriano, M. T. P., Bouwmeester, M. J., Carvajal-Godinez, M. J., Menicucci, A., Watts, M. T., ... & Gill, E. Cubesats To Pocketqubes: Opportunities And Challenges. 67th International Astronautical Congress, Guadalajara, Mexico, 2016, 26-30 September.

[10] Schoemaker, R., Bouwmeester, J.Evaluation of Bluetooth Low Energy wireless internal data communication for Nanosatellites. The 4S Symposium 2014.